The impact of sea surface temperature on the aggregation of deep convective clouds

Sara Shamekh

THÈSE DE DOCTORAT

de l'Université de recherche Paris Sciences et Lettres
PSL Research University

Préparée à l'École Normale Supérieure

The Impact of Sea Surface Temperature on the Aggregation of Deep Convective Clouds

École doctorale n°129

SCIENCES DE L'ENVIRONNEMENT D'ILE-DE-FRANCE

Spécialité OCÉAN, ATMOSPHÈRE, CLIMAT ET OBSERVATIONS SPATIALES

COMPOSITION DU JURY :

M Jean-Philippe Duvel
LMD, ENS PSL, Paris, Co-directeur

M Fabio D'Andrea
LMD, ENS PSL, Paris, Co-directeur

Mme Francoise Guichard
CNRM, Météo France, Toulouse,
Rapporteur

M Adrian Tompkins
International Centre for Theoretical Physics,
Trieste, Rapporteur

M Christopher Holloway
University of Reading, Reading,
Examineur

Mme Sandrine Bony
LMD, Sorbonne Université, Paris, Examineur

M Jean-Pierre Chaboureau
Laboratoire d'Aérologie,
Université de Toulouse, Président

Soutenue par **Sara Shamekh**
le 26 juin 2020

Dirigée par **Caroline Muller**

ENS ÉCOLE NORMALE SUPÉRIEURE | PSL RESEARCH UNIVERSITY PARIS

Abstract

The spontaneous aggregation of deep convective clouds into a single moist region, an ubiquitous phenomenon in numerical modeling of the tropics, has a large impact on mean atmosphere variables such as moisture and radiative cooling. The mechanisms driving the aggregation are known to be sensitive to the choice of sea surface temperature (SST). The objective of this study is to investigate the impact of SST heterogeneities on the occurrence and mechanisms of the aggregation. The cloud-resolving model "System for Atmospheric Modeling", or SAM, is used to perform 3D simulations of radiative-convective equilibrium in a non-rotating framework.

The SST heterogeneities are either imposed or interactive. In imposed cases, a spatiotemporally fixed warm SST anomaly (hereafter Hot-spot) with radius R and temperature anomaly ΔT is introduced at the center of the domain. The hot-spot significantly accelerates aggregation, particularly for warmer/larger hot-spots, and extends the range of SSTs for which aggregation occurs, however at cold SSTs (290 K) the aggregated cluster disaggregates if we remove the hot-spot. A large convective instability over the hot-spot leads to stronger convection and generates a large-scale circulation which forces subsidence drying outside the hot-spot. The hot-spot induced large-scale circulation can enforce the aggregation even without radiative feedbacks for hot-spots sufficiently large/warm. The strength of the large-scale circulation, which defines

the speed of aggregation, is a function of the hot-spot fractional area.

In cases where SST heterogeneities are interactive, the ocean is modeled as one layer slab ocean, with a temporally fixed mean but spatially varying temperature. We find that the interactive SST decelerates the aggregation and that the deceleration is larger with a shallower slab, consistent with earlier studies. The surface temperature anomaly in dry regions is positive at first, thus opposing the diverging shallow circulation known to favor self-aggregation, consistent with the slower aggregation. But interestingly, with further drying, it becomes negative and favors the shallow circulation. This diverging shallow circulation out of dry regions is found to be well correlated with the aggregation speed. It can be linked to a positive surface pressure anomaly, itself the consequence of SST anomalies and boundary layer radiative cooling. Including a diurnal cycle in simulations with interactive SST, results in a faster triggering of dry patches for shallow slabs, reduces the dependency of aggregation on slab depth, and accelerates the aggregation for shallow slabs.

Acknowledgements

Written on the 40th day of quarantine.

It's been a wonderful 3 years as a Ph.D. student at LMD and I can not believe they have gone by already. There are many people to thank for making it a great experience.

First of all, I would like to express my gratitude to my supervisor Caroline Muller, my co-supervisors Jean-Philippe Duvel, and Fabio D'Andrea. I deeply thank Caroline, for her support, dynamism, and for invaluable independence she gave me as a Ph.D. student. I thank her for teaching me that every mistake is just a learning experience. I have learned so much with her. The joy and enthusiasm she has for her research were contagious and motivational for me, even during tough times in the Ph.D. pursuit.

I thank Jean-Philippe for his time, assistance, and for his patience to deal with all my inquiries. It has been great to get his many useful thoughts, suggestions, and constructive criticisms on divers problems and from such a different and valuable perspective. I thank Fabio for providing critical and insightful feedback along the way, which improved greatly this thesis. I thank him for saying "don't worry I take care of it" and helping me with all kinds of challenges that I faced.

I spent a great month at MPI Hambourg working with Cathy Hohenegger. I would like to thank her for her hospitality, time and assistance, and for sharing many inspiring thoughts and suggestions regarding my research.

My Ph.D. experience would have not been nearly enjoyable without the friendship and assistance of my colleagues at LMD. Having their friendship is such a privilege.

I thank Maxime for all his supports and for keeping me happy and sane during the last months of my Ph.D. that passed in confinement. He has made this period much smoother than it could have been. I thank Mahsa for being there for me any time I needed a friend, despite living far away. Finally, I would like to thank my family members for all their love and support.

This project has received funding from the Marie - Sklodowska Curie Actions (MSCA) under the European Union's Horizon 2020 research and innovation programme (grant agreement no 675675)

Contents

1 Introduction **12**

1.1 Motivation 12

1.2 Tropical convective clouds 13

1.3 Aggregation in numerical simulations 15

1.4 Surface temperature dependency 16

1.5 The aggregation mechanisms 18

1.5.1 Radiation 18

1.5.2 Atmospheric Moisture 21

1.5.3 Surface fluxes 22

1.6 Objective and Outline of the thesis 24

2 Model Description, Simulation setup and Diagnostics **27**

2.1 Introduction 27

2.2 Model Description 29

2.2.1 Governing Equations 29

2.2.2 Radiation 31

2.2.3 Cloud Microphysics and water partitioning 31

2.2.4 Surface Fluxes 32

2.2.5 Sub-grid Scale Model 33

2.3 Simulation Setup 34

2.3.1 SST 35

2.4 Diagnostics 36

2.4.1 Dry patch and Aggregation Index 36

2.4.2 Moist Static Energy 39

2.4.3 Stream Function and Circulation 39

3 How do ocean warm anomalies favor the aggregation of deep convective clouds 42

3.1 Introduction 43

3.2 Model description and simulation design 48

3.2.1 Cloud-resolving model 48

3.2.2 Experimental setup 49

3.2.3 Aggregation metrics 51

3.3 Hot-spot impact on aggregation of deep convection 52

3.3.1 Results without and with hot-spot at different SSTs . . . 53

3.3.2 Development of a large-scale circulation 56

3.4 Convective aggregation without radiative feedbacks 60

3.4.1 Hot-spots with or without radiative feedbacks 60

3.4.2 Two-box model: Pulled or pushed aggregation? 64

3.4.3 The aggregation onset phase 66

3.5 Equilibrium phase 69

3.6 Conclusions 71

4 Self-aggregation of convective clouds with interactive sea surface temperature 75

4.1 abstract 75

4.2 Introduction 76

4.3 Method 80

4.3.1 Cloud-resolving model 80

4.3.2 Experimental setup 81

4.3.3 Slab ocean 82

4.3.4 Analysis Framework 84

4.4 The impact of interactive SST on the aggregation of convective clouds 85

4.4.1 Overview of results 85

4.4.2 SST anomalies 87

4.4.3 Surface pressure anomaly 91

4.4.4 Divergent flow 96

4.5 The impact of slab depth and SST on self-aggregation 100

4.5.1 Delayed aggregation with shallow mixed layer and cold SST 100

4.5.2 Link with the strength of the shallow circulation compared to the deep circulation 104

4.6 Conclusions 107

4.A Impact of interactive SST with constant deep ocean sink 112

4.B Surface pressure computation 114

4.C Sensitivity simulations and low-level radiative cooling 116

5 Impact of the diurnal cycle on the aggregation of convective clouds with interactive surface temperature 118

5.1 Introduction 119

5.2 Experimental setup 121

5.3 Results 123

5.3.1 The diurnal cycle in aggregating simulation 124

5.3.2 Diurnal cycle vs constant solar radiation 127

5.4 Conclusion 137

5.A Sensitivity to relaxation time 140

6 Conclusions and Future Research Directions 142

6.1 Conclusions 142

6.2 Future Research Directions 146

6.2.1 Ocean Eddies 146

6.2.2 Boundary Layer Divergent Flow 147

6.2.3 Dry patch triggering 148

6.2.4 Shallow Circulation 149

6.2.5 Interactive SST with adjusted mean energy removal . . . 150

Chapter 1

Introduction

1.1 Motivation

In the tropics, deep moist convection, which is the main source of free tropospheric water vapor (Grabowski and Moncrieff, 2004), is mostly organized into clusters rather than being randomly distributed. The organization of convection occurs on a wide range of scales such as squall lines (Houze, 1977), mesoscale convective systems (Houze, 2004), tropical cyclones (Simpson et al., 1997), and the Madden Julian oscillation (Madden and Julian, 1971). Organization has an important impact on the atmosphere and weather. For example, Hennon et al. (2013) show that approximately 1600 tropical cloud clusters form around the globe each year, from which 6.4 develop into tropical cyclones. Also, a large part of cloudiness and precipitation over the tropics is due to organized clusters. Tobin et al. (2012) find that for a larger degree of organization, the middle and upper troposphere in non-convective areas is drier, and shallow cloudiness is reduced. This can have an important impact on climate sensitivity. Later on, two studies Mauritsen and Stevens (2015); Tan et al. (2015) showed that the change in organized convection with global

warming can modulate precipitation and climate sensitivity. In the models, without any external forcing, moist convection can spontaneously organize into a cluster, this process is know as self-aggregation (or aggregation). The ubiquitous presence of aggregation in different models with a variety of boundary conditions and simulation setups, and its potential importance for weather and climate, brings forward a need to understand its mechanisms and feedbacks. This work tries to shade light on these mechanisms and gain a better understanding on what drives the aggregation.

This chapter presents the necessary concepts, reviews the previous studies of aggregation, discusses the mechanism proposed to drive the aggregation, and how SST plays a role. The chapter ends with the objective and the outline of the thesis.

1.2 Tropical convective clouds

The tropics are usually defined as the region between 23 N to 23 S in which incoming solar radiation is larger than outgoing longwave radiation (OLR), and the sea surface temperature is larger than that at higher latitude. Different processes (large scale deep convection, Hadley cell, ocean transport, ...) are in charge of transporting this surplus of energy out of the tropics and regulating the tropical SST and atmospheric temperature profile.

In the absence of convection and conduction, the only heat source in the atmosphere is radiation, which brings the surface and the atmosphere towards an equilibrium state that is gravitationally unstable, thus moist convection can develop. Convection redistributes heat vertically by latent heat release of condensation through the free troposphere. In the absence of external forcing or lateral transport of energy, this process brings the atmosphere towards a

new equilibrium in which the radiative cooling is in balance with convective heating:

$$LHF_{condensation} = Qrad \tag{1.1}$$

where $LHF_{condensation}$ is the latent heat released by condensation, and $Qrad$ is the radiative cooling of the atmosphere. Though simple, this paradigm, referred to as "radiative-convective equilibrium" or RCE, provides a useful framework to understand the interaction between convection, (internally-developed) large scale circulation, and radiation. It has first been introduced by Manabe and Strickler (1964) using a single column model. Since then, RCE has been widely used as an idealisation of the tropical atmosphere (Held et al., 1993; Tompkins and Craig, 1998; Bretherton et al., 2005).

The tropics has a variety of cloud types, however the most frequent ones are shallow and deep convective clouds (Johnson 1999). Deep convective clouds represents the dominant transport process of moisture, momentum and heat to the free troposphere. Deep convection thus changes the temperature profile of the atmosphere towards a more stable one. In the free troposphere, the heat released by condensation produces gravity waves that redistribute the heat over large areas (Bretherton and Smolarkiewicz, 1989). So the stabilising effect of convection is not local, especially over the tropics where the Rossby radius of deformation is very large due to a small Coriolis force there, and gravity waves can travel far before dissipating. The moistening effect of deep convection though is more local. Convection moistens the free troposphere locally while it dries the non-convective regions due to the subsidence drying forced by mass balance between convective regions and non-convective ones.

Most moist convective clouds have a small spatial scale, typically a few kilometers in the horizontal. They often merge into clusters of approximately 10 km in horizontal dimension. In the tropics, convective clouds can also be

organized into larger clusters (O(100 km)) by synoptic dynamical systems such as equatorial waves or tropical depressions. Convective clouds can also have their own organization sources such as in squall lines, or more generally in mesoscale convective systems (MCS). A broad definition of a mesoscale system is "a cumulonimbus cloud system that produces a contiguous precipitation area$\sim$100 km or more in at least one direction" (Houze, 2004). MCSs are associated with extreme weather conditions and strong precipitation: in fact tropical precipitation - which accounts for two thirds of global precipitation - mostly occurs in MCSs (Nesbitt et al., 2006). MCSs, which contain many deep convective cells, become gravity wave generators, propagating momentum outward, displacing the environment mass downward, and thus warming and drying the atmosphere (Bretherton and Smolarkiewicz, 1989). A drier atmosphere cools more efficiently by longwave radiation, so that OLR potentially increases in response to MCSs formation.

1.3 Aggregation in numerical simulations

Aggregation is the spontaneous clustering of convective clouds in an initially homogeneous environment. It is driven by internal feedbacks and has been found to occur in numerical simulations. The aggregation of convective clouds has been first studied by Nakajima and Matsuno (1988) in an idealised study of the tropics using a two-dimensional cloud convection model (1 km horizontal resolution and 512 km horizontal domain length). In their simulation, with a constant SST and a fixed rate of atmospheric radiative cooling, they found that the individual clouds can spontaneously organize into a cluster (30 - 100 km) with lifetime longer than 10 hours. In a similar setup, Held et al. (1993) also found the clustering of convection when no wind shear is allowed to form. Since then, aggregation has been widely studied using 2D (Grabowski and Moncrieff,

2001; Stephens et al., 2008), and 3D cloud resolving models (CRMs) in a square domain (Tompkins and Craig, 1998; Bretherton et al., 2005; Muller and Held, 2012; Wing and Emanuel, 2014; Hohenegger and Stevens, 2016; Holloway, 2017) or a channel (Tompkins, 2001b; Wing and Cronin, 2016), as well as in global models with clouds and convection parametrization (Coppin and Bony, 2015).

In a CRM simulation over a small square domain, the aggregation of convective clouds typically starts with the appearance and expansion of non-convective regions that become progressively drier and expand horizontally. These dry patches merge and by the end of the simulation the domain is divided into a single (or few when the domain is very large, O(10^4 km)) isolated cloud cluster, which is surrounded by the largely dry and subsiding environment. The domain averaged water vapor significantly decreases with aggregation, allowing the surface and atmosphere to radiatively cool thus increasing OLR. This is of significant importance as it changes the surface and atmospheric energy budget. If this process is found relevant to the natural world, its effect would be to reduce climate sensitivity. A better understanding of the aggregation of convective clouds and its representation in GCMs is consequently very important for climate prediction.

1.4 Surface temperature dependency

Most studies on aggregation make use of numerical simulations in idealised settings, typically with fixed and uniform SST as lower boundary condition. Virtually all studies have found a sensitivity to the value of the (fixed) SST. This sensitivity partially arises from SST dependency of mechanisms developing the aggregation (Wing and Emanuel, 2014), however, the range of SST

for which the aggregation is favored seems to be model and set-up dependent (Held et al., 1993; Emanuel et al., 2014; Coppin and Bony, 2015; Wing and Cronin, 2016). Held et al. (1993) show that the aggregation is favored at 30 C compared to 25 C. Using 3D cloud-resolving simulations and a small square domain, Wing and Emanuel (2014) show that aggregation is favored over an intermediate range of (fixed) SSTs 300 - 307 K, though increasing the domain size yields aggregation at warmer SSTs as well. These results suggest favored aggregation at warmer temperatures. Later on, using the same setup but a large channel domain, Wing and Cronin (2016) show that aggregation is favored over a large range of SSTs 280-310 K when SST is fixed. Conversely, Coppin and Bony (2015) show that aggregation occurs at low (< 298K) and high SST (> 305) in a GCM, while in the intermediate range it is sensitive to the initial condition and is not systematic.

Beside sensitivity to the absolute value of SST, the spatial or temporal changes of SST also impact convection and the atmospheric circulation (Lau, 1997; Tompkins, 2001b; Back and Bretherton, 2009; Robinson et al., 2011). Back and Bretherton (2009) show that over the tropics, the distribution of boundary layer divergence is predominantly dictated by boundary layer temperature gradients which are closely related to SST gradients. They conclude that deep convection is generated in response to boundary layer divergent flows, themselves a consequence of SST patterns. A boundary layer divergent flow from dry regions (often referred to as shallow circulation in numerical modelling of aggregation) has been found to be key for the aggregation process. Indeed, this shallow circulation redistributes moisture horizontally, transporting moisture from dry into moist regions, thus upgradient (Bretherton et al., 2005; Coppin and Bony, 2015). This upgradient transport of moisture, and the concomitant upgradient transport of moist static energy, result in a larger variance of moisture and localization of convection.

Although this shallow circulation accompanying self-aggregation is believed to be radiatively-driven (Muller and Bony, 2015), Hohenegger and Stevens (2016) show that an interactive SST allows the formation of SST gradients, which can also impact the strength of the shallow circulation, thus the aggregation. In a conceptual model of the boundary layer, Naumann et al. (2019) find that a radiatively-driven shallow circulations can be as strong as those driven by typical SST gradients.

1.5 The aggregation mechanisms

Self-aggregation studies identify several physical mechanisms that can drive the aggregation, involving radiation, surface fluxes or water vapor. These mechanisms seems to depend on model, simulation configurations (such as domain size and shape), and boundary conditions (for instance SST). Here we briefly review these mechanisms.

1.5.1 Radiation

The importance of interactive radiation in driving the aggregation has been confirmed by many studies. The radiation related mechanisms include longwave radiative cooling from clear sky (Wing and Emanuel, 2014; Emanuel et al., 2014) or cloud top (Muller and Held, 2012) as well as shortwave radiation (Wing and Cronin, 2016). The importance of each radiation mechanism and how they drive the aggregation differ among the studies. Here we review the main ones.

Tompkins and Craig (1998) find that replacing the interactive radiation scheme with a horizontally uniform radiation profile destroys the convective

organization in few days. Thus they conclude that the differential radiative heating rate is necessary for the maintenance of the aggregated cluster by converging into cloudy region.

Using a 3D CRM in a RCE frame work, Bretherton et al. (2005) find that homogenizing the longwave radiation suppresses the aggregation. They suggests that an enhanced lower tropospheric longwave radiation in dry region compared to moist region drives a shallow circulation which transports low level moist air to the moist region. Consequently the already dry region dries further and cools more efficiently by radiation while the mosit region radiation reduces. Thus the differential radiative cooling increases as well as shallow circulation hence creating a positive feedback, as was firstly presented by Gray and Jacobson (1977). The finding of Muller and Held (2012) further confirms the role of longwave radiation: in their simulation, removing low clouds from the computation of radiation prevents the aggregation. They thus emphasize the importance of cloud top longwave radiation: the boundary layer circulation, which transport moisture up-gradient, is driven by downward motion in the dry region which itself is forced by enhanced cloud top longwave radiation.

Wing and Emanuel (2014) find that the both the differential shortwave or longwave heating rate due to upper tropospheric moisture difference between the moist and dry region (clear sky effects) is necessary for the aggregation. They find that, for a sea surface temperature in the range of the current temperature of the tropical ocean, the shortwave radiation effect is to favor aggregation in its early and middle stage. The shortwave absorption in clear sky region reduces with reduction of moisture, thus the net differential radiative cooling increases hence results in stronger subsidence and further dryness. The longwave radiation feedbacks though can be positive or negative depending on the relative emissivity of upper and lower troposphere. At the early stage of

aggregation, when the upper troposphere is dry compared to the lower troposphere, the longwave radiative cooling increases with further dryness and creates a positive feedback. While when aggregation is established, the lower troposphere also has a small amount of moisture thus the longwave radiative cooling decreases and results in a negative feedback. Wing and Cronin (2016) confirm these finding in a channel domain, but they suggest that driving feedbacks are SST dependent so that the shortwave radiative feedbacks remains positive across all SSTs but weaken with increasing the temperature, while the longwave radiative feedback is negative at low SST but then turn positive for warmer SSTs.

Emanuel et al. (2014) used a toy model with two atmospheric layers to show the importance of clear-sky longwave radiation. Above a critical SST, the lower tropospheric longwave radiative cooling becomes very large due to its large amount of water vapor and comparatively a dry free troposphere. The enhanced low-level clear-sky longwave radiative cooling increases the large scale subsidence and drives the aggregation. The aggregation drives the atmospheric to a dry profile far from typical RCE approximation. Thus they suggest that "the ordinary RCE state becomes linearly unstable to large-scale overturning circulations" and the aggregation drives the atmosphere towards a new RCE.

The importance of radiative feedbacks have been also investigated in GCM by Coppin and Bony (2015). They show that the low level radiative cooling in dry non convective region drives a circulation which leads to aggregation. They call these dry region "radiatively driven cold pools". These cold pools can expand as they cool more efficiently thus they become denser than the moist region. They find that this feedback is more effective at cold SSTs ($< 300K$).

1.5.2 Atmospheric Moisture

While convective moistening of the free troposphere has a stabilising effect on the large scale, the local moistening by convective clouds favors successive convection (Grabowski and Moncrieff, 2004). This is known as moisture-convection feedback (Held et al., 1993; Tompkins, 2001b; Craig and Mack, 2013). The free tropospheric moisture-convection feedback has been firstly mentioned by Held et al. (1993) in a two dimensional setup. In their simulation with no imposed wind shear, convection becomes organized in a small part of the domain. Adding even a weak wind shear to an already organized simulation, homogenizes moisture over the domain followed by convection being activated outside the organized cluster. However, before losing its organization, convection follows the region with moist low level free troposphere which is advected by wind shear. They suggests that, as in moist region the entertained air into the cloud is also moist, it doesn't have a negative impact on the buoyancy of convective updraft, convection is more successful thus favored. The reduced entrainment of dry air mentioned above is then the key for the organisation of convection.

In 3D cloud-resolving simulations, Tompkins (2001b) suggests that convection moistens its local environment and a moist environment favors more convection thus moisture-convection feedback is important for aggregation. . This study further examines this hypothesis in two sensitivity tests in which the free tropospheric and upper free tropospheric moisture is reduced by 70 percent in the convective area. The consequence is a cut off of the convective activities especially for the case in which the lower free tropospheric water vapor has been reduced. The drier free troposphere enhances the strength of downdraft and also weakens the convective updrafts due to the entrainment of dry air. In a recent study, Tompkins and Semie (2017) shows that a higher

entrainment rate (represented by the sub-grid mixing parameterization in numerical simulations) favors aggregation. A higher entrainment rate increases the interaction between the convective plume and its local environment's moisture thus it enhances convection-moisture memory

Beside the role of free tropospheric moisture, the boundary layer moisture can also play a role in aggregation. Yang (2018), using a boundary layer framework shows that a negative boundary layer water vapor anomaly is necessary for the formation of the dry regions thus for the aggregation. A negative moisture anomaly creates a locally higher density thus a pressure gradient that is necessary for the horizontal mass transport between non-convective and convective regions. He argues that cold pools formed by the evaporation of rain disfavor aggregation by homogenizing the boundary layer moisture. This impact of cold pools on the aggregation has been confirmed firstly by Nakajima and Matsuno (1988) in a simple 2D simulation in which they show that suppressing the evaporation of rain - thus suppressing the cold pools - leads to clustering of convection. Further, Jeevanjee and Romps (2013) show that the aggregation can occur even in small domains when they prevents the formation of cold pools. They reinforce the idea that cold pools transport moisture to dry region and homogenize water vapor in the boundary layer. This redistribution of moisture is even more effective over small domains.

1.5.3 Surface fluxes

The surface fluxes (latent heat and sensible heat fluxes) are functions of wind speed, air-sea moisture and temperature disequilibrium. The spatial variation of surface fluxes arises from variation in surface wind speed or air-sea disequilibrium. The wind-speed surface flux feedback which is often referred to as WISHE (wind-induced surface heat exchange) is a positive feedback mecha-

nism in which a stronger wind enhances surface fluxes and the enhanced surface fluxes favors stronger atmospheric circulation (wind speed). On the one hand, the interaction of convection and the surface results in a locally enhanced heat and moisture fluxes due to increased surface wind, which in return can feed the convection and favor aggregation. On the other hand, the surface fluxes are enhanced in a dry non-convective area due to an increased moisture disequilibrium at the surface, and thus disfavor aggregation. Tompkins and Craig (1998); Bretherton et al. (2005) show that homogenizing the surface fluxes can destroy the aggregation. However Muller and Held (2012) show that the surface fluxes are not necessary but helpful for the aggregation and conclude that the aggregation proceeds even with homogenized surface fluxes as long as radiative feedbacks are strong and the domain is large.

Wing and Emanuel (2014) show that the surface fluxes create a positive feedbacks with aggregation at the early stage, when the aggregation is proceeding, but when well established, the surface fluxes feedback becomes negative. This change of sing is due to the fact at the early stage the wind effect dominates (WISHE effect), while at a longer times it is the evaporative demand of dry regions that dominates. In other words, at early stage, the surface fluxes are stronger in convective regions (positive feedback) while when aggregation is established, surface fluxes become stronger in dry regions due to enhanced air-sea moisture disequilibrium.

Another surface flux related mechanism that can play a role in aggregation of convection is wind-induced surface heat exchange (WISHE, Emanuel et al. (1994)).

Coppin and Bony (2015), using a GCM, show that the surface flux are necessary at warm SSTs (> 305K).They suggest that a WISHE mechanism initiates and develops aggregation at high SST as the deep convection enhances

surface fluxes and the convection becomes more likely in a region with high surface fluxes.

1.6 Objective and Outline of the thesis

While a lot has been done identifying the mechanisms triggering and governing the aggregation of convective clouds, there is still a need to better understand how these mechanisms are affected by SST. More specifically, the majority of these studies use idealized simulation designs that exclude any SST heterogeneity which potentially impacts surface fluxes, atmospheric circulation, and convective activities. This study works towards achieving a better understanding of the physics of aggregation and how it is affected by SST heterogeneities. The key questions to address are:

- How does the aggregation of convective clouds depend on the surface temperature, when SST is fixed in time and space?
- How does the presence of a spatiotemporally fixed SST anomaly impact the aggregation, and what role do the amplitude and the fractional coverage of the SST anomaly play?
- How does an interactive surface temperature feedback on convection its aggregation?
- Does including a diurnal cycle affect the progress of aggregation when the surface temperature is interactive?

To that end, we will use radiative-convective equilibrium simulations performed with the cloud-resolving model SAM. Chapter 2 describes this cloud-resolving model in more detail, as well as the simulation settings, and the

diagnostics used to quantify the aggregation of convective clouds in our simulations.

In chapter 3, we first investigate the range of fixed SST that favors the aggregation in SAM, as this range is model and setup dependent. Then for SST = 300 K, we impose a spatially and temporally constant warm SST anomaly at the center of the domain (but keeping the domain-mean SST constant by reducing the SST outside of the warm anomaly) to investigate how fast the aggregation progresses, and how its progress depends on the size and magnitude of the warm anomaly. One of the interesting questions is whether a simulation with homogeneous SST which does not aggregate, does with a hot spot, and in that case whether removing the warm anomaly after reaching the aggregation leads to disaggregation. In other words, does this forced aggregation drive the system to a new stable equilibrium? The chapter continues by exploring the importance of radiative feedbacks for the aggregation when a warm anomaly is present. To do so, we spatially homogenize the radiation profile for simulations with different warm anomalies. These results are published in Shamekh et al. (2019).

In chapter 4, we investigate the feedbacks between the SST and the aggregation when the SST is interactive. To allow the SST to interact, a slab ocean with fixed mean SST is implemented. Thus the domain-mean SST is held fixed, but the local SST can evolve according to the surface energy budget. When SST is interactive, reaching equilibrium can take significantly longer (Cronin et al., 2015), but keeping the domain mean SST constant excludes this problem. Using this setup, we investigate the sensitivity to the slab depth and to mean SST. As the radiation feedbacks are known to be necessary for aggregation, we further investigate separately the role of free tropospheric versus boundary layer radiation, in order to determine which part is more important

to drive the aggregation. These results are submitted in Shamekh et al. (2020).

Chapter 5 is devoted to the importance of the diurnal cycle for the aggregation. Indeed, the previous chapters neglected the diurnal cycle for simplicity, and used constant incoming solar radiation. But the diurnal cycle can modify the SST anomalies by intensifying them spatially but damping them temporally. We therefore use the same setup but adding a diurnal cycle to the simulations with interactive surface temperatures. We find that the diurnal cycle can significantly accelerate the aggregation, particularly for shallow ocean slab depths. We believe that this is linked to a new onset mechanism for aggregation, namely cold pools serving as seeds for the expanding dry regions. The results are being written for publication (in preparation).

In chapter 6, we present a summary of the key results from the 3 research chapters, a discussion of their implications, and potential directions for further research.

Chapter 2

Model Description, Simulation setup and Diagnostics

2.1 Introduction

In an atmosphere at rest or for large scale circulation, acceleration of vertical velocity is negligible, thus the vertical momentum equation reduces to the balance between the vertical pressure gradient force and gravity:

$$\frac{dp}{dz} = -\rho g$$

where p is pressure, rho is the air density and g is the gravitational acceleration. This balance holds for the atmospheric phenomena in which the horizontal length scale is much wider than the vertical one, approximately where the vertical velocity is smaller than 1cm/s. Considering deep convection, the vertical velocity fluctuation becomes large enough that it can not be ignored in the third momentum equation thus the hydrostatic balance breaks down. Consequently, to study the convective cloud and mesoscale circulation a non-

hydrostatic vertical momentum equation is used.

$$\frac{Dw}{Dt} = -\frac{1}{\rho}\frac{\partial p}{\partial z} - g \tag{2.1}$$

where w is the vertical component of the velocity.

Anther approximation made in CRMs is the anelasticity by assuming that the changes in air density are small compared to its reference value. This assumption rules out the sound waves. To explain why this is an advantage, we briefly review that the requirement for the stability of the numerical solution is set by the Courant–Friedrichs–Lewy or CFL condition as follow:

$$C = c\frac{\Delta t}{\Delta x} \tag{2.2}$$

where C is known as Courant number, c is the fluid velocity, Δx is the length interval and Δt is the time step. The meteorological phenomena have a speed much smaller than the sound waves, thus for a length interval of 1 km (typical for cloud and convection modeling), a simulation time step of up to a few seconds fulfills the CFL condition. The sounds waves which have a much larger speed thus require a much smaller time step; if not fulfilled, the numerical solutions become unstable. So the anelasticity approximation is an advantage by removing the sound waves from the equation and allowing the time step to be adequate for the meteorological phenomena.

A type of numerical weather forecast models used to study the convective clouds and storms is Cloud resolving model (CRM). The grid spacing of CRMs which varies between a few tens of meters to a few kilometers makes them suitable for resolving these phenomena.

2.2 Model Description

The CRM used in this study is the model System for Atmospheric Modeling (SAM) version 6.11.1 (Khairoutdinov and Randall, 2003). SAM is an evolved version of a Large Eddy Simulation developed by Khairoutdinov and Kogan (1999). The governing equation, as well as a short description of the radiation scheme, microphysics, subgrid-scale scheme, and surface flux computation, is provided in this chapter.

2.2.1 Governing Equations

SAM uses the anelastic assumption for air density that means the changes in density can be treated as small fluctuation around its reference value thus rules out the sounds waves from the equation. The presence of sound waves that have a velocity much larger than the atmospheric phenomenon requires a small numerical simulation time step to have stable solutions. smoothing them out of the equations allows increasing the time step without The prognostic governing equations are:

1. The momentum equation:

$$\frac{\partial u_i}{\partial t} = -\frac{1}{\overline{\rho}}\frac{\partial}{\partial x_i}(\overline{\rho}u_i u_j + \tau_{ij}) - \frac{\partial}{\partial x_i}\frac{p\prime}{\overline{\rho}} + \delta_{i3}B + \epsilon_{ijz}f(u_j - U_{gj}) + \left(\frac{\partial u_i}{\partial t}\right)_{l.s.} \tag{2.3}$$

2. The continuity equation:

$$\frac{\partial}{\partial x_i}\overline{\rho}u_i = 0 \tag{2.4}$$

3. The thermodynamic equation: as thermodynamic prognistic variable, SAM

uses the liquid/ice water vapor static energy defined as :

$$h_L = c_p T + gz - L_c(q_c + q_r) - L_s(q_i + q_s + q_g) \tag{2.5}$$

$$\frac{\partial h_L}{\partial t} = -\frac{1}{\overline{\rho}}\frac{\partial}{\partial x_i}(\overline{\rho} u_i h_L + F_{h_L i}) - \frac{1}{\overline{\rho}}\frac{\partial}{\partial z}(L_c P_r + L_s P_s + L_s P_g) + \left(\frac{\partial h_L}{\partial t}\right)_{rad} + \left(\frac{\partial h_L}{\partial t}\right)_{l.s.} \tag{2.6}$$

4. The prognostic equation of hydrometeors: SAM separates the hydrometeors in two categories 1. Total non-precipitating water (water vapor, cloud water cloud ice) shown in equation 2.7.a. 2. Total precipitating water (rain, ice, graupel) presented in equation 2.7.b.

$$\frac{\partial q_T}{\partial t} = -\frac{1}{\overline{\rho}}\frac{\partial}{\partial x_i}(\overline{\rho} u_i q_T + F_{q_T i}) - \left(\frac{\partial q_p}{\partial t}\right)_{mic} + \left(\frac{\partial q_T}{\partial t}\right)_{l.s.} \tag{2.7a}$$

$$\frac{\partial q_p}{\partial t} = -\frac{1}{\overline{\rho}}\frac{\partial}{\partial x_i}(\overline{\rho} u_i q_p + F_{q_p i}) + \frac{1}{\overline{\rho}}\frac{\partial}{\partial z}(P_r + P_s + P_g) + \left(\frac{\partial q_p}{\partial t}\right)_{mic} \tag{2.7b}$$

where B is buoyancy $= -g(\rho\prime/\rho) \approx g(T\prime/T + 0.608 q_v' - q_n - q_p - p\prime/\overline{p})$. The subscript "rad" denotes the tendency due to radiative heating; "mic" denotes the tendency of precipitation water to evaporation; "l.s." denotes the prescribed large-scale tendencies. Overbars and prime represent the horizontal mean and perturbation from the mean, respectively. The rest of the symbols are defined in Table 2.1

2.2.2 Radiation

The longwave and shortwave radiation scheme is adopted from the National Center for Atmospheric Research (NCAR) Community Climate Model (CAM3.0 ; Collins et al. (2004)). The radiative transfer is computed for each individual grid column. The cloud radiative and optical properties are explicitly calculated using the simulated cloud water and cloud ice mixing ratios. To reduce the computational expense, radiation heating rates are updated every 5 minutes rather than every time step. For this computation, the temperature, moisture, and cloud water/ice fields averaged over the time interval between two calls to the radiation is used.

2.2.3 Cloud Microphysics and water partitioning

In this study, we used single moment bulk microphyiscs package of SAM that are developed based on Marshall and Palmer (1948). The scheme assumes a form of the gamma distribution for precipitating hydrometeor type m:

$$\frac{\partial N_m}{\partial D} = n_m(D_m) = N_{0m} exp(-\lambda_m D_m) \tag{2.8}$$

N_m is is the number concentration ($m_1 m_3$) and D_m is the hydrometeor diameter.

The scheme has 6 water type :water vapor, cloud liquid, cloud ice, precipitating rain, precipitating snow, and precipitating graupel, and the partitioning between the hydrometeor is as follow:

$$q_c = w_n q_n \tag{2.9a}$$

$$q_i = (1 - w_n) q_n \tag{2.9b}$$

$$q_r = w_p q_p \tag{2.9c}$$

$$q_s = (1 - w_p)(1 - w_g) q_p \tag{2.9d}$$

$$q_g = (1 - w_p) w_g q_p \tag{2.9e}$$

where w_n, w_p and w_g only depend on temperature (m=n,p,g):

$$w_m = max(0, min(1, \frac{T - T_{00m}}{T_{0m} - T_{00m}}) \tag{2.10}$$

2.2.4 Surface Fluxes

The turbulent fluxes of latent heat (LH) and sensible heat (SH) into the atmosphere over the ocean surface are determined by the bulk formulas:

$$LH = C_E \rho_A |v| (\Delta q) \tag{2.11}$$

$$SH = C_p C_H \rho_A |v| (\Delta \theta) \tag{2.12}$$

where ρ is atmospheric surface density and c_p is the specific heat. v is the velocity of the lowest model level. In SAM the wind speed in bulk formula is set to be above a minimum so that: $v = min(1(m/s), v)$. The potential temperature deference is $\Delta\theta = \theta_A - T_s$ where T_s and θ_A are the ocean and the lowest model level temperature respectively. The specific humidity difference is $\Delta q = q_A - q_s(T_s)$, where $q_s(T_s)$ is the saturation specific humidity at the

sea-surface temperature.

2.2.5 Sub-grid Scale Model

In the numerical modeling, the turbulent motion can be separate to the large scale or resolved scale which is represented by the model equation directly, and the small scale or subgrid-scale (SGS) which occurs at the length scale smaller than the resolution of the model thus is not resolved. One way to represent the SGS turbulent motion (eddies, vortices) in the equation is to model them based on the resolved scale motion. Most of the time, the SGS turbulence is parametrized assuming that it is a function of the local gradient of the resolved value:

$$\overline{u_i' c'} = -K_c(\frac{\overline{dc}}{dx_i}) \tag{2.13}$$

where K_c is the eddy diffusivity coefficient for variable c. In our simulations using SAM, the sub-grid scale mixing is a 3D Samgorinsky closure scheme that models the coefficient K_c as:

$$K_c = C_k^2 l_s^2 max\left(0, D^2 - (PrN^2)^{1/2}\right) \tag{2.14}$$

where C_k is a constant (set to 0.1 in SAM), l is the mixing length, D represents the deformation, Pr (Prandtl number) is set to one. N is Brunt–Väisälä frequency which defined by equation 2.15 for outside the clouds and by equation 2.16 inside the clouds.

$$N^2 = \left(\frac{g}{\overline{T}}\right)\frac{\partial}{\partial z}\left(\frac{h_L + 0.61 T c_p q_T + (L - c_p T) q_p}{c_p}\right) \tag{2.15}$$

$$N^2 = \left(\frac{g}{\overline{T}}\right)\frac{\partial}{\partial z}\left(\frac{h_L + 0.61Tc_pq_T + (L - c_pT)(q_p + q_T)}{c_p + L\frac{\partial q_s}{\partial T}}\right) \tag{2.16}$$

The length scale is:

$$l_s = (\Delta x \Delta y \Delta z)^{1/3}, \tag{2.17}$$

where Δk (k=x,y,z) represents the grid spacing in direction k. When the horizontal spacing is much coarser than the vertical (i. e. near the surface) the vertical mixing becomes artificially large as the coefficient is more representative of the larger grid spacing. In this case, only the vertical grid spacing is used to calculate Δ. In SAM, the vertical grid spacing increases from 25 near the surface to 500 meters near the top of the model, while the horizontal grid spacing is larger (a few kilometers). As the vertical grid spacing is smaller than the horizontal one everywhere in the simulation domain, the length scale is set to its vertical value Δz.

2.3 Simulation Setup

The model domain is square, doubly-periodic in both horizontal directions x and y. We run simulations with domain size (576 km)^2 (plus two more domain sizes, (288 km)^2 (96 km)^2, for sensitivity tests in chapter 3). The horizontal resolution is 3 km and the vertical grid spacing increases gradually with height, with the first level at 25 m and a resolution of 50 m close to the sea surface, reaching a vertical resolution of 500 m in the mid troposphere. There are 64 vertical levels which span 27 km in the vertical. This includes a sponge layer in the upper third of the domain (from z = 18 km to 27 km) where the

wind is relaxed to zero in order to reduce gravity wave reflection and buildup. No large-scale forcing or wind is imposed. We neglect the Earth's rotation, a reasonable approximation in the tropics where the Coriolis parameter is small.

The initial conditions for the different mean SSTs are obtained from a smaller domain run with the corresponding SST at RCE ((96 km)^2 run to 50 days), then using time and domain averaged profiles of the last 5 days.

In chapters 3 and 4 the incoming solar radiation is constant and equal to 413 W/m^2. In chapter 5, a diurnal cycle is included and its total amount at the top of the atmosphere is 1367 W/m^2

2.3.1 SST

Hot-Spot

Chapter 3 investigates the impact of a hot-spot on the aggregation. The hot-spot is a circular area with a higher temperature than the surrounding ocean, located at the center of the domain. The temperature of hot-spot and the ocean surrounding it are both constant.

Slab Ocean

In chapters 4 and 5, a slab ocean is implemented to couple ocean with the atmosphere. Using a realistic incoming solar radiation when performing numerical simulations of the tropics results in an increase in SST and likely a greenhouse gas run-away (section 4.6 Pierrehumbert (2010)). This is due the fact that, in nature over the tropical region, the surplus of energy is exported poleward by large scale circulation or by deep ocean. In numerical simulations we have to artificially remove the surplus of energy in order to take into account the poleward export of energy. To do so, we follow Semie and Tompkins (2016)

and relax the domain-averaged ocean mixed layer temperature $\overline{SST}$ toward a fixed target temperature SST_0. This relaxation method allows us to keep the domain-averaged SST constant over time (domain mean SST affects the aggregation mechanism and progress) while it allows the SST to vary locally according to the evolution equation:

$$\rho_w c_{p,w} H \left(\frac{dSST}{dt} + \frac{\overline{SST} - SST_0}{\tau_0} \right) = Q^N_{SW} + Q^N_{LW} + LHF + SHF \quad (2.18)$$

where ρ_w denotes water density, $c_{p,w}$ is the specific heat capacity of water at constant pressure, H the depth of the slab, τ_0 the relaxation time scale, which is constant and equal to two hours in all of our simulations (this value was empirically determined to avoid significant drift in the domain mean SST). All the terms on the right hand side of 2.18 are positive downward (increase SST) and negative upward (decrease SST). LHF and SHF denote surface latent and sensible heat fluxes (up to a minus sign), and Q^N_{SW} and Q^N_{LW} stand respectively for shortwave and longwave net radiative flux at the surface

2.4 Diagnostics

2.4.1 Dry patch and Aggregation Index

The aggregation starts with the appearance and expansion of dry patches. A dry patch is a region that becomes cloud-free and progressively dry with the progress of aggregation. As with aggregation, the domain separates into moist and cloudy and dry and clear-sky regions, one can follow the progress of aggregation by quantifying moisture variation in the domain.

To identify the dry patches and define an index for aggregation progress, we use vertically integrated relative humidity (Bretherton et al., 2005). Verti-

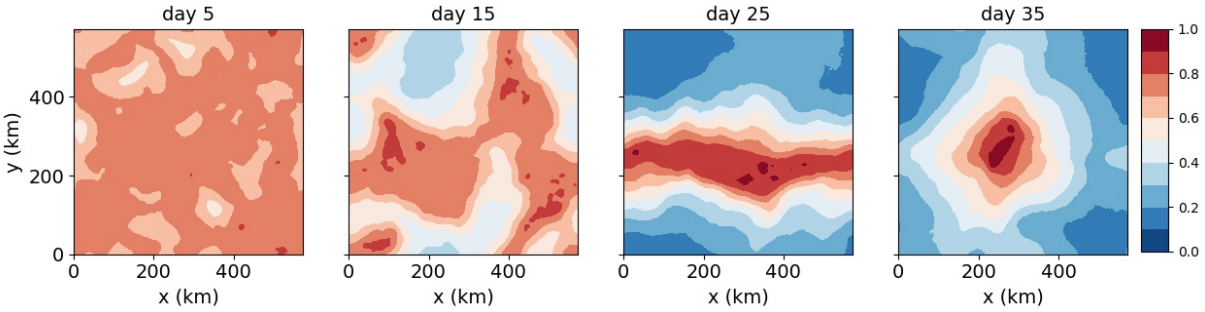

Figure 2.1: Time evolution of column relative humidity in a simulation with fixed SST=305 K, where convection aggregates.

cally integrated relative humidity or column relative humidity (CRH) is defined as:

$$CRH = \frac{\int q_v \rho dz}{\int q_{v,sat} \rho dz}, \tag{2.19}$$

where q_v denotes the water vapor mixing ratio, $q_{v,sat}$ denotes the saturation water vapor mixing ratio, ρ density and the vertical integration done over the troposphere. Figure 2.1 shows the time evolution of CRH in an aggregating simulation with constant SST that started from a homogeneous initial condition.

In chapter 3 the dry patch is defined as the area where CRH is below the 25^{th} percentile and an aggregation index as the difference between the 75^{th} and 25^{th} percentiles of column relative humidity, ΔCRH_{75-25}. Figure 2.2 shows the time series of aggregation index, CRH averaged over 25 lowest ($\overline{CRH}_{25}$) and 25 highest percentile ($\overline{CRH}_{75}$).

$\overline{CRH_{25}}$ decreases, reaches a minimum and then slightly increases again while $\overline{CRH_{75}}$ is constant at the beginning and starts reducing toward a new constant. $\overline{CRH_{75}}$ reduces as the moist region with high CRH (> 0.7) shrinks to an area smaller than 25 percent. Thus averaging CRH over 25 percentile includes some points with low values of CRH resulting in a reduction. The aggregation index has an increase due to the decrease of $\overline{CRH_{25}}$, while it

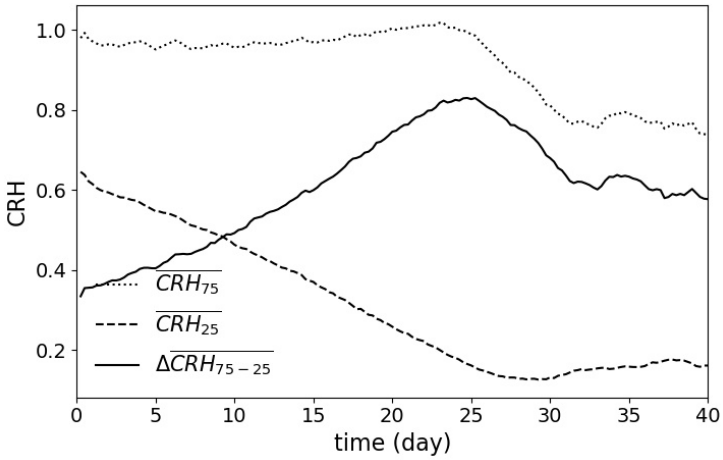

Figure 2.2: Time progress of aggregation index, $\overline{CRH}_{25}$ and $\overline{CRH}_{75}$ for the same simulation as in Figure 2.1

decreases after reaching a maximum, because of the reduction of $\overline{CRH_{75}}$.

$\overline{CRH_{25}}$ shows a modest increase when the aggregation is well established. This increase is due to the enhancement of latent heat flux in dry regions, the negative surface flux feedback mentioned in the introduction: the latent heat flux increases as the first layer of the atmosphere becomes very dry leading to increased air-sea moisture disequilibrium thus increased evaporation and supplying moisture into the first quartile.

Although using a percentile-based index for aggregation is a simple but useful way to follow moisture variation with aggregation, a dry patch defined by percentile does not correspond to all non-convective regions. This becomes important when the first appearance and evolution of non-convective regions are of interest. Therefore in chapters 4 and 5, where we investigate the dry patch appearance and expansion, a dry patch is defined as a region where CRH < 0.6. In our simulations, 0.6 is a threshold under which convective activities have not been observed. Following the new definition of dry patches, the aggregation index is also modified to the fraction area of dry patches.

2.4.2 Moist Static Energy

Moist static energy is the combination of dry air enthalpy, the latent heat of condensation, and gravitational potential energy :

$$MSE = c_p T + L_v q_v + gz, \tag{2.20}$$

with the specific heat capacity of air at constant pressure c_p, temperature T, gravity g, height z, latent heat of evaporation L_v, water vapor mixing ratio q_v. One impact of aggregation is an increase in the spacial variance of vertically integrated moist static energy. In a typical simulation of aggregation, the variance of MSE is mostly due to the variance of moisture.

2.4.3 Stream Function and Circulation

The aggregation is associated with circulations that transport moisture up-gradient. In this work, to diagnose the circulations, we use the stream function introduced firstly by Bretherton et al. (2005). The stream function, defined as the net mass transport between dry to moist region, is computed in sorted CRH and height space:

$$\Psi_i(z) = \Psi_{i-1}(z) + \sum_{CRH \in [CRH_{i-1}, CRH_i]} \overline{\rho(z)} w(z) \tag{2.21}$$

where Ψ is the stream function, i is the index of CRH bin (sorted), w is the vertical velocity summed in the CRH bin i, $\overline{\rho}$ is the domain-mean density profile, and $\Psi_0 = 0$ for all z.

Figure 2.3 shows an example of stream function in an aggregation simulation. The stream function has two maxima: one at the low level (below

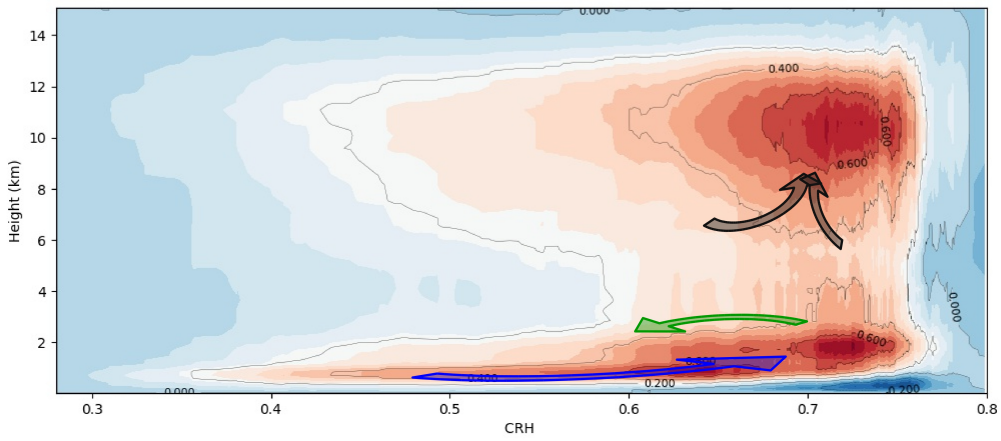

Figure 2.3: Stream function (color and contours) in Height - sorted CRH space. The arrows show shallow flux (blue), shallow circulation (green), and deep circulation (black)

3 km) corresponds to the boundary layer convergence of moisture, and the second one at a higher level corresponds to higher up mass convergence into the convective clouds. We refer to the blue arrow as shallow flux, part of the shallow flux that stays below 3 km (green arrow) as shallow circulation, and black arrow as deep circulation. The shallow flux transports low-level air with high moisture and MSE into the high CRH bins. The green arrow transports moist air (moist compared to dry bins) with low MSE (low compared to shallow flux) out of high CRH bins. The deep circulation transports air with high MSE but low moisture out of high CRH bins. Thus the shallow circulation favors up-gradient transport of MSE while deep circulation opposes it.

Symbol	Description
u_i	Resolved wind components
ρ	air density
p	pressure
q_v	water vapor
q_c	cloud water
q_i	cloud ice
q_n	cloud condensate
q_T	total non-precipitation water ($q_v + q_c + q_i$)
q_r	rain
q_s	snow
q_g	graupel
q_p	total precipitating water ($q_r + q_s + q_g$)
f	Coriolis force
U_g	prescribed geostrophic wind
g	gravitational acceleration
c_p	specific heat at constant pressure
L_c	latent heat of evaporation
L_s	latent heat of sublimation
τ	subgrid-scale stress tensor
F_{var}	subgrid-scale scalar fluxes
P_r	rain precipitation flux
P_s	snow precipitation flux
P_g	graupel precipitation flux

Table 2.1: List of symbols

Chapter 3

How do ocean warm anomalies favor the aggregation of deep convective clouds

We investigate the role of a warm sea-surface temperature (SST) anomaly (hot-spot of typically 3 K to 5 K) on the aggregation of convection using cloud resolving simulations in a non-rotating framework. It is well known that SST gradients can spatially organize convection. Even with uniform SST, the spontaneous self-aggregation of convection is possible above a critical SST (here 295 K), arising mainly from radiative feedbacks. We investigate how a circular hot-spot helps organize convection, and how self-aggregation feedbacks modulate this organization. The hot-spot significantly accelerates aggregation, particularly for warmer/larger hot-spots, and extends the range of SSTs for which aggregation occurs, however at cold SSTs (290 K) the aggregated cluster disaggregates if we remove the hot-spot. A large convective instability over the hot-spot leads to stronger convection and generates a large-scale circulation which forces the subsidence drying outside the hot-spot. Indeed, convection over the hot-spot brings the atmosphere towards a warmer temperature. The warmer

temperatures are imprinted over the whole domain by gravity waves and subsidence warming. The initial transient warming and concomitant subsidence drying suppress convection outside the hot-spot, thus driving the aggregation. The hot-spot induced large-scale circulation can enforce the aggregation even without radiative feedbacks for hot-spots sufficiently large/warm. The strength of the large-scale circulation, which defines the speed of aggregation, is a function of the hot-spot fractional area. At equilibrium, once the aggregation is well established, the moist convective region with upward mid-tropospheric motion, centered over the hot-spot, has an area surprisingly independent of the hot-spot size.

3.1 Introduction

In the tropics, convection can be organized by synoptic dynamical systems such as equatorial waves or tropical depressions, but it may also have its own organization sources such as in squall lines, or more generally in mesoscale convective systems. Organized convection is associated with extreme weather conditions (Houze, 2004), and can strongly impact the hydrological cycle and the top-of-atmosphere radiation budget (Tan et al., 2015; Tobin et al., 2012). For large-scale processes such as the Madden Julian Oscillation, the aggregation of the convection may generate non-linear effects modifying the average circulation at basin scale (Bellenger et al., 2009). However, the physical processes responsible for the mesoscale organization of convection are still not clearly identified and are typically not specifically accounted for in global climate models (GCMs) (Mapes and Neale, 2011).

The spontaneous clustering of convective clouds in simulations in idealized settings, typically non-rotating Radiative-Convective Equilibrium (RCE),

provides a manageable framework to gain fundamental understanding of the physical processes at stake. Non-rotating RCE is an idealization of the tropical atmosphere where the Earth's rotation is neglected, a reasonable approximation in the deep tropics where the Coriolis parameter is small, and where the large-scale circulation (larger than the model domain) is neglected. In other words, in RCE, there is no advection of energy into or out of the domain. Thus in the domain mean, surface latent and sensible heat fluxes are in balance with the net radiative cooling of the atmosphere (top-of-atmosphere minus surface).

In the tropics, such equilibrium is only reached at large, thousands of kilometers scales (Muller and O'Gorman, 2011). The idealized framework of RCE has proven to be useful to study and improve our understanding of numerous aspects of tropical convection, including precipitation extremes (Muller et al., 2011; Muller, 2013), entrainment (Romps, 2010), cold pools (Tompkins, 2001a), atmospheric thermodynamics (Pauluis and Held, 2002) or rain evaporation (Muller and Bony, 2015). Notably, it has led to the discovery of the remarkable ability of deep convection to spontaneously cluster in space despite homogeneous forcing in cloud-resolving models (CRMs). These are models with sufficient kilometr-scale horizontal resolutions to resolve the main features of deep convection, instead of parameterizing them.

Typical RCE simulations with homogeneous forcing (doubly-periodic geometry, square domain, constant sea-surface temperature (SST) in space and time) reach a statistically steady state in which convection and clouds are somewhat randomly distributed. But under certain conditions, including large domains, deep clouds aggregate into a region of the domain, surrounded by a dry environment devoid of deep convection. This phenomenon, known as self-aggregation in the literature (see, e.g., Wing et al. (2017) for a review), leads to an equilibrium state with dry and warm mean thermodynamic pro-

files, and enhanced outgoing longwave radiation (OLR) to space (Bretherton et al., 2005; Tobin et al., 2012). Since its discovery in idealized CRM simulations, the self-aggregation of deep convection has been confirmed to occur in more realistic settings (Holloway, 2017) and even in GCMs with parameterized convection (Coppin and Bony, 2015).

Radiative feedbacks are believed to be key for self-aggregation, at least at temperatures observed in the tropical atmosphere (Wing et al., 2017). It is the circulation generated by the differential longwave radiative cooling rates between dry (strong cooling) and moist (little cooling or even warming) regions which is believed to trigger and maintain the convective aggregation (Bretherton et al., 2005; Muller and Held, 2012). Strong cooling in dry regions yields subsidence down to low levels, and a near-surface flow from dry to moist regions. Such a process was already proposed by Gray and Jacobson (1977) to explain the observed reinforcement of large convective systems at the end of the night. This circulation transports near-surface high moist static energy (MSE) from dry to moist regions. This MSE upgradient transport maintains high MSE in the moist region, helping to maintain deep convection there. In fact, in the CRM used in this study (System for Atmospheric Modeling, or SAM (Khairoutdinov and Randall, 2003)), there is no self-aggregation without interactive radiation (unless the evaporation of rain is artificially suppressed (Muller and Bony, 2015), a particular case which will not be discussed here). Because of the idealized settings in which self-aggregation was discovered, its relevance to the real world is still debated. Notably, the aforementioned CRM studies used spatially and temporally constant and uniform sea-surface temperatures (SSTs).

The impact of SST anomalies on deep convection has already been widely studied in the literature (Tompkins, 2001b; Kuang, 2012; Ramsay and Sobel,

2011; Sobel and Bretherton, 2000). Tompkins (2001b) found in particular that a sudden inverting of an imposed SST anomaly leads to the migration of the convective clusters over the warm anomaly. The migration of aggregated convective clusters over warm anomalies has been confirmed by other studies which used a slab ocean in order to have interactive SSTs (Coppin and Bony, 2015; Grabowski, 2006). Using a single column model (SCM) and CRM, Ramsay and Sobel (2011) and Wang and Sobel (2011) showed that precipitation rate increases over local warm SSTs and is determined by the temperature anomaly rather than by the mean SST. Daleu et al. (2017) confirmed this result using two adjacent SCMs with different SSTs. The SST difference, if large enough, can suppress convection in the cold column and strengthen it in the warm column. Notably, SST gradients can generate a large-scale circulation that can lead to a migration of deep convection towards the warmest SST.

Another type of surface temperature anomalies are tropical islands with different surface properties, which act as a surface forcing and change the intensity of convection (Crook, 2001; Beringer and Tapper, 2002) and thermal structure of the atmosphere (Cronin et al., 2015). Rainfall over tropical islands is larger than over the surrounding ocean (Cronin et al., 2015; Sobel et al., 2011; Qian, 2008; Wang and Sobel, 2017), however the strength of the thunderstorms and precipitation depends on several factors such as the size of the islands, wind speed and direction and the island's topography (Wang and Sobel, 2017; Crook, 2001). Convective events over tropical islands show large diurnal variations, however they build up an average ascent (Cronin et al., 2015) .

Ocean mesoscale eddies (Chelton, 2011) can also be associated with SST anomalies reaching a few degrees in cold core cyclonic eddies or warm core anticyclonic eddies. These persistent ocean eddies have a typical radius varying with latitude, from a hundred to a few hundreds of kilometers in the tropics ($\pm$

20° latitude), to around 50 km or less in mid-latitudes. As a surface forcing, eddies can impact the atmosphere locally (Sugimoto et al., 2017) by enhancing low level convergence and thus convective precipitation. Potentially, the eddies change the cloudiness and wind field which can impact the large scale circulation .

Whether and how such persistent SST anomalies, as an external forcing, can favor or suppress the aggregation of convection is, to our knowledge, still not well covered in the literature. In this paper, we investigate the aggregation response to an idealized, circular SST anomaly referred to as a "hot-spot'. We must emphasize that the aggregation forced by a hot-spot, when it is the case, is not anymore "self-aggregation" but rather a forced aggregation. Of particular interest are the following questions:

- How does the presence of an ocean hot-spot modify or enforce the aggregation process of the deep convection? And how does this modification depend on the hot-spot radius and temperature anomaly?
- How does the hot-spot impact the large-scale circulation?
- In the presence of a hot-spot, how does the aggregation physics differ from the self-aggregation ones; specifically, does aggregation disappear in the absence of radiative feedbacks (known to be crucial for self-aggregation over homogeneous SST)?

The next section, § 3.2, describes the cloud-resolving model used and the experimental setup, as well as the metrics used to measure (self-)aggregation. § 3.3 investigates the impact of the hot-spot on convective aggregation, and the sensitivity to hot-spot properties. § 3.4 investigates whether radiative feedbacks are still necessary for aggregation to occur when a hot-spot is present. Additionally, we derive a simple, two-box model to help comparison between

the onset of self-aggregation and aggregation. In § 3.5 we briefly discuss the equilibrium phase, once aggregation has occurred. Conclusions are given in § 3.6.

3.2 Model description and simulation design

3.2.1 Cloud-resolving model

The CRM used is the model System for Atmospheric Modeling (SAM) version 6.11.1 (Khairoutdinov and Randall, 2003). This model solves the anelastic equations of conservation of momentum, water (with 6 species present in the model, water vapor, cloud liquid, cloud ice, precipitating rain, precipitating snow, and precipitating graupel), and energy. The relevant energy for moist convection is the moist static energy, as it is conserved (approximately, i.e. neglecting viscous and subgrid-scale effects) under adiabatic processes including the phase change of water. More precisely in this model, the so-called "frozen" MSE is conserved during moist adiabatic processes, including the freezing of precipitation. The frozen MSE is given by

$$MSE = c_p T + gz + L_v q_v - L_f q_{ice}, \tag{3.1}$$

with the specific heat capacity of air at constant pressure c_p, temperature T, gravity g, height z, latent heat of evaporation L_v, water vapor mixing ratio q_v, latent heat of fusion L_f, and mixing ratio of all ice phase condensates q_{ice}.

The subgrid-scale turbulence is modeled using a Smagorinsky-type parameterization, and we use the 1-moment microphysics formulation, following Bretherton et al. (2005) and Muller and Held (2012). Bulk formulae are used to compute surface fluxes. Further information about the model can be found

in Khairoutdinov and Randall (2003).

Most simulations use interactive radiation, using the radiation code from the National Center for Atmospheric Research (NCAR) Community Atmosphere Model version 3 (CAM3; (Collins et al., 2006)). For simplicity, we neglect the diurnal cycle and use the daily mean incoming solar insolation of 413 W m^{-2} (same setting as Tompkins and Craig (1998)). Studies of self-aggregation over the ocean with a diurnal cycle show that, quantitatively, a diurnal cycle can change the strength of the hydrological cycle, increasing the daily precipitation range. But qualitatively, beyond this daily modulation of amplitude, it does not seem to affect the fact that deep convection self-aggregates or not.

In some simulations, radiative feedbacks are turned off by homogenizing radiative cooling rates horizontally, at each height and time step, following Muller and Held (2012). Note that in that case, the domain average radiative cooling rates can still evolve in time.

3.2.2 Experimental setup

The model domain is square, doubly-periodic in both horizontal directions x and y. We run simulations with two domain sizes, (288 km)^2 and (576 km)^2 (except for one simulation shown in Figure 3.1 with a smaller (96 km)^2 domain). The horizontal resolution is 3 km and the vertical grid spacing increases gradually with height, with the first level at 25 m and a resolution of 50 m close to the sea surface, reaching a vertical resolution of 500 m in the mid troposphere. There are 64 vertical levels which span 27 km in the vertical. This includes a sponge layer in the upper third of the domain (from $z = 18$ km to 27 km) where the wind is relaxed to zero in order to reduce gravity

wave reflection and buildup. No large-scale forcing or wind is imposed. We neglect the Earth's rotation, a reasonable approximation in the tropics where the Coriolis parameter is small.

The initial conditions for the different mean SSTs (horizontal mean SSTs in our simulations with and without hotspot) are obtained from a smaller domain run with the corresponding SST at RCE ($(96\text{ km})^2$ run to 50 days), then using time and domain averaged profiles of the last 5 days. We run two different types of simulations: simulations with a uniform and constant sea surface temperature that we refer to as ocean experiments, and simulations with a warm temperature anomaly referred to as hot-spot experiments. The hot-spot is a circular area with a higher temperature than the surrounding ocean, located at the center of the domain. A given hot-spot simulation will be defined by its temperature anomaly dT and its radius R so that, for example, simulation dT5R60 is for a hot-spot with a temperature anomaly of 5 Kelvin and a radius of 60 km. The upper two panels of Figure 3.1 show snapshots of near-surface air temperature and cloud water for two simulations with a different domain size and hot-spot radius. This illustration shows that, although there is some organization of convection on the small domain in the presence of a hot-spot, the self-aggregation of convection surrounded by extremely dry air only occurs in the large-domain simulation. This is well captured by the metrics used to quantify the degree of aggregation described next and shown in Figure 3.1c. In the following, in both ocean and hot-spot experiments, we also investigate the role of radiative feedbacks by repeating some simulations with homogenized radiation.

3.2.3 Aggregation metrics

The convective aggregation is associated with progressive drying of the dry environment surrounding deep clouds, and progressive moistening of the moist region where deep convection occurs. This leads to increased horizontal moisture variability. Thus a common index for self-aggregation is the difference between the 75^{th} and 25^{th} percentiles of precipitable water, ΔPW_{75-25} (Muller and Held, 2012; Muller and Bony, 2015). Since here we will compare simulations with different SSTs, we will use precipitable water normalized by the saturation water vapor path, i.e. we will use column relative humidity CRH (Wing and Cronin, 2016),

$$CRH = \frac{\int q_v \rho dz}{\int q_{v,sat} \rho dz}, \tag{3.2}$$

where $q_{v,sat}$ denotes the saturation water vapor mixing ratio, ρ density and the vertical integration done over the troposphere. Our aggregation index is the difference between the 75^{th} and 25^{th} percentiles of column relative humidity, ΔCRH_{75-25}. Figure 3.1 illustrates the increase of this index (bottom panel) in the simulation that aggregates (middle panel).

In SAM, self-aggregation has been shown to start with the strengthening and the expansion of a dry patch, becoming drier and larger. This dry region, devoid of deep convection, was sometimes referred to as the "radiative dry pool" (Coppin and Bony, 2015; Zuidema et al., 2017), as it is believed to be radiatively driven. The dry patches are thus of primary importance, as the self-aggregation of convection can eventually result from the confinement of the deep convection in a restricted region because of the expansion of a dry patch in our doubly-periodic geometry. In the following, the dry patch is defined as the area where the CRH is below the 25^{th} percentile.

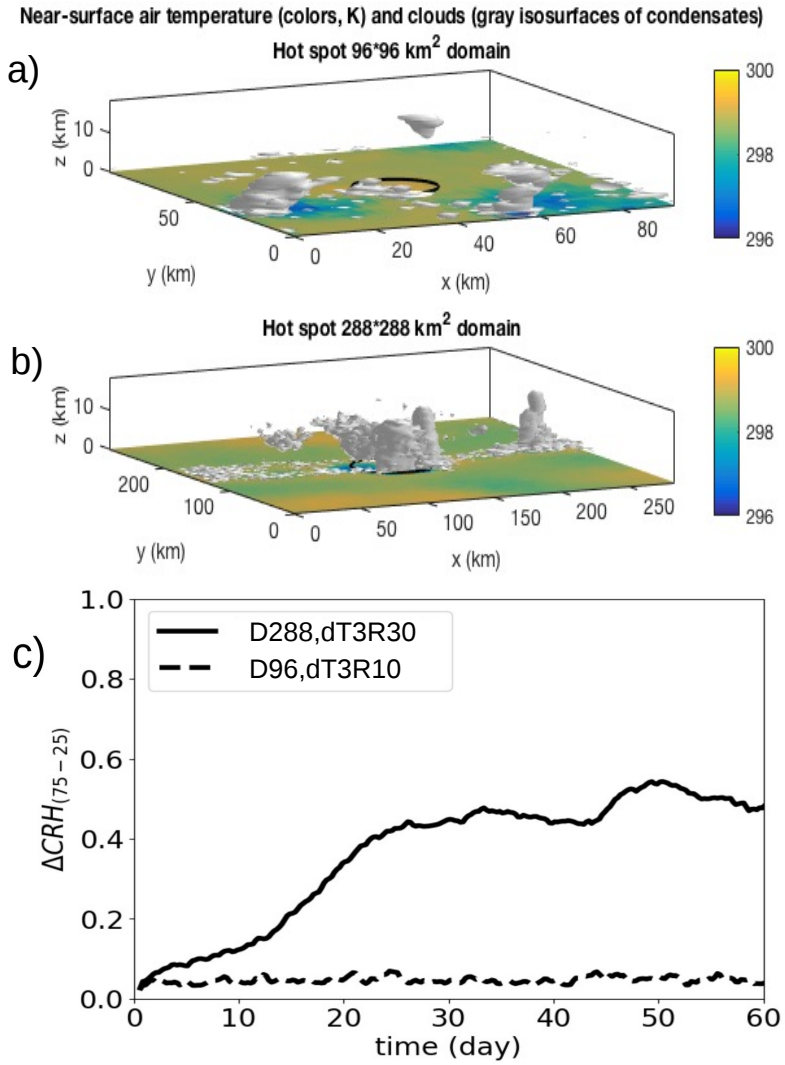

Figure 3.1: Snapshots of near-surface air temperature (colors, K) and cloud water (grey shades) from two simulations with a hot-spot in the center of the domain (circle) for (a) a domain size 96*96km^2 and (b) 288*288 km^2. (c) Time evolution of the aggregation index for those two simulations.

3.3 Hot-spot impact on aggregation of deep convection

Here, we first investigate how the presence of a hot-spot impacts the aggregation of convection in the presence of radiative feedbacks. Of particular interest is whether the aggregation is faster, and whether the deep convection area ends up being localized over the hot-spot.

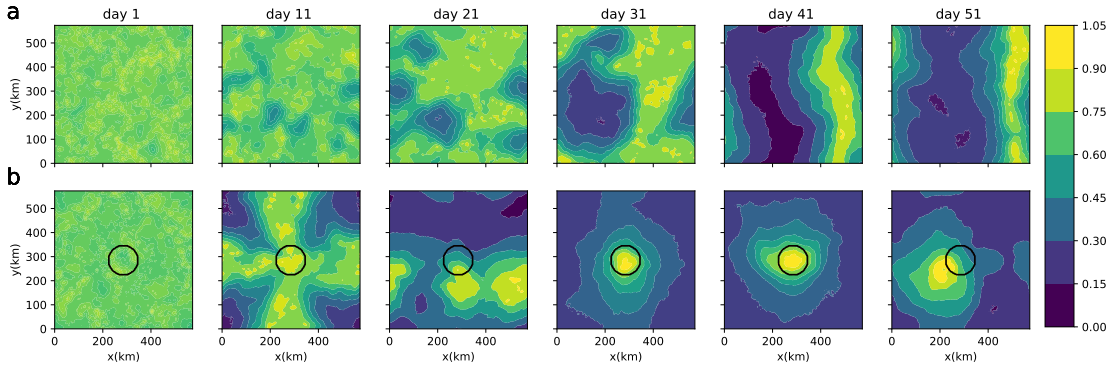

Figure 3.2: Snapshots of CRH for simulations with (a) a uniform surface temperature and (b) a hot-spot with a SST anomaly of 5 K and a radius of 60 km. The black circle shows the hot-spot boundary. For both simulations the domain average SST is 300K and the domain size is 576*576 km^2

3.3.1 Results without and with hot-spot at different SSTs

The upper row of Figure 3.2 shows the CRH maps in a control ocean experiment with a mean SST of 300 K at different times started from homogeneous conditions. We observe the typical evolution of self-aggregation: the appearance of a dry patches after a few days (day 11) and thus the extension and merge of these dry patches into a single patch (day 31). At day 41, the CRH in the dry region reaches extremely low values, and convection and moisture are confined to a small part of the domain. After day 41, the moist patch shrinks to a narrow region surrounded by a very dry environment. The increased spatial moisture variability between dry and moist regions, largely due to enhanced drying, is also visible in ΔCRH_{75-25} (Figure 3.3a). It increases up to day 40 and then starts to decrease slowly. With further progress of aggregation, the high CRH region shrinks to a circular area smaller than 25 percent of the domain, thus CRH_{75} decreases, leading to the decrease of the aggregation index.

Self-aggregation over fixed SSTs is known to depend on the domain mean

SST. Using the same SAM model, Wing and Emanuel (2014) find that warm SSTs favor aggregation, while Coppin and Bony (2015) find in a GCM that self-aggregation is surprisingly favored both for SSTs larger than 295K or smaller than 285K. In very cold snowball simulations, aggregation can also occur (Abbot, 2014), though in that case a weak wind shear can prevent the aggregation. The exact relation between an average SST and the self-aggregation response is hence still unclear, but the general consensus is that self-aggregation is favored at warm SSTs (Emanuel et al., 2014). Consistently, we find that for a colder SST of 290 K aggregation does not occur, and that the aggregation speed increases regularly with the SST for SST values between 295 K and 305 K (Figure 3.3a).

Simulations with the same mean SST, but with different hot-spot characteristics are performed to analyze the role of the SST anomaly on the convective aggregation. Here the domain-mean SST is kept constant at 300 K in order to isolate the effect of the hot-spot temperature anomaly. Consequently, the surrounding ocean temperature is slightly lower than 300 K in the hot-spot simulations. However, it has been argued in previous studies (Ramsay and Sobel (2011); Wang and Sobel (2011)) that the control parameter is the SST anomaly (dT) and not the absolute SST, at least for a reasonable temperature change. Figure 3.2b shows the hot-spot experiment dT5R60 (dT=5 K and R=60 km). Spatially, the main aspects of aggregation in the presence of a hot-spot are similar to the ocean experiment, with a progressive expansion of dry regions. The aggregation is however much faster with the hot-spot and the convection is eventually organized over or near the hot-spot. Note that the location of the aggregation is not stable, and whether the aggregated convective cluster stays over the hot-spot depends on hot-spot radius and temperature. If the hot-spot is sufficiently large and/or warm, it sustains the convective cluster over it, otherwise, it does not necessarily stay over the hot-spot after

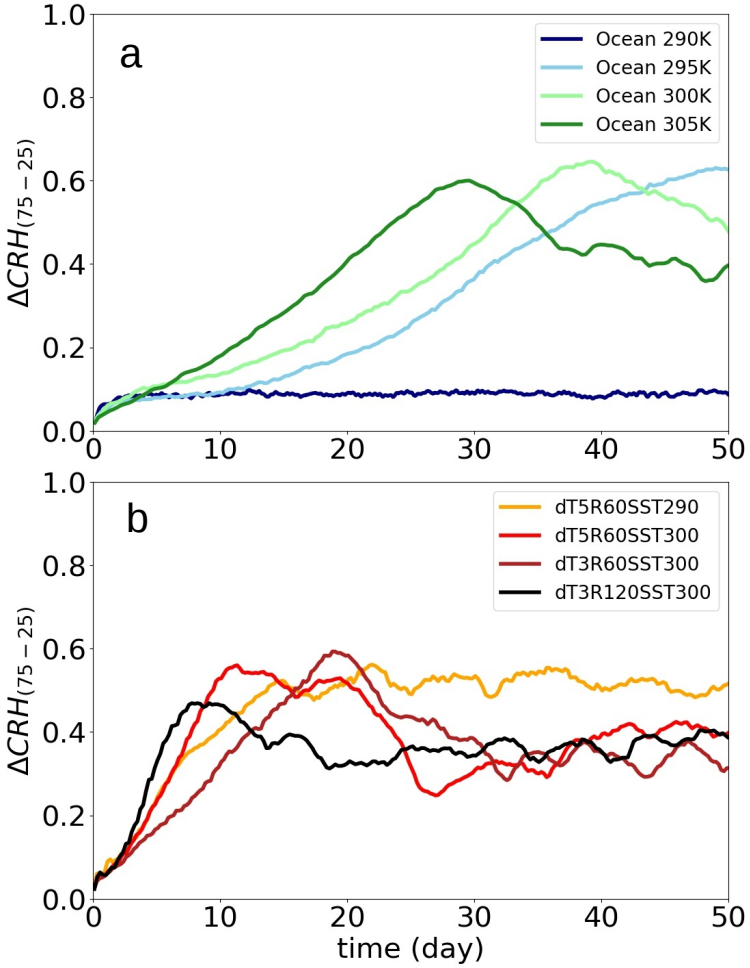

Figure 3.3: Time evolution of the aggregation index for simulations with full radiative feedback for: (a) simulations with a uniform surface temperature (referred to as "Ocean" see §3.23.2.2 for a detailed description of the simulations); (b) simulations with a hot-spot of different sizes and SST anomalies.

its formation. We will discuss this in more detail in § 3.5.

Looking at the aggregation index (Figure 3.3b), the maximum aggregation is in fact reached after only 10 days in dT5R60 compared to 40 days in the ocean simulation at 300K. Thus, the presence of a hot-spot may accelerate the aggregation by a factor of 4. However, the aggregation is much faster with a hot-spot. When the aggregation is fully reached, the aggregation index is fairly comparable between the simulations with and without a hot-spot. The hot-spot temperature anomaly plays a significant role in accelerating or enforcing

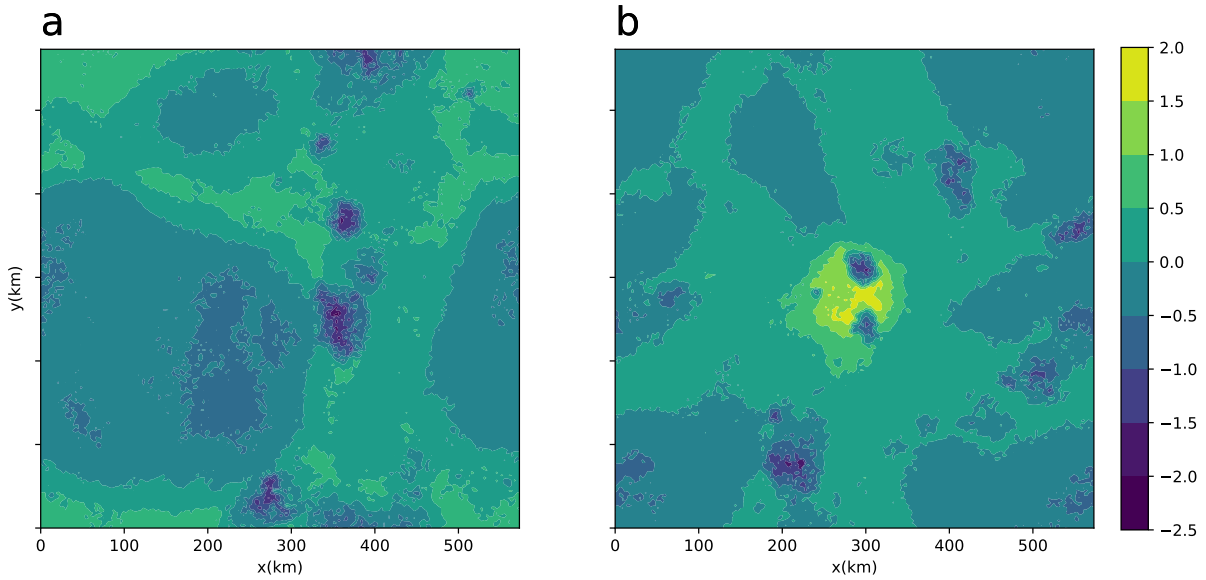

Figure 3.4: θv anomaly averaged over the boundary layer (from surface to 1000 m) for a) day 31 of ocean experiment at 300 K , b) day 11 of Hot-spot experiment dT5R60 and mean SST=300 K.

the aggregation, as can be seen in Figure 3.3b. For dT5R60 the aggregation index reaches a maximum after only 10 days while for dT3R60 the maximum is reached in 20 days. Thus, the aggregation speed is favored by larger hot-spot temperature anomaly. The hot-spot size also plays a role with a maximum aggregation index reached in less that 10 days for dT3R120. Therefore, the larger the hot-spot, the faster the aggregation. Note though that for very large hot-spots relative to the domain size (see below), this can not hold anymore. A hot-spot can also extend the range of SSTs for which an aggregation occurs. For example, with an average SST of 290 K, there is no self-aggregation for uniform SST (3.3a), but the dT5R60 experiment at 290 K aggregates even faster than uniform ocean simulations at 305 K. (3.3b).

3.3.2 Development of a large-scale circulation

Here, we hypothesize that the presence of the hot-spot favors and accelerates the formation of a large-scale circulation that triggers the onset of convective

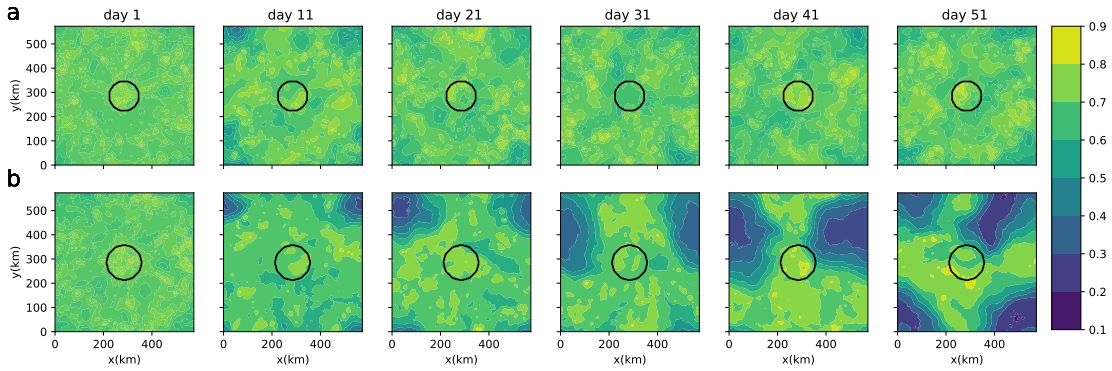

Figure 3.5: Snapshots of CRH for hot-spot simulations with homogenized radiation for: (a) SST anomaly of 5 K and a radius of 60 km and (b) SST anomaly of 5 K and a radius of 70 km. The black circle shows the hot-spot boundary. For both simulations, the domain average SST is 300 K and the domain size is 576*576 km^2.

aggregation, and thus extends the range of SSTs at which aggregation occurs.

To explain the acceleration of aggregation with a hot-spot, we look at virtual potential temperature (θ_v) anomaly. In the free troposphere, gravity waves remove horizontal θ_v anomalies very efficiently (Bretherton and Smolarkiewicz, 1989; Ruppert and Hohenegger, 2018) so that θ_v profile above the boundary layer is fairly uniform over the domain especially when it is averaged over a few hours. So the main source of instability is the buoyancy anomaly in the boundary layer. Figure 3.4 shows θ_v anomaly averaged over the boundary layer for the ocean experiment at SST=300 K at day 31 and the hot-spot experiment dT5R60 with a mean SST equal to 300 K at day 11 (Figure 3.2 shows the CRH evolution for these two simulations). We compare these two days as the aggregation index and the fraction of area covered with low (high) CRH are comparable between the two simulations. In general there is a positive θ_v anomaly in moist areas (except directly below clouds where cold pools result from the partial evaporation of rain), that enforces convergence of low-level air toward the moist area. Consistent with the faster aggregation, the θ_v anomaly is larger over the hot-spot. θ_v depends on both temperature and water va-

por. In both the ocean and hot-spot simulations, the moisture contribution to the θ_v anomaly in moist regions is positive. But the temperature contribution is smaller in the ocean experiment. In the hot-spot simulations, over the hot-spot, both temperature and moisture have a positive contribution to θ_v resulting in a slightly larger θ_v anomaly and a stronger instability over the hot-spot that leads to stronger convection.

The corresponding pressure gradient at the first few levels enforces a convergence of moisture toward the moist region. With a hot-spot, the pressure gradient is larger and it stays over the hot-spot. This convergence favors convection over the hot-spot by transporting low level moist air and by providing energy to lift the air above the hot-spot. Additionally, the convergence of moisture removes moisture from the environment and inhibits convection there. This process (low-level transport of moisture toward the moist region) thus seems common to both self-aggregation and aggregation but is stronger in the latter case. There is a difference though: in aggregation with a hot-spot, it is the strength of the upward mass flux over the hot-spot which seems to control the large-scale circulation and thus the aggregation speed. Ascent over the hot-spot forces compensating subsidence in the environment, which dries the troposphere and results in further suppression of convection there and enhancement of moisture transport toward the hot-spot. This upward motion over the hot-spot and thus subsidence in the environment, is partly a consequence of our periodic boundary conditions, and it builds up a large scale circulation that accelerates the aggregation. Instead, with self-aggregation, it has been hypothesized (Tompkins and Craig, 1998) that it is the subsidence in dry regions which initiates and controls the large-scale circulation, and thus the self-aggregation speed. This development of a large-scale circulation will be further investigated in the next section.

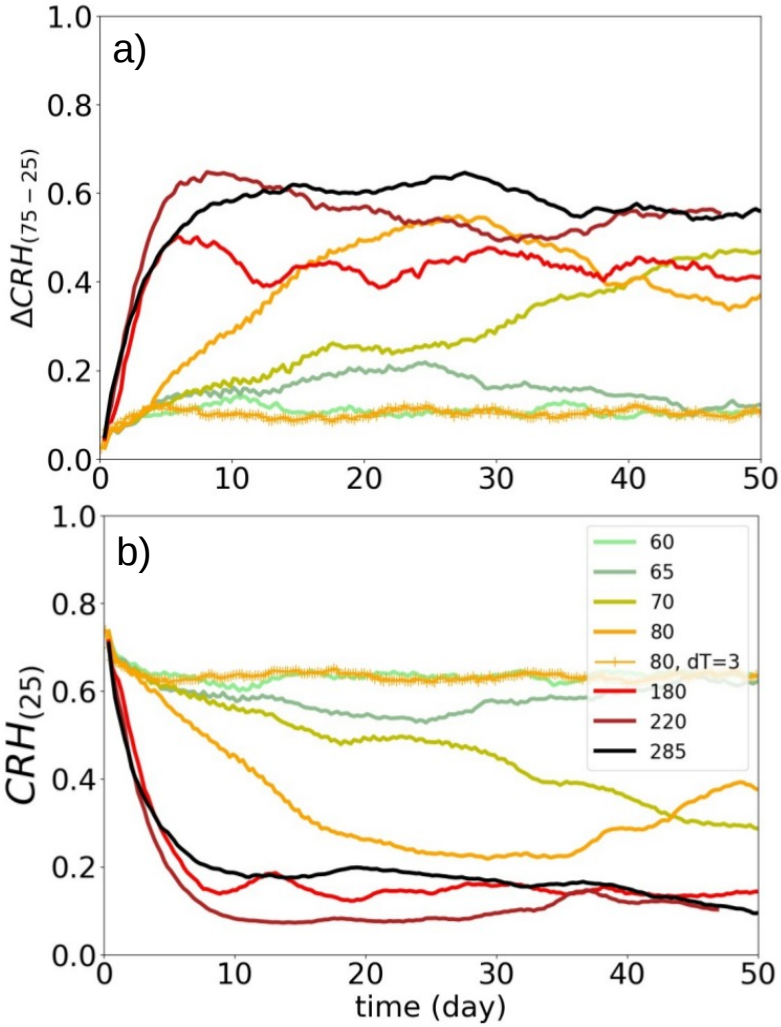

Figure 3.6: Time evolution of (a) the aggregation index and (b) CRH averaged over driest quartile for different hot-spot radius for simulations with homogenized radiation. All the simulations have a domain size of 576*576 km^2 and a hot-spot SST anomaly of 5 K except for one simulation with a radius of 80 km and a SST anomaly of 3 K.

A natural question then, is whether the large-scale circulation enforced by the hot-spot can be maintained even in the absence of a hot-spot, solely by internal self-aggregation feedbacks. The sensitivity of self-aggregation to initial conditions is well documented. Aggregated states that are imposed as initial conditions can persist, even under conditions which do not favor the spontaneous self-aggregation from homogeneous initial conditions (Khairoutdinov and Emanuel, 2010; Muller and Held, 2012). To investigate whether the hot-spot aggregation exhibits hysteresis, we repeat the dT5R60 with SST=290 K simulation, which does not self-aggregate without a hot-spot, for 30 days, and then remove the hot-spot (by simply setting dT to zero) and run for another 30 days. The aggregated cluster spreads over the domain and disaggregates. Therefore the aggregation is not maintained without the hot-spot in this case.

3.4 Convective aggregation without radiative feedbacks

3.4.1 Hot-spots with or without radiative feedbacks

Radiative feedbacks have been shown by many studies to be necessary for convective self-aggregation, at least for typical tropical SSTs around 300 K (Wing et al., 2017). The balance between radiative cooling and subsidence warming in dry regions (Mapes, 2001) creates a positive feedback that results in radiatively enhanced subsidence and drying of already dry regions. Sensitivity studies show that removing radiative feedbacks, by homogenizing radiative cooling rates, prevents the self-aggregation. Here we test the occurrence of aggregation without radiative feedbacks in hot-spot experiments, listed in Table 3.1.

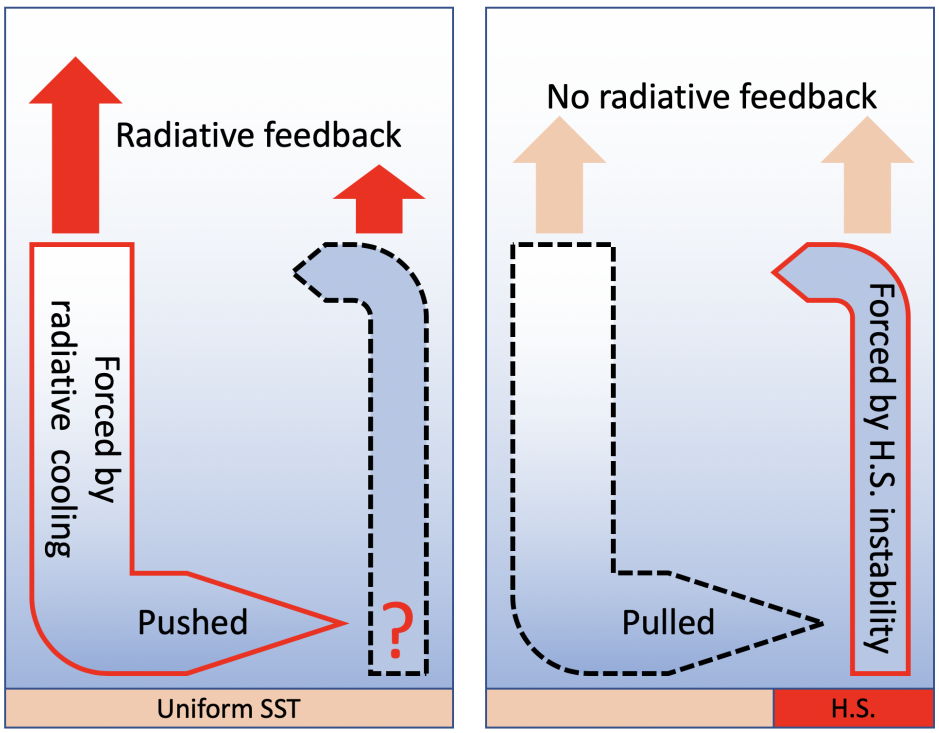

Figure 3.7: Schematic two-box model representing either a self-aggregation by radiative feedbacks or an aggregation forced by a hot-spot induced circulation. (a) Self-aggregation by radiative feedbacks is caused by a progressive expansion of a dry subsidence region under the effect of a strong radiative cooling, "pushing" the low-level moisture toward a constricted moist and warm convective region. (b) The aggregation is due to the large-scale circulation induced by the hot-spot persistent SST anomaly, "pulling" the moisture toward the warm anomaly.

Comparing the dT5R60 simulation with (Figure 3.2b) or without (Figure 3.5a) radiative feedbacks, we see that homogenizing the radiation prevents aggregation for a hot-spot radius of 60 km. However, increasing the hot-spot radius to 70 km (Figure 3.5b) yields aggregation even without radiative feedback. For R=70 km, the aggregation is very slow, but it becomes much faster at larger radius (Figure 3.6). It is worth noting that simulations with R=70 and 80 km give a banded aggregation. For larger hot-spots, a circular aggregation of the convection develops in a few days, with a maximum aggregation index reached in less than 10 days with R=180 km. This is fast compared to typical overturning time scale of the atmosphere (Grabowski and Moncrieff, 2001), suggesting that the circulation between dry and moist regions is greatly accelerated by the presence of the SST anomaly. By reducing this anomaly to 3K instead of 5K, there is no convective aggregation, even for a radius of 80 km (Figure 3.6). A persistent SST anomaly can thus clearly trigger a convective aggregation in SAM, even without radiative feedbacks. This aggregation requires a minimum size and amplitude of the SST anomaly, and is faster for warm and large hot-spots. In order to clarify the physical processes responsible for convective aggregation in that case, we look in the next section at the large-scale circulation in more detail, in particular the subsidence in the dry regions.

Note that because we keep the mean SST constant, changing the hot-spot radius R and temperature anomaly dT, also changes the temperature outside the hot-spot and the absolute temperature of the hot-spot (both reduced to keep the domain mean SST constant). To verify that the leading order parameter determining the onset and speed of aggregation is the hot-spot temperature anomaly dT, not its absolute temperature, we redo some of the simulations keeping the temperature equal to 300 K outside the hot-spot, and simply adding a hot-spot with dT=5 K to the domain (so that the domain

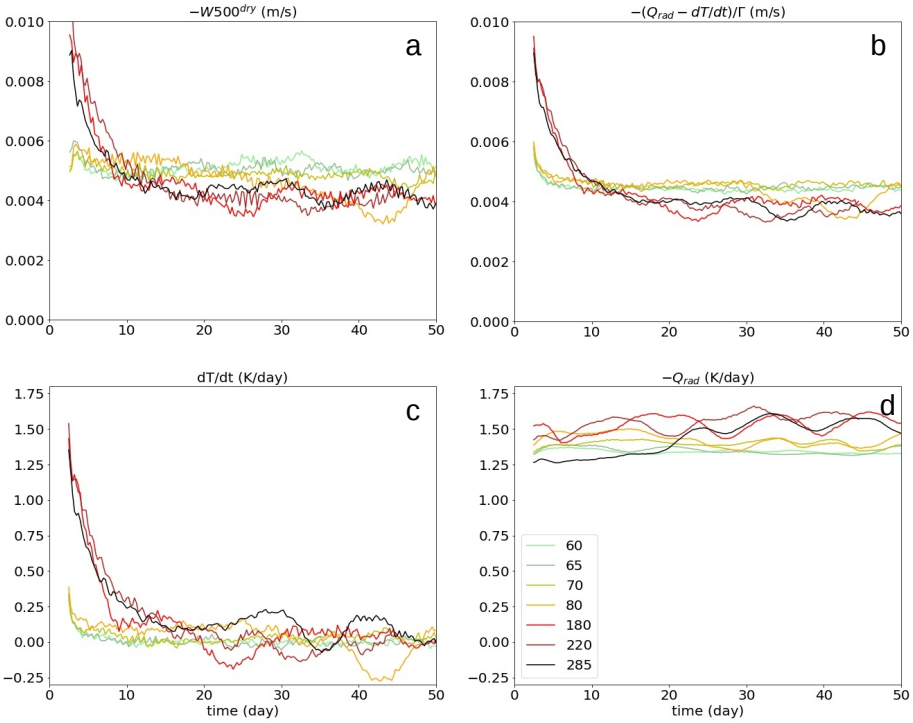

Figure 3.8: Time evolution of atmospheric parameters at 500 hPa averaged over the dry patch for different hot-spot sizes: (a) vertical velocity; (b) the right hand side of Equation 3.4; c) the time derivative of temperature and; (d) radiative cooling. The domain average SST is 300 K and the domain size is 576*576 km^2.

mean SST is now larger than 300 K). We find that the speed of aggregation, based on the aggregation index, is similar, and is determined to leading order by dT. This gives us confidence that the hot-spot temperature anomaly is indeed the main control parameter, not its absolute temperature.

Previous studies showed that the self-aggregation of convective clouds is sensitive to initial conditions so that just by changing initial noise which are small compared to the initial condition, the aggregation onset may delay or hasten. To check the robustness of our results regarding the timing of the onset and the speed of aggregation, we ran two small ensembles of 5 members for dT5R70 and dT5R80 with homogenized radiation, using different initial noises. The ensemble simulations show that the aggregation onset and speed do not

vary significantly among the members, in particular the R=80 km simulations are all faster than the R=70 km. This suggests that the aggregation speed is set mostly by the hot-spot forcing, and dependency on the initial conditions is small.

3.4.2 Two-box model: Pulled or pushed aggregation?

Here we further investigate the mechanisms involved in the aggregation of the convection in the absence of radiative feedbacks (Figure 3.6). Given the potential importance of expansion and strengthening of the dry patch for the onset of convective aggregation (consistent with the drying in Figure 3.6b), we will interpret the results in light of a conceptual, two-box model with a dry and a moist region, illustrated in Figure 3.7. In the moist region, there is upward motion in deep convection. In the dry region, there is subsidence and no deep convection (thus no latent heat release). Therefore, given the small horizontal gradients of temperature in the tropics (so-called weak temperature gradient approximation or WTG (Sobel et al., 2001)), to first order the temperature equation for a given pressure level (500 hPa in the following) yields:

$$\frac{\partial T}{\partial t} + \Gamma w^{dry} = Q_{rad} \tag{3.3}$$

$$\Rightarrow \quad w^{dry} = \frac{Q_{rad} - \partial T/\partial t}{\Gamma}, \tag{3.4}$$

where w^{dry} is the (negative) subsidence velocity (m/s), Q_{rad} the (negative) radiative cooling (K/s), and

$$\Gamma = \frac{T}{\theta}\frac{d\theta}{dz} \tag{3.5}$$

the static stability (θ denotes potential temperature in K). At equilibrium (i.e. $\partial T/\partial t = 0$), there is a balance between subsidence warming and radiative cooling in the dry environment. We nevertheless retain the temperature term

$\partial T/\partial t$ in anticipation of w^{dry} that it may be important during the onset of self-aggregation, before equilibrium is reached. Recall that in these simulations without radiative feedback, the radiative cooling rates are homogenized in space, but is allowed to evolve in time.

As stated in the introduction for self-aggregation with radiative feedbacks, the stronger radiative cooling in dry regions compared to the moist regions causes further subsidence drying and generates a circulation that "pushes" the moisture towards the deep convection area (Figure 3.7). Thus self-aggregation is rather a self-confinement of moisture, as dry regions expand and strengthen, pushing the convection in a small part of the domain in our doubly-periodic geometry. In the hot-spot aggregation however, the hot-spot increases the convective instability and leads to deep convection localized over the hot-spot. Warmer and moister low level conditions over the hot spot increases the convective instability compare to the environment if we assume that the free troposphere temperature is horizontally homogeneous (Bretherton and Smolarkiewicz, 1989). This generates a large-scale circulation with upward motion over the hot-spot and subsidence in its environment, yielding subsidence drying and convectively suppressed conditions in the region surrounding the hot-spot. The moisture is thus "pulled" in the convective region by the large-scale circulation induced by the convective instability over the hot-spot.

The aggregation may be separated into two different phases (Figure 3.6): the aggregation onset phase where dry regions expand and dry further, and the equilibrium phase when aggregation is well established and the simulation is statistically in equilibrium. The mechanisms which govern aggregation at each of these phases might be different (Muller and Held, 2012). For instance, Wing and Emanuel (2014) find that in the onset phase, surface latent heat fluxes act as a positive feedback largely due to enhanced latent heat fluxes in

the moist region, while in the equilibrium phase the aggregation is opposed by enhanced surface fluxes in dry regions. Previous studies using the SAM model with homogeneous SST show that the radiative feedback is necessary for both the onset and the maintenance of aggregation, so that homogenizing the radiation profile even after the formation of aggregation leads to a non-aggregated convection. We showed above that a persistent SST anomaly can generate and sustain aggregation even with homogenized radiation. In the following sections we further focus on the hot-spot simulations with homogenized radiation (Figure 3.6). We analyze first the aggregation processes by considering separately dry and moist regions and by focusing on the aggregation onset phase. The equilibrium state will be addressed later in § 3.5. We define the onset phase as the time between the beginning of the simulation and the first maximum of the aggregation index. The onset phase varies from less than 10 days to more than 50 days for the simulations considered in Figure 3.6 and Table 3.1. Figure 3.6b shows that the aggregation index is mostly driven by the CRH values in the dry patches ($CRH < 25^{th}$ percentile).

3.4.3 The aggregation onset phase

The strength of the subsidence in the dry patch is characterized by its average vertical velocity at 500 hPa ($\overline{W_{500}}^{dry}$). Our hypothesis is that the subsidence strength is correlated with the aggregation onset and time scale. Stronger subsidence outside the hot-spot leads to an enhanced subsidence drying in dry regions, this is an important process that is mostly driven by the positive radiative feedback in the self-aggregation, but it is driven here only by the enhanced vertical motion over the hot-spot (Figure 7). Consistent with this hypothesis, at the beginning of the simulations, the subsidence over the dry patch is larger for larger hot-spots (Figure 3.8a). This can be interpreted as a

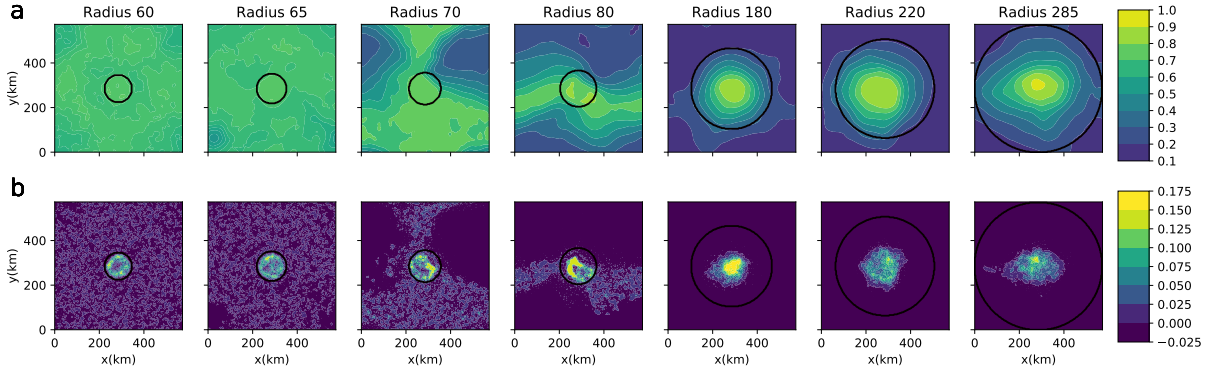

Figure 3.9: (top) CRH and (bottom) W500 (m/s) averaged between day 35 and day 50 of the simulation for hot-spot of different sizes. The domain average SST is 300K, the hot-spot SST anomaly is 5 K and the domain size is 576*576 km^2. The black circle shows the hot-spot.

very fast response to the convective activity over the hot-spot giving a strong subsidence over the surrounding cold ocean region. This response, much faster for larger hot-spots, is largely due to the fact that the initial conditions of the atmosphere (based on a SST of 300 K) enhanced the convective instability over the hot-spot. This plays a role in the aggregation speed, in a manner that may be exaggerated in regard to a hot-spot formation related, for example, to the diurnal surface temperature warming over an island. In that case, our results suggest that the adjustment is too slow (a few days) for such a diurnal variation to reach an equilibrium. Once the aggregation progresses, for hot-spot radius larger than 70 km, $\overline{W_{500}}^{dry}$ becomes progressively weaker so that by the end of the aggregation onset phase, it becomes even weaker than for simulations without aggregation.

Equation 3.4 gives a good estimate of the evolution of the actual $\overline{W_{500}}^{dry}$ (Figure 3.8b) that makes it possible to analyze further the contributions of the radiative cooling term Q_{rad} and of the warming term $\partial T/\partial t$ in the weakening of the subsidence over the dry patch (Figure 3.8c and 3.8d). The difference in the time evolution of the subsidence is largely controlled by the warming term $\partial T/\partial t$ and not by Q_{rad} during the aggregation onset phase. The warming

term $\partial T/\partial t$ is large as the domain is adjusting to the warmer condition over the hot-spot. The adjusting time is about 10 days for large hot-spots. We note that this warming term is much smaller if we use atmospheric initial conditions corresponding to the hot-spot temperature. The larger temperature above the hot-spot yields warmer atmospheric temperatures there, which are progressively impressed on the whole domain through compensating subsidence and via propagating gravity waves (Bretherton and Smolarkiewicz, 1989). As shown in Figure 3.8, this effect is stronger for larger hot-spots for which the term $\partial T/\partial t$ decreases dramatically during the aggregation onset phase. For large hot-spots, Q_{rad} is slightly larger at the end of the aggregation onset phase, showing the effect of a well organized dry patch compared to simulations without organized convection.

This moisture "pulling" leading to convective aggregation is associated to different overturning time scales in these simulations, with typically faster aggregation for larger hot-spots. Note however that for R=285 km, the subsidence is found to be slightly smaller compared to R=180 km or R=220 km, in good agreement with a longer aggregation onset phase (Figure 3.6). For R=285 km, the subsidence is smaller because the potential upward mass flux over the hot-spot is too large to be compensated by subsidence outside of the hot-spot, so that a relatively large part of the hot-spot is included in the subsiding region.

Thus, the aggregation is closely related to the large-scale circulation, as measured by the subsidence velocity in dry regions. The larger fractional area that hot-spot covers, the larger $\overline{W_{500}}^{dry}$ becomes. This can be well seen in Figure 3.8a.

The decrease of $\overline{W_{500}}^{dry}$ during the aggregation onset phase for large hot-spots is caused by the initial transient warming (Equation 3.4 and Figure

3.8c). Eventually, $\overline{W_{500}}^{dry}$ becomes nearly constant in time, as the equilibrium is reached. Then the main balance in dry regions is between subsidence warming and radiative cooling ($\partial T/\partial t \approx 0$). The warming-induced enhanced static stability (large Γ in Equation 3.4) reduces the subsidence velocity in aggregating simulations (Figure 3.8a). Thus the vertical subsiding velocities in dry regions of aggregated simulations become smaller than non-aggregating ones once equilibrium is reached. This is how the expansion and strengthening of the dry patch is halted and equilibrium is reached, despite the stronger radiative cooling rates. This equilibrium phase will be further analyzed in the following section.

3.5 Equilibrium phase

Here we investigate how the strongest convective cells and updrafts are distributed in the equilibrium phase, and whether the aggregated cluster stays over the hot spot. To study the equilibrium state, we consider a period of 15 days starting at day 35 and ending at day 50 for which the simulations already reached the equilibrium phase (Figure 3.6), except for a hot-spot of R70 for which we look at the last five days as this period is closer to the equilibrium.

Figure 3.9 shows CRH and W_{500} fields averaged over this period. For $R \leq 65$ km, there is no aggregation visible on the CRH field or detected by aggregation index, however W_{500} is much stronger over the hot-spot compared to its environment. For $R = 70$ the aggregation is still on progress. The CRH map of this simulation shows both dry and moist area, however, similar to $R = 60$ and 65, the convection over the hot-spot is much stronger than over the environment. For $R = 80$ km, the convection is not totally centered on the hot-spot for this equilibrium phase. For the largest hot-spots, the region of

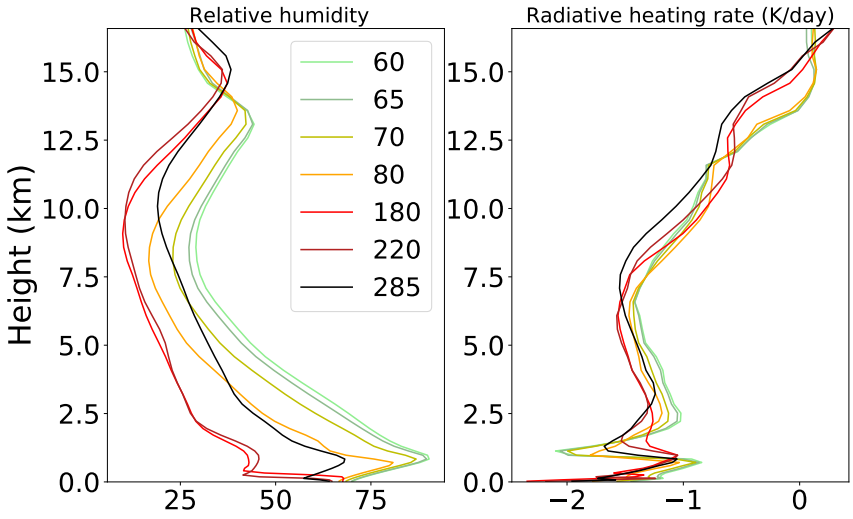

Figure 3.10: Domain average vertical profiles averaged between day 35 and day 50 of the simulation for hot-spot of different sizes. The domain average SST is 300 K, the hot-spot SST anomaly is 5 K and the domain size is 576*576 km^2.

large CRH is well centered on the center of the hot-spots. The concentration of the moist patch over the hot-spot for aggregated simulations is not systematic. In the simulations with interactive radiation (not homogenized in space), the aggregated cluster is indeed not always centered over the hot-spot (Figure 3.2.b). In fact, once equilibrium is reached in the simulations with radiative feedbacks, the moist patch seems to decouple from the surface. It does not stay in the same location and can move across the domain. Thus this result that the convection is located over the hot-spot is not robust once radiative feedbacks are accounted for. With radiative feedbacks, whether the convective cluster stays over the hot-spot probably depends on the strength of radiative feedbacks compared to the hot-spot effects.

Despite the large variability of the aggregation index and of the CRH pattern among the simulations without radiative feedbacks, maximum values of W_{500} are always located over the hot-spot (with an annular shape for $R \leq$ 65 km) during the equilibrium phase (Fig.3.9). A striking result is that the

fractional area of large W_{500} (e.g. $W_{500} > 0.08$ m/s) is relatively independent of the radius of the hot-spot. This region with large W_{500} (Figure 3.9b) has a fractional area of approximately 10 % for all hot-spot radii.

Figure 3.10 shows the vertical profiles of the domain mean relative humidity and radiative cooling rates at equilibrium. Simulations with large aggregation index have a drier average profile in agreement with low CRH in the dry patch (Fig.3.6) and with earlier studies of self-aggregation. Average radiative cooling profiles are similar among the simulations which aggregate, with a large radiative cooling rate near the surface. These profiles are consistent with the very dry conditions and strong low-level radiative cooling accompanying aggregation found in earlier studies (Muller and Bony, 2015).

3.6 Conclusions

In this paper, we investigate the role of persistent warm SST anomalies (hot-spots) on the aggregation of deep convective clouds in cloud-resolving simulations. To this end, we perform simulations in radiative-convective equilibrium with SST anomalies of varying size and amplitude, but keeping the domain mean SST constant between simulations. Earlier studies with homogeneous SSTs find that radiative feedbacks are necessary for both the onset and maintenance of a self-aggregation of the convection for typical tropical temperatures ($\sim$ 300 K). As for previous studies, we find that self-aggregation over homogeneous SSTs is favored at warm temperatures. We also find that the presence of a hot-spot significantly accelerates the aggregation process and extends the range of average SSTs for which aggregation occurs.

We interpret these different behaviors by the fact that the mechanisms for convective aggregation with a hot-spot or with homogeneous SSTs are

different. With homogeneous SSTs, the aggregation of convection starts by a strengthening and an expansion of a dry region. Strong radiative cooling in dry regions yields enhanced subsidence that further dries the dry regions and that "pushes" low-level moisture toward the convective region (Figure 3.7a). In other words, radiatively-driven subsidence inhibits convection in the dry region (Wing et al., 2017; Bretherton et al., 2005; Muller and Held, 2012).

With a hot-spot, we find that aggregation (it is no more a self-aggregation since it is forced by the persistent SST anomaly) can occur even in the absence of radiative feedbacks (removed by homogenizing horizontally radiative cooling rates) if the hot-spot is warm and large enough. The hot-spot triggers aggregation by locally increasing the convective instability. Indeed, the warmer and moister conditions at low level over the hot-spot favor deep convection, which brings the atmosphere towards a warmer condition. These warmer temperatures are imprinted over the whole domain through compensating subsidence warming in drier regions and via the propagation of gravity waves (Bretherton and Smolarkiewicz, 1989). This subsidence favors further drying in dry regions. This is the positive feedback responsible for the expansion and strengthening of dry regions in hot-spot simulations that aggregate. In other words, the hot-spot "pulls" convection over itself, by generating a large-scale circulation with subsidence outside the hot-spot (Figure 3.7b).

In our simulations, planetary rotation is neglected so there is no limiting scale (beyond the dissipative scale) for the propagation of waves. So in our doubly-periodic geometry, the subsidence compensates upward convective motion and is thus potentially stronger when the fractional area of the hot-spot increases. In particular, for a given hot-spot radius, the subsidence is sensitive to the domain size. This highlights the importance of using large domains when investigating island convection in similar non-rotating doubly-periodic

settings, in order to either avoid or control the triggering of self-aggregation feedbacks. In particular, the doubly-periodic confinement of the large scale circulation induced by surface heterogeneities may explain the non-monotonic responses of precipitation to an island found in idealized simulations of convection over tropical islands. In such simulations, precipitation is found to increase and then decrease as a function of island radius holding the domain size fixed. Our results suggest that the large-scale circulation induced by the island may be impacted by the domain size if the domain is not large enough compared to the island.

In reality, with planetary rotation, the scale of the large-scale circulation induced by SST anomalies is likely determined by the Rossby radius of deformation. Our results suggest that for a large enough fractional area of SST anomalies compared to this large-scale circulation, self-aggregation feedbacks could play a role in organizing deep convection over SST anomalies. In the ocean, SST anomalies of the size studied here ($\mathcal{O}(100$ km$)$) are not uncommon, taking the form of mesoscale eddies (Chelton, 2011). Their contribution to convective organization deserves further investigation. Finally, these findings raise questions on the organization of deep convection over tropical islands, e.g. of the maritime continent. There, a strong diurnal cycle further interacts with aggregation feedbacks and tendencies (Cronin et al., 2015). Our results show that the adjustment of the average temperature profile to the hot-spot SST anomaly takes a few days for large hot-spots, which is very slow compared to diurnal variability of surface temperature over tropical islands (reaching to a maximum typically in 6h between sunrise and noon). Therefore, the atmosphere, and the convective aggregation pattern itself, will not have time to fully adjust before the island starts cooling down in the afternoon. Further work is needed to investigate the implication of our results on the diurnal cycle of convection over tropical islands.

Table 3.1: List of all the simulations with homogenized radiation. Shown are the hot-spot radius, the fractional area covered by it (with one digit for values below 10 %), its temperature anomaly (dT), ocean temperature and domain mean SST.

HS Radius (km)	$A^{hs}/(A^{env}+A^{hs})(\%)$	dT (K)	SST^{env} (K)	$\overline{SST}$ (K)
60	3.4	5	299.83	300
65	4.0	5	299.80	300
70	4.6	5	299.77	300
80	6.1	5	299.69	300
80	6.1	3	299.81	300
180	31	5	298.46	300
220	46	5	297.70	300
285	77	5	296.15	300

Chapter 4

Self-aggregation of convective clouds with interactive sea surface temperature

4.1 abstract

This study investigates the feedbacks between an interactive sea surface temperature (SST) and the self-aggregation of deep convective clouds, using a cloud-resolving model in non-rotating radiative-convective equilibrium. The ocean is modeled as one layer slab with a temporally fixed mean but spatially varying temperature. We find that the interactive SST decelerates the aggregation, and that the deceleration is larger with a shallower slab, consistent with earlier studies. The surface temperature anomaly in dry regions is positive at first, thus opposing the diverging shallow circulation known to favor self-aggregation, consistent with the slower aggregation. But surprisingly the driest columns then have a negative SST anomaly, thus strengthening the diverging shallow circulation and favoring aggregation. This diverging circu-

lation out of dry regions is found to be well correlated with the aggregation speed. It can be linked to a positive surface pressure anomaly (PSFC), itself the consequence of SST anomalies and boundary layer radiative cooling. The latter cools and dries the boundary layer, thus increasing PSFC anomalies through virtual effects and hydrostasy. Sensitivity experiments confirm the key role played by boundary layer radiative cooling in determining PSFC anomalies in dry regions, and thus the shallow diverging circulation and the aggregation speed.

4.2 Introduction

The spontaneous organization of deep convective clouds into a single cluster, which is known as self-aggregation, has been found across a wide range of 2D and 3D cloud-resolving models (CRMs) and global climate models (GCMs) with different configurations and domain shapes and sizes (Nakajima and Matsuno, 1988; Held et al., 1993; Muller and Held, 2012; Wing et al., 2017; Wing, 2019). Self-aggregation typically starts with the appearance and growth of persistent dry areas devoid of deep convection. The growth of those dry regions leads to the confinement of convection to a remaining small fraction of the simulation domain. This phenomenon results in a reduction of domain-averaged water vapor content, and consequently a significant enhancement of outgoing longwave radiation to space. If relevant to the real world, this self-aggregation of deep convective clouds could potentially impact the climate sensitivity.

Several studies have investigated the physical processes responsible for this phenomenon. Most of these studies use fixed sea-surface temperature (SST). In a seminal study, Bretherton et al. (2005) point out the importance of surface fluxes and atmospheric radiative cooling for self-aggregation. They

find that enhanced radiative cooling in the lower troposphere in dry regions leads to the formation of a shallow flux from dry to moist regions. This shallow circulation transports moist static energy (MSE) from dry to moist regions, i.e. up-gradient (from low MSE to high MSE regions), thus reinforcing the MSE gradient and the aggregation of convection.

The importance of atmospheric radiative cooling has been confirmed by other studies as well, however, based on model and simulation configuration, different radiative feedbacks can drive the self-aggregation. Muller and Held (2012) show that the low-level clouds longwave radiation is necessary for self-aggregation to occur from homogeneous initial conditions, while clear-sky and high-clouds longwave radiative feedbacks are sufficient to maintain the aggregation. Wing and Emanuel (2014) also highlight the importance of clear-sky free-tropospheric radiative cooling. Other studies mention the importance of free-tropospheric moisture and convection-moisture feedback (Tompkins and Craig, 1998; Craig and Mack, 2013) and also cold pool-convection feedback (Jeevanjee and Romps (2013)). In summary, several physical processes contribute to the onset and maintenance of convective self-aggregation. It is still unclear which one of those feedbacks, if any, dominates. In particular, more work is desirable to clarify the role of low-level versus free-tropospheric radiative feedbacks on driving self-aggregation.

One robust feature though, is the significant increase of MSE variance with self-aggregation (Wing and Emanuel, 2014). As mentioned above, the radiatively-driven shallow circulation, and concomitant up-gradient MSE transport, are believed to play a key role. Indeed, the shallow circulation transports low level air with high MSE to already moist regions. A strong shallow flux can result in a strong up-gradient transport of MSE, thus negative gross moist stability, which is known to favor aggregation (Bretherton et al., 2005). The

importance of boundary-layer differential radiative cooling rates, between dry and moist regions, in driving this shallow circulation has been suggested by Muller and Bony (2015). Using a conceptual, analytical model of the boundary layer, Naumann et al. (2017) and Naumann et al. (2019) further investigate the divergent shallow circulation out of a dry region driven by enhanced boundary layer radiative cooling, and how it compares to the shallow circulation driven by SST anomalies. Their dry theoretical model confirms that a shallow circulation can be maintained for differences in radiative boundary-layer cooling rates larger than 1 K/day. The circulation strength is comparable to that caused by SST differences of a few kelvins (Naumann et al., 2017), or even larger when moisture effects are accounted for (Naumann et al., 2019). The circulation follows from colder boundary layer temperatures, and thus increased hydrostatic surface pressures, in regions with larger boundary layer radiative cooling.

It should be mentioned that all the studies mentioned so far used fixed homogeneous surface temperature. Using a non-homogeneous SST (constant in time but inhomogeneous in space) or an interactive SST (evolving in time) can also change the occurrence of self-aggregation and the dominating feedback. Introducing an SST anomaly can dictate the preferred location of convection (Tompkins, 2001b) and thus impact the self-aggregation. When a circular SST anomaly (constant in time) is imposed, the aggregation process is significantly accelerated (Shamekh et al., 2019), due to the large-scale circulation that develops in response to the stronger upward mass flux over the warm region. Consistently, Back and Bretherton (2009) show that a boundary layer divergent flow forms in response to an SST gradient, that can re-enforce deep convection.

A few studies have also investigated the response of self-aggregation to an interactive SST. In that case, the SST evolves in space and time according

to the local energy budget (see section 4.3.3 for more details). When SST is allowed to interact with the atmosphere, the self-aggregation is typically delayed or prevented (Hohenegger and Stevens, 2016; Grabowski, 2006; Coppin and Bony, 2017). Using a GCM coupled with a slab ocean, Grabowski (2006) shows that warm SST anomalies form under the cloud free area by enhanced shortwave radiation which reaches the surface. In the GCM, convective clusters follow the warm SST anomaly, and results in an easterly propagating convective cluster similar to the Madden Julian oscillation. In a similar set-up, Coppin and Bony (2017) find that the convective aggregates prefer to stay on the maximum of SST gradient, which also results in the similar propagation found by Grabowski (2006).

Using an cloud resolving model and a domain of $(576\ \text{km})^2$, Hohenegger and Stevens (2016) investigate the impact of different slab depths on the aggregation of convection. They find that the coupling between the SST and the atmosphere delays the onset of self-aggregation, or prevents it completely if the slab is very shallow (1 m). They suggest that this delay is the result of the formation of an SST gradient, which opposes the boundary layer divergent flow (shallow circulation mentioned above) known to be important for the development of convective aggregation, a hypothesis that we further investigate and quantify here. Of particular interest are the following questions:

- What is the impact of interactive SST on aggregation, and how do surface variables evolve as the aggregation progresses?
- Do SST anomalies oppose the shallow circulation between dry and moist regions?
- What is the relative importance of the shallow versus the deep circulation in the MSE transport and time scale of aggregation?

The next section describes the CRM and simulations in more detail, as well as the index used to quantify the convective aggregation. Section 4.4 describes the impact of interactive SST on aggregation for various slab depths and mean SST, and describes in detail the evolution of surface properties in one simulation. Section 4.5 investigates the physical processes behind the sensitivity to mixed layer depth and domain-mean SST, notably the relative roles of boundary layer radiative cooling anomalies and SST anomalies in setting up a shallow circulation. Concluding remarks are offered in §4.6.

4.3 Method

4.3.1 Cloud-resolving model

The CRM used is the model System for Atmospheric Modeling (SAM) version 6.11.1 (Khairoutdinov and Randall, 2003). This model solves the anelastic equations of conservation of momentum, water (with 6 species present in the model, water vapor, cloud liquid, cloud ice, precipitating rain, precipitating snow, and precipitating graupel), and energy. The relevant energy for moist convection is the moist static energy (MSE), as it is conserved (approximately, i.e. neglecting viscous and subgrid-scale effects) under adiabatic processes including the phase change of water. More precisely in this model, the so-called "frozen" MSE is conserved during moist adiabatic processes, including the freezing of precipitation. The frozen MSE is given by

$$MSE = c_p T + gz + L_v q - L_f q_{ice}, \tag{4.1}$$

with the specific heat capacity of air at constant pressure c_p, temperature T, gravity g, height z, latent heat of evaporation L_v, water vapor specific humidity

q_v, latent heat of fusion L_f, and specific humidity of all ice phase condensates q_{ice}.

The subgrid-scale turbulence is modeled using a Smagorinsky-type parameterization, and we use the 1-moment microphysics formulation, following Bretherton et al. (2005) and Muller and Held (2012). Surface fluxes are computed using bulk formulae. Further information about the model can be found in Khairoutdinov and Randall (2003).

All simulations use interactive radiation, using the radiation code from the National Center for Atmospheric Research (NCAR) Community Atmosphere Model version 3 (CAM3; Collins et al. (2006)). For simplicity, we neglect the diurnal cycle and use the daily mean incoming solar insolation of 413 W m^{-2} (same setting as Tompkins and Craig (1998)).

4.3.2 Experimental setup

The model domain is square, doubly-periodic in both horizontal directions x and y. We run simulations with horizontal domain size (576 km)^2. The horizontal resolution is 3 km and the vertical grid spacing increases gradually with height, with the first level at 25 m and a resolution of 50 m close to the sea surface, reaching a vertical resolution of 500 m in the mid troposphere. There are 64 vertical levels which span 27 km in the vertical. This includes a sponge layer in the upper third of the domain (from $z = 18$ km to 27 km) where the wind is relaxed to zero in order to reduce gravity wave reflection and buildup. No large-scale forcing or wind is imposed in the domain. We neglect the Earth's rotation, a reasonable approximation in the tropics where the Coriolis parameter is small.

The initial conditions for the different domain averaged SSTs are obtained

from smaller domain runs with the corresponding SST at radiative-convective equilibrium (RCE) ((96 km)^2 run to 50 days), then using time and domain averaged profiles of the last 5 days. We run simulations with three different depths of slab: $H = 5$, 10, and 50 meters, at two domain-averaged SSTs = 300 and 305 K. This allows us to explore the impact of interactive SST on aggregation, and compare the sensitivity to slab depth to the impact of changing domain-averaged SST by 5 K. We also perform fixed SST simulations for both SST = 300 and 305. Note that fixed SST is mathematically equivalent to infinite slab depth, thus the results should converge to the fixed SST simulation when H increases. A simulation will be referred to by its depth of slab and its SST so that, for example, simulation H5SST305 has slab depth of 5 meters and SST = 305 K.

As the time to equilibrium is longer with interactive SST, and thus the computation is more expensive, in particular with shallow slab depth, we stop the simulations when the metric used for the aggregation progress (introduced below in §4.3.4) reaches its maximum and drops back down to its equilibrium value. It is worth mentioning that after this drop, the metric oscillates around a value between 0.4-0.5 and does not depend on slab depth or mean SST.

4.3.3 Slab ocean

One technical complication with tropical simulations using interactive SST, is that the incoming solar radiation in the tropics exceeds the threshold for a runaway greenhouse gas warming (Pierrehumbert, 2010). In the tropics, oceanic and atmospheric transport of energy out of the tropics compensates the energy imbalance at the top of the atmosphere and prevents excessive warming. This is not the case in simulations of an isolated tropical region with periodic boundary conditions that lacks the transport of energy out of

the tropics by the Hadley cell and the ocean circulation.

Several solutions have been proposed to overcome this issue, e.g. reducing the incoming solar flux (Cronin et al., 2015), adding a constant deep ocean flux (Romps, 2011), or relaxing the domain average SST to a target temperature (Semie and Tompkins, 2016) i.e. adding a deep ocean flux which ensures little drift in domain-mean SST.

Aggregation is known to be sensitive to the domain-mean SST (e.g., Wing and Emanuel (2014)). Thus in order to separate the effects of domain-mean SST and of spatial inhomogeneities, here we follow Semie and Tompkins (2016) and relax the domain-averaged ocean mixed layer temperature $\overline{SST}$ toward a fixed target temperature SST_0 (see 4.A for a brief discussion of simulations with a constant deep ocean flux and their domain mean SST drifts). This relaxation method allows us to keep the domain-averaged SST constant over time while it allows the SST to vary locally according to the evolution equation:

$$\rho_w c_{p,w} H \left(\frac{dSST}{dt} + \frac{\overline{SST} - SST_0}{\tau_0} \right) = Q^N_{SW} + Q^N_{LW} + LHF + SHF \quad (4.2)$$

where ρ_w denotes water density, $c_{p,w}$ is the specific heat capacity of water at constant pressure, H the depth of the slab, τ_0 the relaxation time scale, which is constant and equal to two hours in all of our simulations (this value was empirically determined to avoid significant drift in the domain mean SST). All the terms on the right hand side of 4.2 are positive downward (increase SST) and negative upward (decrease SST). LHF and SHF denote surface latent and sensible heat fluxes (up to a minus sign), and Q^N_{SW} and Q^N_{LW} stand respectively for shortwave and longwave net radiative flux at the surface, with

$$Q^N_{LW} = LW_d - \sigma SST^4, \quad (4.3)$$

where σ is the Stephen-Boltzmann constant and LW_d the downward longwave flux at the surface.

Also

$$Q^N_{SW} = (1-\alpha)SW_d = (1-\alpha)SW_{TOA}e^{(-\tau/\mu_0)} \tag{4.4}$$

where α is albedo, SW_d is downward shortwave flux at the surface, μ_0 is a constant which depends on the zenith angle, τ is the shortwave optical depth, and SW_{TOA} is the incoming shortwave flux at the top of the atmosphere. In our simulations, τ changes only by changes in water vapor and cloud water content of the atmosphere as the other factors do not change.

Using equation 4.2, we can find an equation for spatial SST anomalies $SST' = SST - \overline{SST}$:

$$\frac{dSST'}{dt} = \frac{1}{\rho_w c_{p,w} H}\left(Q^N_{SW}{}' + Q^N_{LW}{}' + LHF' + SHF'\right) \tag{4.5}$$

It should be mentioned that the relaxation term disappears as it is the same everywhere in the domain. Thus the spatial variability of SST arises from spatial variations of the energy flux at the surface.

4.3.4 Analysis Framework

To follow the progress of aggregation we use column relative humidity CRH (Wing and Cronin, 2016; Shamekh et al., 2019).

$$CRH = \frac{\int q_v\,\rho\,dz}{\int q_{v,sat}\,\rho\,dz}, \tag{4.6}$$

where $q_{v,sat}$ is the saturation water vapor specific humidity, ρ the air density and the vertical integration is done over the troposphere. We use CRH for our analysis as it is less dependent on surface temperature compared to the inte-

grated column water vapor (PW), thus it allows us to compare the aggregation progress at different SSTs.

In our simulations, deep convection does not occur in regions with $CRH < 0.6$, thus, we define the dry patch as the area with $CRH < 0.6$. With the progress of aggregation, these dry patches grow and merge so that they take a larger and larger fraction of the domain. As the growth of the dry patches is the main feature in all our simulations, to follow the progress of aggregation, we use the fractional area covered by dry patches, whcih we will refer to as the aggregation index.

4.4 The impact of interactive SST on the aggregation of convective clouds

In this section, we first provide an overview of the main results regarding the impact of interactive SST on the progress of self-aggregation in our simulations. We then study in detail one simulation with slab depth = 5 m and domain mean SST = 305 K (hereafter H5SST305) as processes are found to be qualitatively similar in all simulations. Notably, we investigate in detail how interactive surface temperatures affect the surface pressure anomaly in dry regions, and thus the shallow circulation between dry and moist regions known to play an important role in the aggregation process.

4.4.1 Overview of results

Figure 4.1 shows the aggregation index for the simulations with interactive SST with different slab depths and with SSTs 300 and 305 K. To compare the timing of self aggregation in our simulations, we simply compare the time at

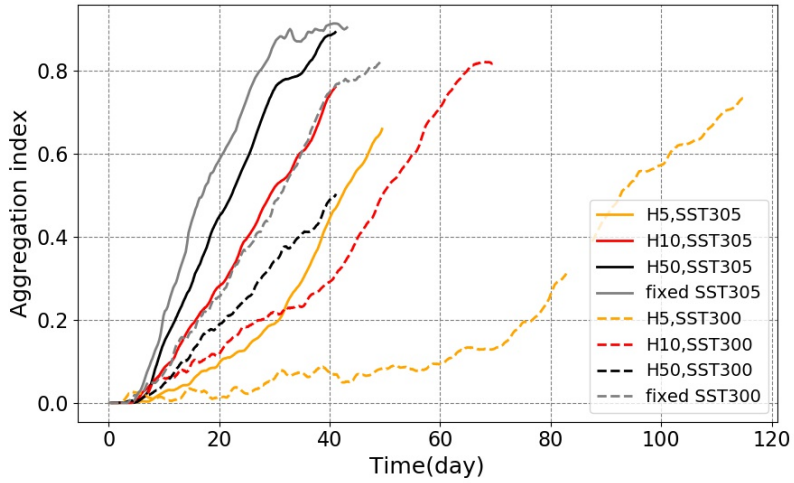

Figure 4.1: Time series of the aggregation index ($\text{Area}_{CRH<0.6}$) for $SST_0 = 300K$ (dashed lines) and $SST_0 = 305K$ (plain lines) and different slab depths. Simulations with fixed SST are also shown for reference (gray lines). (We note in passing that the few days missing in the H5SST300 simulation, around day 85, are due to a technical issue, but do not affect the results discussed here.)

which the aggregation index reaches its maximum.

Generally speaking, introducing a slab ocean with interactive surface temperature delays self-aggregation (Figure 4.1). Consistently, the fixed SST simulations (which correspond to infinite slab depth) are faster at both 300 K and 305 K than the interactive SST simulations with the same mean SST. This is consistent with previous studies on the impact of slab ocean on self-aggregation (Hohenegger and Stevens, 2016; Bretherton et al., 2005). Here, with the slab depths that we examined, the aggregation always proceeds, but it is significantly delayed with a shallow slab as, for example H10SST305 and H5SST305 delay the self-aggregation by 12 and 25 days respectively compared to fixed SST simulation (Figure 4.1). The delays obtained with interactive SST (tens of days) are comparable to the delays obtained when reducing the SST. Indeed, similar tens of days delays are found when decreasing the SST from 305 to 300 K for a given slab depth (Figure 4.1).

Note that in some of the simulations, there is a period of slower increase

of the aggregation index (e.g. H5SST300 before day 70, or H5SST305 before day 30) before the index starts its faster monotonic increase. We refer to this delayed period, for which the aggregation index is not increasing significantly, as latency.

We now investigate in more detail surface properties in one of the simulations since, as mentioned earlier, properties are found to be qualitatively robust in all the runs. Of particular interest are the evolution of surface temperature and surface pressure in dry regions, and how these impact the circulation.

4.4.2 SST anomalies

Figure 4.2 shows the time evolution of several variables, including SST anomaly and the surface energy budget anomaly (right hand side of equation 4.5) in the simulation H5SST305. The first dry patches are well detectable at day 16 (Figure 4.2.a). These dry patches grow where they firstly appear without significant displacement. By day 40, a single circular dry patch exists and covers half of the domain. It worth mentioning that the dryness is more pronounced in the free troposphere, specially at early time, and reaches the boundary layer by day 24 (Figure 4.3).

We see that the SST anomalies exhibit two different stages of evolution: 1. an early stage warming which happens when the dry patch is newly formed and still has large amount of column water vapor, so that shortwave warming dominates; 2. a later stage cooling which appears with further dryness of the dry patch, so that longwave cooling dominates. In the following we investigate each of these stages separately.

a. Early stage warming

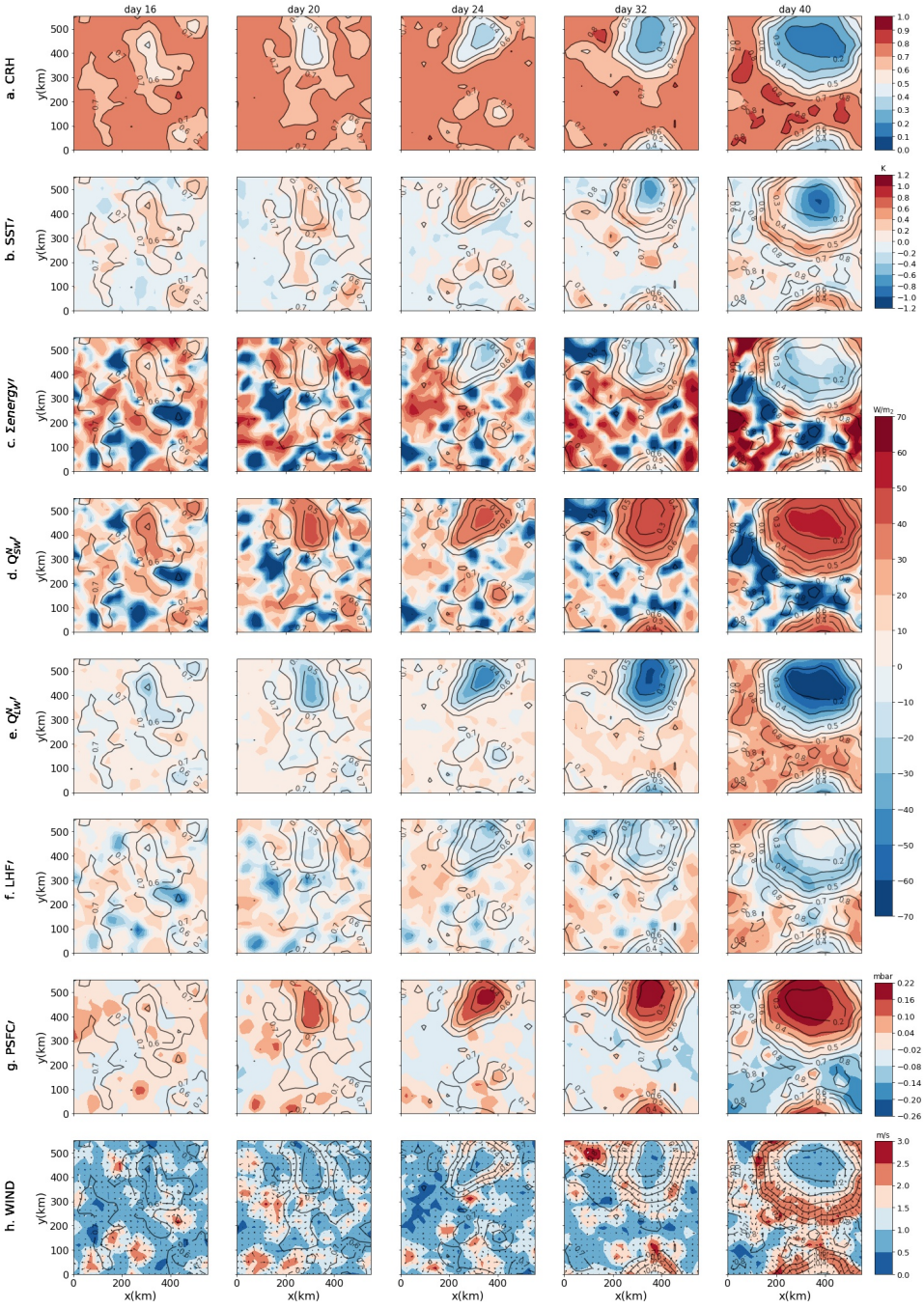

Figure 4.2: The rows show daily mean of: a) CRH, b) SST anomaly, c) Net energy flux at the surface, d) net shortwave radiative flux anomaly at the surface, e) net longwave radiative flux anomaly at the surface, f) surface latent heat flux anomaly, g) surface pressure anomaly, and h) surface wind (color) with arrows showing the direction of the wind. Columns show the time progress of each variable.The data are taken from the simulation H5SST305 averaged over 6 hours of the day mentioned on the top of each column. Each panel is further smoother by 16*16 grids column averaging The contours of CRH are repeated in all panels to ease comparison. In all flux plots (c, d, e, and f) downward (upward) flux is shown with positive (negative) sign.

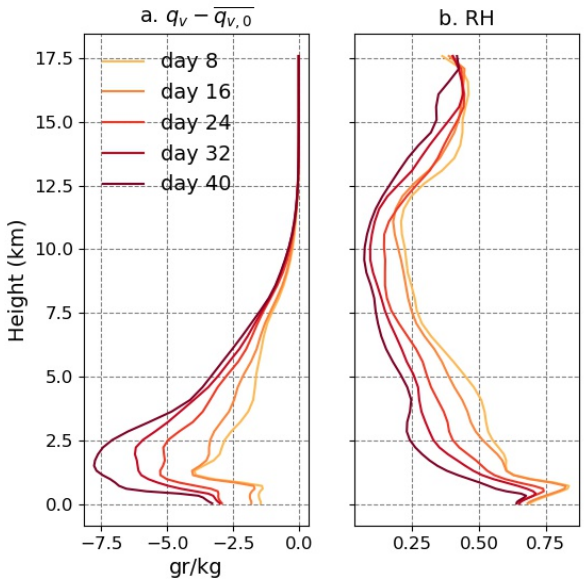

Figure 4.3: The vertical profiles of a) total change in specific humidity ($qv-\overline{q_{v,0}}$) and b) relative humidity averaged over the dry patch (defined by CRH<0.6) for the simulation H5SST305.

The temperature anomaly underneath the dry patches at their early appearance (up to day 16) is positive, thus the first impact of a dry patch on the surface temperature is warming (Figure 4.2.b). This early stage warming in dry regions can be understood by looking at the net energy flux anomaly (hereafter $\Sigma EF\prime$) at the surface (Equation 4.5 and Figure 4.2.c). In dry regions, $\Sigma EF\prime$ is initially positive, thus leading to an SST increase with time. $\Sigma EF\prime$ is predominantly determined by shortwave and longwave radiative fluxes at the surface, with also a small contribution by surface latent heat flux. The sensible heat flux is very small thus negligible.

The early stage warming is mainly because of an enhancement in the shortwave radiative flux at the surface (SWNS), as the dry patches become cloud free and more transparent from the very beginning, letting larger amounts of shortwave radiation reach the surface and building up positive SST anomalies locally (Figure 4.2.b and d). These cloud free dry patches experience a reduction in total column water vapor (Figure 4.3). As noted above, the dryness

starts from the free troposphere and is not significant in the boundary layer (up to day 16).

When the free troposphere becomes dry, the boundary layer and the surface can radiatively cool more efficiently in the longwave (Emanuel et al., 2014). The enhancement of net longwave radiative flux at the surface (LWNS) is clear in Figure 4.2.e, however, as the dry patches still have a large amount of water vapor, especially in the boundary layer, the surface cooling by LWNS is smaller than warming by enhanced shortwave radiative flux. All together, at early stage of dry patches, surface warming by SWNS is more efficient compared to cooling by LWNS (and LHF) leading to the formation of warm SST anomalies.

b. Later stage cooling

By day 24, with further dryness and expansion of the dry patches, surprisingly the surface at the center of one of the dry patches with lowest CRH becomes colder than the area around it (Figure 4.2.b, the dry patch at x=400 km and y=500 km) so that a cold anomaly surrounded by a ring of warm water forms. CRH over the ring of warm water is large (roughly comparable with CRH in the dry patches at day 16) thus its warming is caused by the dominance of SWNS versus LWNS and LHF. The cooling at the center of the dry patch indicates that further drying of the dry patches can have a cooling effect on the surface temperature underneath them by increasing LWNS with an additional albeit small contribution from enhanced LHF. The surface latent heat fluxes (Figure 4.2.f) increases mainly as a result of increased gradient of specific humidity between the surface and the first layer of the atmosphere, as the dryness has already reached the boundary layer (Figure 4.3). The enhanced LWNS is the result of low amount of column water vapor that results in a smaller downward longwave radiative flux at the surface and allows the

LWNS to increase. This enhancement is well seen in Figure 4.2.e, day 24 at x=400 km and y=500 km.

To summarize, at the center of the dry patch, around day 24, cooling by LWNS dominates and results in a negative trend in surface temperature anomaly, while at the edge of the dry patch, shortwave warming overcomes longwave cooling (and the small contribution from latent heat flux) so that a ring of warm water forms. This pattern of warm ring-cold center further intensifies with dryness of dry patch. At this stage, the cold patch persists as LWNS remains larger than SWNS and LHF.

After day 40, the reduction in LHF results in an increase in surface temperature anomaly at the center of the dry patch (not shown). The warmer center in return increases LHF, so that the SST anomaly and LHF at the center of the dry patch oscillate slowly around an equilibrium value.

These SST anomalies can potentially affect the aggregation speed by impacting the surface pressure anomaly in dry regions, an aspect which we further investigate in the following section.

4.4.3 Surface pressure anomaly

At the early stage of the simulation, the surface pressure anomaly (hereafter PSFC) is slightly positive under some of the dry patches (Figure 4.2.g, day 16). A positive PSFC anomaly builds up a divergent flow at the surface, which exports low level moist air from the dry to the moist regions (figure 4.2.h). This flow further dries the dry regions which strengthen and expand. The divergent flow then increases the horizontal variance of water vapor which is correlated with the progress of aggregation. As mentioned in the introduction, this low-level divergent circulation and the concomitant up-gradient MSE transport are

well documented in aggregation simulations (Bretherton et al., 2005; Muller and Held, 2012; Muller and Bony, 2015). Here we further investigate the origin of this high surface pressure anomaly in dry regions, and its link with specific humidity, radiation, and SST anomaly.

Assuming hydrostatic balance, the surface pressure anomaly in the dry region depends on the virtual temperature anomaly, itself a function of temperature and humidity anomalies. Since horizontal gradients of virtual temperature are small in the free troposphere (Figure 4.4 and Figure 4.6.d, consistent with the weak temperature gradients of tropical regions where the Coriolis parameter is small (Sobel et al., 2001)), the surface pressure anomaly in dry regions is related to virtual temperature anomalies in the boundary layer. Neglecting variations in boundary layer height z_{BL}, from hydrostasy and the ideal gas law (see 4.B for a derivation):

$$PSFC' \approx \overline{PSFC}\frac{g}{R_d}\int_0^{z_{BL}} \frac{-1}{\overline{T_v(z)}}\left(\frac{T\prime(z)}{\overline{T(z)}} + \frac{0.61q_v\prime(z)}{(1+0.61\overline{q_v(z)})}\right)dz, \qquad (4.7)$$

where $PSFC$ denotes surface pressure, T_v virtual temperature, T temperature, q_v specific humidity, R_d the gas constant of dry air. Primes denote anomalies in dry regions compared to the domain mean denoted with an overbar (i.e. for a variable x, $x\prime = x_d - \overline{x}$). Based on this equation, a positive anomaly of temperature or of q_v reduces the high PSFC anomaly (consistent with lighter warmer and moister air).

From the early stage of the dry patch (day 16), the boundary layer water vapor anomaly is negative and creates a negative θ_v anomaly (Figure 4.4.a). The temperature anomaly is slightly positive at the beginning but then becomes negative with further progress of the dry patch (Figure 4.4.b). So, up to day 20, the temperature profile of the boundary layer opposes the formation of a positive PSFC anomaly but after turning negative, it favors the positive

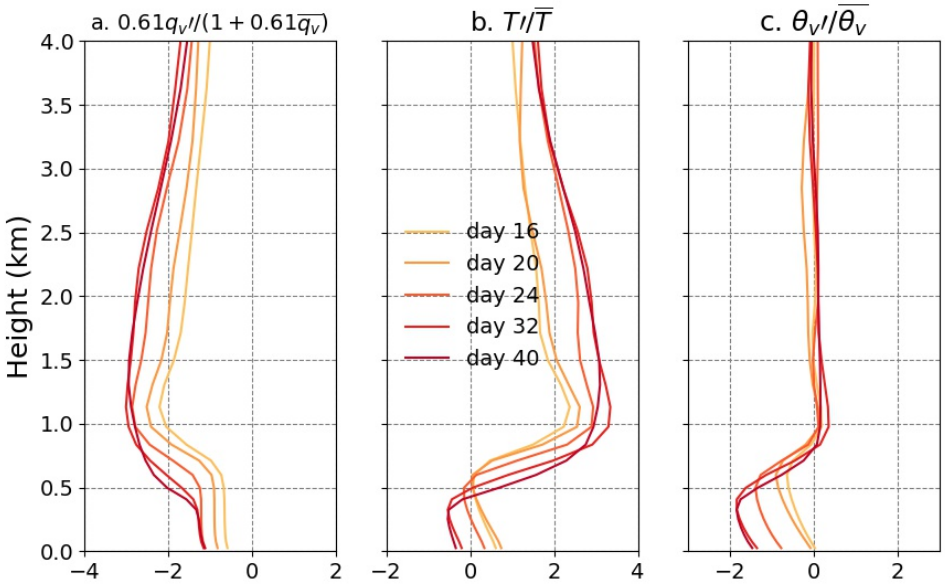

Figure 4.4: Plots show the contribution of a) qv anomalies and b) temperature anomalies into c) virtual potential temperature anomalies. Each line is one day averaged over the dry patch (CRH <0.6) for the simulation H5SST305.

PSFC anomaly, consistent with the SST anomaly discussed in the previous section, first positive opposing and second negative favoring aggregation.

In fact, we interpret the surface pressure anomaly in the dry regions as being the consequence of SST anomalies and boundary layer radiative cooling anomalies there. This is motivated by earlier work showing the key role played by low-tropospheric radiation in self-aggregation (Muller and Bony, 2015), and by the theoretical model of Naumann et al. (2017, 2019) showing the similar or even larger radiatively driven shallow circulation compared to that driven by SST gradients. A locally warmer SST tends to warm and moisten (through enhanced surface latent heat flux) the column and oppose the positive PSFC anomaly. On the other hand, a locally enhanced boundary layer radiative cooling (hereafter Q_{BL}, negative for a cooling) can cool and dry through subsidence, the boundary layer, and generate a positive PSFC anomaly. In 4.C, we confirm the key role played by boundary layer radiative cooling in sensitivity simulations: homogenizing it prevents the aggregation in our simulations,

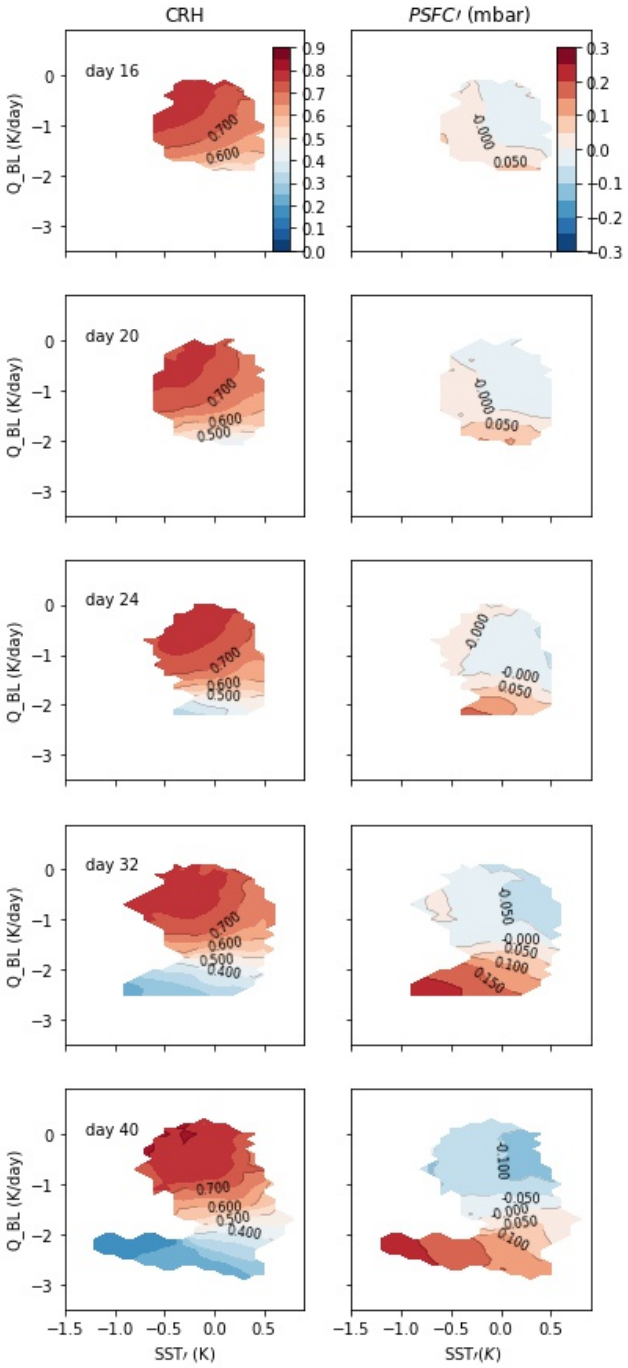

Figure 4.5: CRH (left column) and PSFC anomaly (right column) for simulation H5SST305. The x axis is SST anomaly, and the y axis is radiative cooling averaged over the boundary layer Q_{BL}. To compute the top of the boundary layer, we use the q_v profile and determine the first altitude above ground where it has a maximum curvature.

while homogenizing radiation in the free troposphere has little impact.

Figure 4.5 shows the evolution of PSFC' in Q_{BL} and SST' space. At day 16, on the lower part of the panel (i.e. at more negative Q_{BL}), SST anomaly is positive thus warming the column while Q_{BL} is large and cooling the column. Figure 4.4.b shows that the temperature anomaly of the dry region is still opposing the positive PSFC anomaly. But this opposition has been reduced by boundary layer radiative cooling. Indeed, the cooling generates subsidence (not shown), yielding a drying and concomitant virtual effects, which dominate the temperature effects and lead to the formation of a positive PSFC anomaly (Figure 4.4.a).

As Figure 4.4 shows, the opposite effects of q_v and T on θ_v, up to day 20, might explain why some of the dry patches do not persist at early stage and disappear. This opposing impact results in a small θ_v anomaly thus small PSFC anomaly that has a low chance of persistence. By day 24, the center of the dry patch has a cold SST anomaly (§ 4.4.2), furthermore, Q_{BL} is enhanced as the column is drier (Figure 4.5). Thus the temperature of boundary layer also favors positive PSFC anomaly, so that PSFC anomaly shows a significant enhancement (Figure 4.2.g and 4.5).

The high pressure in dry region results in divergence and further expansion of dry patches, and also their stickiness: they grow larger wherever they firstly appear without significant migration. Note that this is at odds with GCM studies of aggregation with interactive SST (Grabowski, 2006; Coppin and Bony, 2017), where the moist patch always follows the warm SST anomaly which forms under the dry patch: a "cat and mouse" dynamics. In our cloud-resolving simulations, this migration is absent as the dry patches have a persistent positive PSFC anomaly which guarantees their growth and stickiness. We interpret this discrepancy as resulting from a strong sensitivity

of convection to local SST in GCMs. In our simulations, the enhanced boundary layer cooling by Q_{BL} compensates the warming by positive SST anomaly, thus along with a negative boundary layer moisture anomaly create a positive PSFC anomaly. So higher pressure remains located over the dry regions, and convection remains localized in moist regions.

The picture that emerges is that enhanced boundary layer radiative cooling in dry regions dries the boundary layer and thus through virtual effects creates a high pressure anomaly there. This positive PSFC anomaly is partially offset by warmer SSTs at early stages of the aggregation process. Once the dry patch is dry enough, the SST anomaly reverses because of enhanced surface cooling by longwave radiation and the colder SST adds to the boundary layer cooling in dry regions, and by hydrostasy to positive PSFC anomaly. The sign and magnitude of PSFC anomaly has a large impact on the persistence and growth of dry patches. More precisely, a positive PSFC anomaly ensures the expansion of dry patches by exporting moist static energy via a boundary layer divergent flow out of dry patches. As this divergent flow is found to be crucial for the speed of aggregation, we explore it in more detail in the following section.

4.4.4 Divergent flow

The surface wind is divergent in dry patches from their early stage (Figure 4.2.e). From earlier studies on aggregation, it is known that this low-level divergent circulation is key in transporting moisture and MSE out of dry patches, strengthening moisture and MSE gradients. The dry patches then expand (e.g., Bretherton et al. (2005)). Consistent with the theoretical model of Naumann et al. (2017), we saw that this low-level circulation can be related to the persistence of a high surface pressure anomaly, itself related to negative moisture

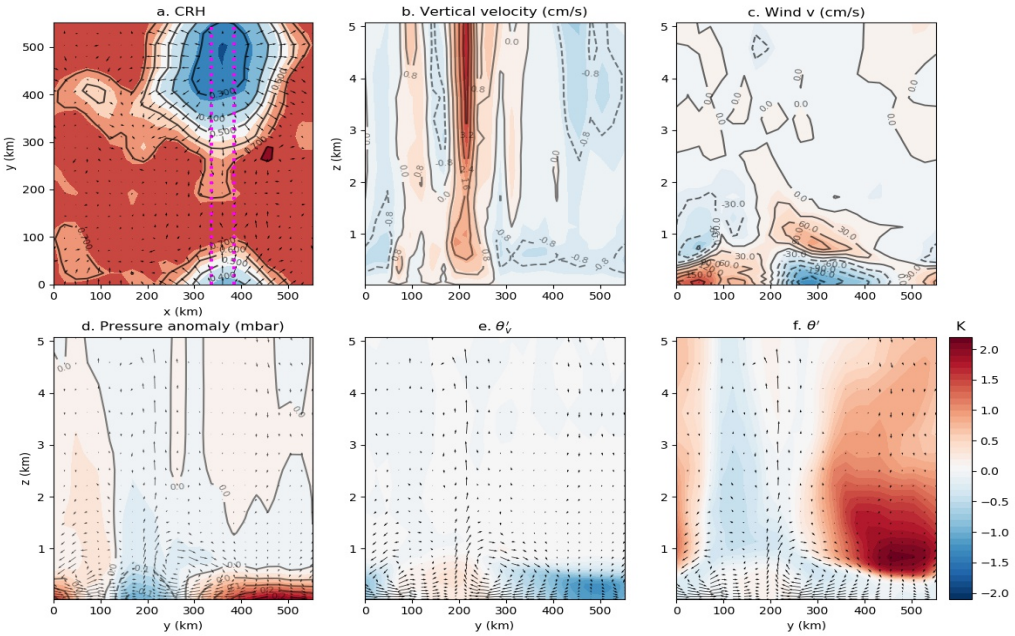

Figure 4.6: Simulation H5SST305, (a) shows CRH profile from day 32. (b)-(e) are the vertical profile between magenta line in panel (a) averaged in x direction. The dry patch is centered around $y = 500$ km. (b) and (c) shows respectively the vertical profile of vertical and horizontal velocity. (d), (e), and (f) shows respectively pressure anomaly (mbar), θ_v anomaly and θ anomaly. colorbar corresponds to panels (e) and (f).

anomaly, stronger boundary layer cooling, and SST anomaly. Here we investigate further the vertical structure of this circulation. Figure 4.6 shows a vertical cross section of winds, pressure, potential temperature (θ) and virtual potential temperature (θ_v) anomalies at day 32. We see that the divergent flow is indeed located in the boundary layer (below 1 km or so, see Figure 4.6.c) where θ_v has a large variance (Figure 4.6.e). In the free troposphere, consistent with theoretical expectations in the tropics (Sobel et al., 2001), θ_v anomalies are small.

The divergent flow can also be shown using the stream function (Ψ) in CRH - height space (Bretherton et al., 2005):

$$\Psi_i(z) = \Psi_{i-1}(z) + \sum_{CRH \in [CRH_{i-1}, CRH_i]} \overline{\rho(z)} w(z), \tag{4.8}$$

where i is the index of CRH bin (sorted), w is the vertical velocity summed in the CRH bin i, $\overline{\rho}$ is the domain-mean density profile, and $\Psi_0 = 0$ for all z. This stream function represents the total mass transport between low and high CRH bins. The stream function is negative everywhere but here for simplicity we use the absolute values. Figure 4.7 shows that it has one maximum below 3 km (which we refer to as the boundary layer divergence) and one maximum in the free troposphere (which we refer to as the deep circulation). The boundary layer divergence extends from dry to moist regions where the PSFC gradient is maximum, consistent with the boundary layer divergence of the snapshot shown in Figure 4.6.

Indeed, the maximum of the stream function Ψ at low levels is exactly equal to the boundary layer divergence out of dry regions and into moist regions:

$$\Psi_{max} = \int_0^{z_{max}} \rho u_{max}\, dz, \tag{4.9}$$

where z_{max} denotes the height of the stream function maximum, and ρu_{max} is the total mass transport through the CRH bin of the stream function maximum (about 0.65 on Figure 4.7), i.e. total mass transport from low CRH to high CRH values.

As figure 4.6 and figure 4.7 show, part of the boundary layer divergence returns to the dry region higher in the boundary layer (around ≈ 2 km), while the rest of it is transported upward. Here we define the shallow circulation as part of the flux that stays in the boundary layer (circulation below 4 km or so). It is given by $\Psi_{max} - \Psi_{min}$, where Ψ_{min} is the minimum of the streamfunction (around 4 km). It is this shallow circulation which exports low-level air with high MSE from dry regions, and imports air with low MSE at the top of the boundary layer into dry regions, i.e. up-gradient. This shallow circulation thus has negative gross moist stability, leading to aggregation, e.g. Neelin and Held

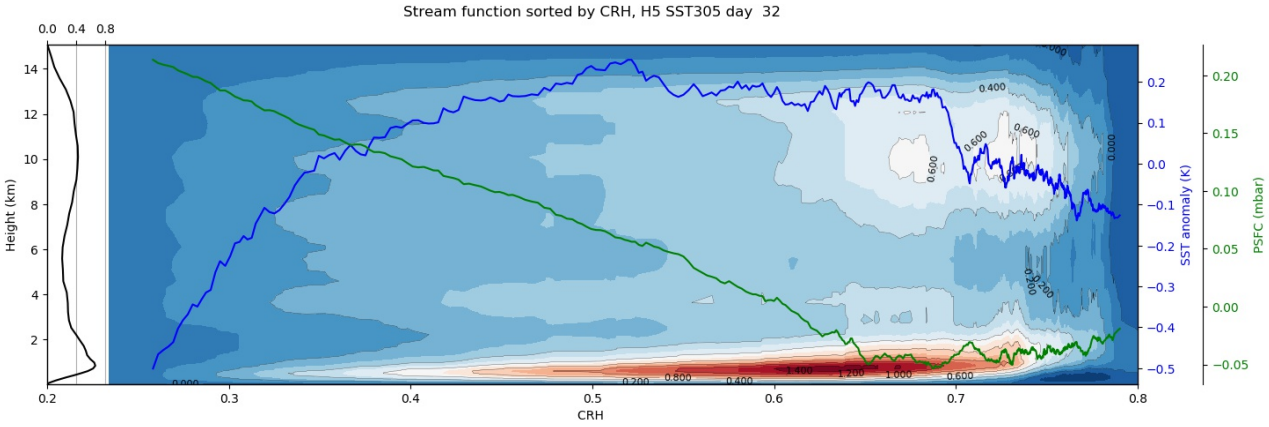

Figure 4.7: Stream function for simulation H5SST305 at day 32 (color and contours, $Kg.m^{-2}.s^{-1}$). Black line on the left side of the panel shows the stream function averaged over the domain. For simplicity, we plotted the absolute values of the stream function. Blue line shows the SST anomaly and green line shows PSFC anomaly both sorted by CRH.

(1987); Bretherton et al. (2005); Raymond et al. (2009).

The deep circulation on the other hand (which is given by $\Psi_{max,deep}$ secondary streamfunction maximum around 10 km) disfavors aggregation by transporting air with high MSE (found at high altitudes, above 10 km on Figure 4.7) out of the moist convective region, thus down-gradient (positive gross moist stability). Therefore, the more bottom heavy the circulation, the more favored the aggregation. We further explore the role of this shallow circulation, and the importance of the ratio of shallow to deep circulation on the speed of aggregation, in the following section, where we extend our study to various slab ocean depths and mean SSTs.

4.5 The impact of slab depth and SST on self-aggregation

4.5.1 Delayed aggregation with shallow mixed layer and cold SST

To investigate the impact of slab depth and domain mean SST on our findings, we extend the analysis of § 4.4 to two more depths of the slab, H= 10 and 50 meters, and one more domain mean surface temperature SST_0 = 300 K. As was shown earlier (figure 4.1 and § 4.4.1), introducing an interactive SST typically slows down the aggregation, and the delay obtained (tens of days) is comparable to the delay due to decreasing the mean SST in fixed SST simulations (from 305 K to 300 K). Based on the aggregation index (figure 4.1), we define two regimes: Regime 1 when the aggregation index stays around a constant value (ΔCRH $\approx$ 0.1) before starting its monotonic increase. We refer to this period as Latency. And regime 2 with monotonic increase of the aggregation index to its maximum value. We refer to this period as Transient. In the following we elaborate on the impact of slab depth and domain mean sea-surface temperature on each of these periods.

a. Latency

Figure 4.8 shows the relative contributions of SST anomaly and boundary layer cooling in dry regions in the different simulations. We see that with a shallower mixed layer depth, the warm SST anomaly in dry regions is larger and persists longer than with a deeper mixed layer. Thus with a shallower slab, the probability that a dry patch, at its first stage, recovers its moisture and disappears, is larger. This process can significantly delay the aggregation or potentially prevent it if the warm anomalies are large enough. For example,

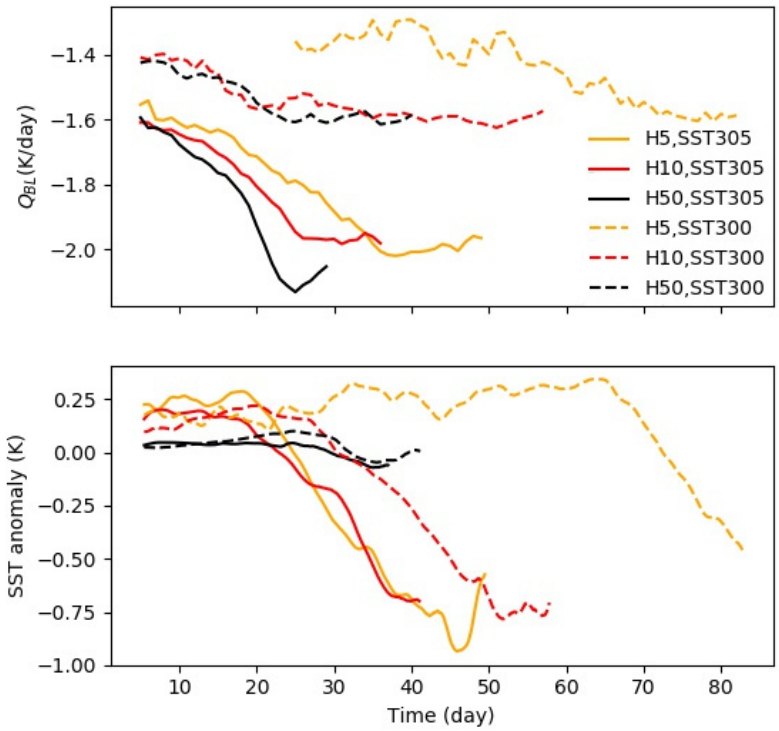

Figure 4.8: Time series of (top) differential boundary layer radiative cooling, and (bottom) surface temperature anomaly averaged over the dry patch.

the aggregation indices in the simulations with slab depth=5 m (both at 300 and 305 K) have longer latency. Thus the larger the warm SST anomalies (or the shallower the slab), the longer the latency. As Figure 4.1 shows, when the slab depth is large (especially at 305 K), the latency goes to zero. As expected, the deepest slab are close to simulations with fixed SST.

We also find that for a given slab depth, the latency is longer at 300 K compared to 305 K. Specifically, the latency for H5SST305 is about 13 days while for H5SST300 it is around 40 days. We interpret this longer latency as being the result of the significantly weaker Q_{BL} at 300 K (Figure 4.8), while SST anomalies have similar magnitudes. Weaker Q_{BL} has a smaller contribution to the high pressure PSFC, so that the chance that a dry patch with a warm SST underneath it disappears becomes larger, leading to a longer latency.

The reason why Q_{BL} is smaller at 300 K is not clear, however, it could be related to the specific humidity of the free troposphere. At 305 K, the free tropospheric specific humidity is larger (due to the thermodynamic constraint given by the Clausius-Clapeyron equation, which predicts an approximately exponential increase of specific humidity with temperature for constant relative humidity). Consequently, the decrease of specific humidity due to subsidence in dry regions, which is proportional to the specific humidity, is more rapid at 305 K compared to 300 K. The free tropospheric dryness allows the boundary layer to radiatively cool more efficiently and have a stronger contribution to PSFC. We will come back to this large scale circulation in § 4.5.2.

In summary, the longer latency at shallower slabs can be understood by the warmer SST anomaly in dry regions (Figure 4.8.b), leading to reduced surface pressure and thus reduced boundary layer divergence. But the SST anomaly is very similar at cold (300) and warm (305) SST, at least at early times. Thus the longer latency at colder SSTs is instead due to weaker boundary layer cooling (Figure 4.8.a), reducing the radiatively-driven divergence.

b. Transient

During the transient period, the aggregation index (Figure 4.1) monotonically increases to reach its maximum. As we will see here, the slope of the index evolution, which determines the timing of the aggregation, depends on the strength of the shallow circulation and associated up-gradient transport of MSE, itself function of Q_{BL} and SST anomalies.

Figure 4.8 shows that, after the latency period, both stronger radiative cooling and colder SST anomalies contribute to the high surface pressure in dry regions. The largest change comes from the SST anomaly, which drops sharply in the H10 and H5 simulations (Figure 4.8.b); the increase in radiative

cooling is more gradual and stronger in the 305 K simulations. Once these two cooling effects both contribute to higher surface pressure, aggregation progresses faster, consistent with the increase in the aggregation index (Figure 4.1).

Thus, with interactive SST, the SST anomalies have an opposition - acceleration impact on the shallow circulation. The early warm anomaly in dry regions opposes the virtually- and radiatively-driven divergent flow and concomitant export of MSE, thus opposing the aggregation; but the later cold anomaly in dry regions reinforces the divergent flow, thus reinforcing the aggregation.

This is well captured in Figure 4.9.a, which shows the strength of the shallow circulation ($\Psi_{max} - \Psi_{min}$, see § 4.4.4) in the various simulations. For the shallower slabs, the shallow circulation has a fairly constant value at the beginning followed by a rapid monotonic increase, while for deeper slabs, the SST anomalies are very small so the 'opposition-acceleration' impact is absent and the shallow circulation has a monotonic increase from the beginning. The deep circulation on the other hand (Figure 4.9.b) does not show a strong dependence on slab depth or on SST.

These results suggest that the aggregation speed is determined by the shallow circulation between dry and moist regions. Figure 4.9.b also suggests that the deep circulation is not directly linked to the aggregation progress, though we note that the free-tropospheric drying (Figure 4.3), which strongly affects the boundary layer cooling and thus the shallow circulation, is closely related to the deep circulation. Although not directly linked to the dry region strengthening and expansion, the deep circulation could therefore play a role in the onset of aggregation, through its impact on boundary layer radiation. We explore this in more detail in the next section.

4.5.2 Link with the strength of the shallow circulation compared to the deep circulation

The vertical structure of the streamfunction (Figure 4.7) shows two cells: a shallow circulation with a maximum below 3 km or so, and a deeper cell with a maximum around 10 km or so. As noted earlier § 4.4.4, the shallow circulation is given by $\Psi_{max} - \Psi_{min}$ and is associated with the boundary layer divergence out of the dry column, which occurs below the height of the maximum.

To capture more accurately the shallow circulation and its relative amplitude compared to the deep circulation (which, as noted in § 4.4.4, is given by $\Psi_{max,deep}$), we introduce a circulation efficiency η:

$$\eta = \frac{\Psi_{max} - \Psi_{min}}{\Psi_{max,deep} + \Psi_{max} - \Psi_{min}}. \tag{4.10}$$

The numerator is the fraction of boundary layer divergence out of dry regions into moist regions, which returns to the dry regions below the height of the minimum, 4 km or so. It thus indeed quantifies the shallow circulation. The denominator is the sum of this shallow circulation and of the deep circulation. The latter includes air that has converged into moist regions at low levels as well as in the free troposphere (between the minimum and the deep maximum), and returns to the dry regions above the height of the deep maximum, above 10 km or so. The denominator thus quantifies the overall large-scale circulation, measured by the total mass transport between dry and moist regions. So η (between 0 and 1) measures the fraction of mass transport between dry and moist regions which is done by the shallow circulation.

Figure 4.9.c shows the time evolution of the circulation efficiency in the various simulations. The link with the aggregation evolution is clear: the

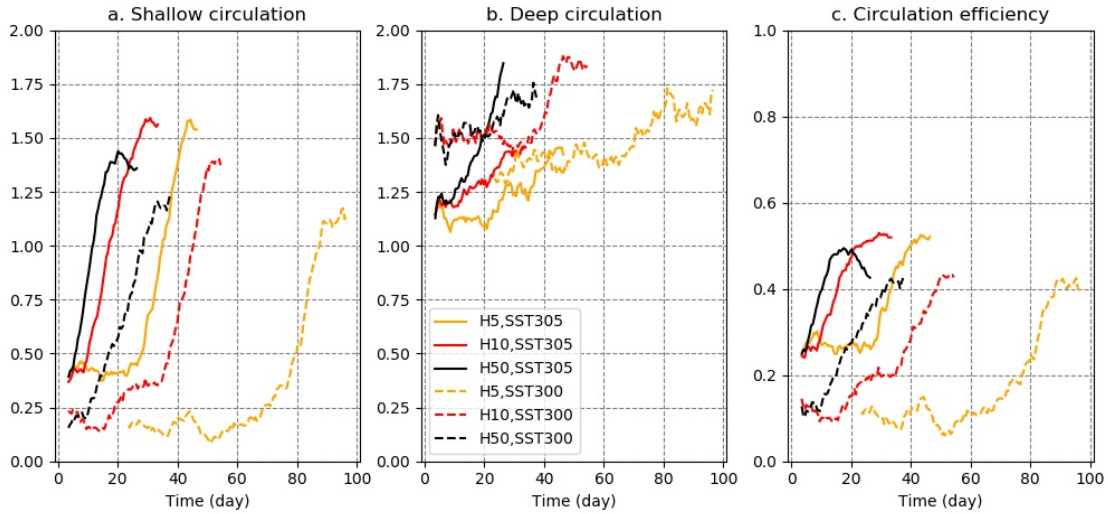

Figure 4.9: Time evolution of the (a) shallow, (b) deep circulation strength and (c) the circulation efficiency η. Plots are smoothed using a running mean with a 7 day window.

simulations with higher circulation efficiency have faster aggregation (Figure 4.1). This is consistent with earlier studies of self-aggregation, which highlight the key role played by the MSE transport of the shallow circulation. From the previous section, the shallow circulation is driven by boundary layer radiative cooling and SST anomalies in dry regions, generating hydrostatic high surface pressure anomalies through cooling and virtual effects.

As noted earlier, Figure 4.9.b suggests little contribution from the deep circulation. But larger Q_{BL} can occur in response to relatively drier upper free troposphere, itself connected to the efficiency of the deep circulation via subsidence drying. Thus, although the deep circulation has little contribution to the aggregation progress or dry region strengthening, we can not rule out its contribution to the onset of aggregation and of dry regions. The subsidence drying in the free troposphere, which can be seen in Figure 4.3, could play an important role in initiating the boundary layer cooling enhancement in dry regions, which then amplifies the drying, high pressure and low-level divergence.

The deep circulation is determined by the upward mass transport in deep moist convection, and in our doubly-periodic domain by the compensating subsidence in cloud-free areas. The strength of the subsidence velocity in cloud-free areas can be quantified using the weak temperature gradient (WTG) approximation as follows:

$$w_{WTG} = \frac{Qrad}{\Gamma}, \tag{4.11}$$

where

$$\Gamma = \frac{T}{\theta}\frac{d\theta}{dz} \tag{4.12}$$

is the stratification, $Qrad$ is the radiative cooling, T is temperature, and θ is potential temperature. Our findings show that (Figure 4.10) $Qrad$ in the dry region is larger at higher SST (Figure 4.10.b), but so is Γ (Figure 4.10.a), so that W_{WTG} does not explain the different timings of aggregation between the two SSTs (Figure 4.10.c): for instance 5-305 and 5-500 have approximately the same maximum W_{WTG} while their aggregation speed is very different (Figure 4.1; we note in passing that the maximum W has similar magnitude but occurs higher in the warmer simulation, consistent with theoretical expectations; Singh and O'Gorman (2012)).

But enhanced drying is still expected from subsidence, as it is given by $W_{WTG}\partial q_v/\partial z$, and the gradient of specific humidity $\partial q_v/\partial z$ is larger at warmer SSTs (Figure 4.10.d). It should be mentioned that the horizontal tendency is similar between the simulations with different SSTs and slab depths (not shown) so that, to the first order, the total tendency is dictated by the vertical term, $W_{WTG}\partial q_v/\partial z$. In the subsiding regions, the free tropospheric drying is thus expected to be stronger at warmer SST, enhancing the boundary layer cooling and the radiatively-driven divergence. We suggest that the positive PSFC anomaly in the dry region is the organizer of the convective clouds by exporting low level moist air from the dry patches and expanding them. But

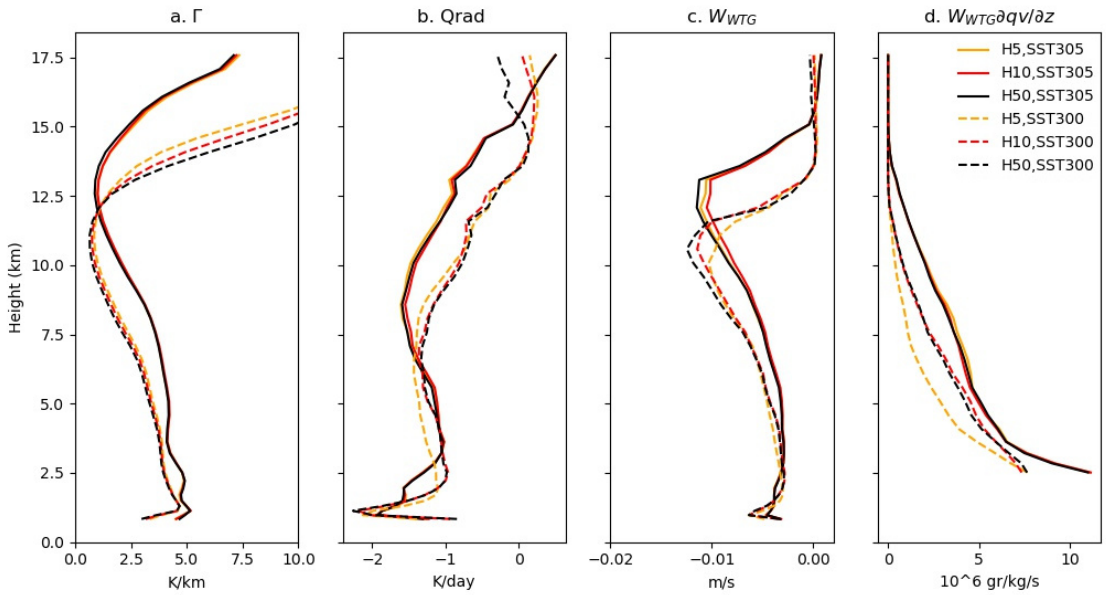

Figure 4.10: Plot shows: a) the stratification, b) atmospheric radiative cooling, c) vertical velocity computed by WTG, and c) dryness tendency. The variables are averaged over transient part ($0.2 < \delta CRH < 0.5$ in Figure 4.1)

the formation of a positive PSFC anomaly is a response to the large-scale deep circulation and free-tropospheric drying, and is necessary for the persistence and expansion of dry patches leading to the confinement of convection.

4.6 Conclusions

The importance of sea surface temperature on the aggregation of convective clouds has been shown in earlier studies, however mostly using a constant and uniform SST (e.g., Wing (2019)). Here we study the feedbacks between an interactive SST and the aggregation of convective clouds using a 3D RCE setup. To have an interactive surface temperature, we use an slab ocean with fixed mean SST but locally varying temperature.

Consistent with earlier studies, we find that the presence of an interactive SST delays the aggregation of convection, and the stronger the interaction (smaller slab depth) the longer the delay. It has been suggested (Hoheneg-

ger and Stevens, 2016) that this delay could be due to the development of an SST gradient between dry and moist regions, with a warm anomaly in dry regions opposing the shallow circulation believed to play a crucial role in the aggregation process. Indeed, the onset of aggregation, and the associated strengthening and expansion of dry regions, is associated with a shallow circulation (below 4 km or so). This shallow circulation diverges from dry regions near the surface and in the boundary layer, and returns back into dry regions just above the boundary layer. It thus transport MSE from dry into moist regions, i.e. up-gradient, and has negative gross moist stability, reinforcing MSE gradients and leading to aggregation (Bretherton et al., 2005; Muller and Held, 2012).

We find that the surface temperature anomaly underneath the dry patches actually depends on their dryness. At first, the dryness is small, and warming by shortwave radiation dominates the cooling by latent heat flux and surface longwave radiation, so that the surface under the dry patch warms. But when the dryness becomes large, the surface can cool more efficiently due to predominantly enhanced surface longwave radiative cooling as the column is dry and downward longwave radiation reduces (the dryness also results in the enhancement of LHF though it is small compared to longwave radiative cooling).

This first positive and then negative SST anomaly in dry regions has an impact on the surface pressure anomaly in dry regions, which is important for driving the aforementioned shallow circulation and guaranteeing the growth and expansion of the dry patch. When positive, the SST anomaly under the dry patch opposes the divergent boundary layer flow out of the dry patch, while if negative it adds to the positive PSFC anomaly and further helps the divergent flow and concomitant expansion of the dry patch. However, even with an initially positive SST anomaly, the dry patch has a positive PSFC,

due to enhanced boundary layer radiative cooling. This radiative cooling decreases the boundary layer temperature and humidity via subsidence drying, resulting in higher PSFC (by virtual effects). Then, when the SST anomaly becomes negative, it adds to the high PSFC anomaly and thus enhances the divergent flow from dry regions and the aggregation. So the SST anomaly has an opposition - acceleration impact on aggregation, and the differential boundary layer radiative cooling and virtual effects are necessary for triggering the aggregation.

In the Earth's tropics, the surface temperature in clear-sky areas is usually warmer than the surrounding as a result of enhanced shortwave radiation at the surface, broadly corresponding to the initial warming discussed above. The second cooling phase discussed above, which occurs after tens of days, requires a dry atmosphere. In our simulation at 300 K, when the precipitable water at the center of the dry patch reaches below about 15 mm (corresponds to CRH ≈ 0.4) the net surface radiation can have a cooling effect. Using ERA5 reanalysis, we find that over the tropics, PW $\leq$ 15 mm is not rare. However, the cooling effect is a slow process and its time scale depends on the depth of ocean mixed layer. In our CRM simulations with double periodicity, the dry patches are persistent enough for the surface cooling by radiation to become important. Whether this can be the case over the tropics deserves further investigation.

We note that although the PSFC anomalies originate from boundary layer virtual temperature anomalies, they are the result of the response of the boundary layer to the free tropospheric moisture reduction. It is indeed the free-tropospheric drying which allows larger boundary layer radiative cooling and injection of free tropospheric dry air into the boundary layer. The PSFC anomaly is thus the organizer of convection, or the amplifier of ag-

gregation, by creating the shallow circulation which transports low-level air with high MSE up-gradient and favors aggregation. But the free-tropospheric drying appears to be initiating the process. A circulation efficiency, which measures the strength of the shallow circulation relative to the overall circulation (shallow + deep), is found to correlate well with the speed of aggregation. Interestingly, the shallow circulation strength increases strongly in the simulations as aggregation proceeds, while the deep circulation remains much more constant. When the SST anomaly in the dry patch turns negative, the shallow circulation shows a clear strengthening due to the increased high PSFC anomaly.

Using different slab depths and SSTs, our findings confirm that the aggregation is faster with deeper slab and at higher SST. When the slab is shallow, warm SST anomalies that form at the early stage of dry patches weakens the pressure anomalies thus the shallow circulation. This weakening delays the aggregation. We also find that at higher SST, the boundary layer radiative cooling is larger for the same dryness, so that the negative impact of the warm SST anomaly on PSFC is less important compared to the positive impact of the stronger boundary layer radiative cooling.

The initial free-tropospheric drying is also found to be sensitive to SST. The free tropospheric radiative cooling is stronger at higher SST (but largely independent of slab depth for a given SST). However, the atmospheric stratification is also larger at higher SST so that the free-tropospheric subsidence velocity calculated using the WTG approximation (Sobel et al., 2001) does not explain the different speeds of aggregation in our simulations. But the resulting free-tropospheric moisture tendency is larger at higher SST. Larger free-tropospheric drying at warmer SST yields enhanced boundary layer radiative cooling, itself leading to the formation of positive PSFC anomalies. Therefore

the boundary layer shallow circulation determines the speed of aggregation, but the deep circulation, and the associated free-tropospheric drying, appear to be necessary for the formation of a high surface pressure anomaly in dry regions leading to the shallow circulation.

Acknowledgments This project has received funding from the Marie - Sklodowska Curie Actions (MSCA) under the European Union's Horizon 2020 research and innovation programme (grant agreement No. 675675). CJM gratefully acknowledges funding from the European Research Council (ERC) under the European Union's Horizon 2020 research and innovation programme (Project CLUSTER, grant agreement No. 805041). The authors also thank Grand Équipement National De Calcul Intensif (GENCI), France, for providing access and support to their computing platforms Très Grand Centre de Calcul (TGCC). The data that support the findings of this study are available from the corresponding author upon request.

Appendices

4.A Impact of interactive SST with constant deep ocean sink

As mentioned in § 4.3.3, the incoming solar flux in the tropics exceeds the threshold for runaway greenhouse warming (Pierrehumbert, 2010). As a consequence, in closed domain simulations with interactive SST such as those used here, without the oceanic and atmospheric transport of energy out of the tropics, the SST increases without bound (Hohenegger and Stevens, 2016). Relaxing the domain mean SST to a target SST, as is done in this study, allows to prevent this runaway greenhouse warming, and maintains the domain mean SST close to constant.

Another possibility to avoid the runaway greenhouse warming is to add a sink of energy, e.g. into the deep ocean (following Romps (2011)). Figure 4.11 shows the time evolution of the aggregation index, domain-mean PW, and domain-mean SST for simulations where a spatially and temporally constant ocean sink of energy of varying strength (from 0 to 120 W m^{-2}) is added to the surface energy budget (negative term added to the right-hand side of equation 4.2 instead of the relaxation term on the left-hand side). The slab depth is 10 meters and the initial temperature is 300 K for all simulations. In order to investigate the sensitivity to the amount of sink, four different sinks of energy are tested: 0, 30, 60, and 120 W m^{-2}.

For all 4 sinks, the aggregation proceeds. For sink = 0 W m^{-2}, as expected, the domain-mean SST increases quickly. The aggregation reduces the increasing trend of SST (as aggregation is associated with increased Outgoing

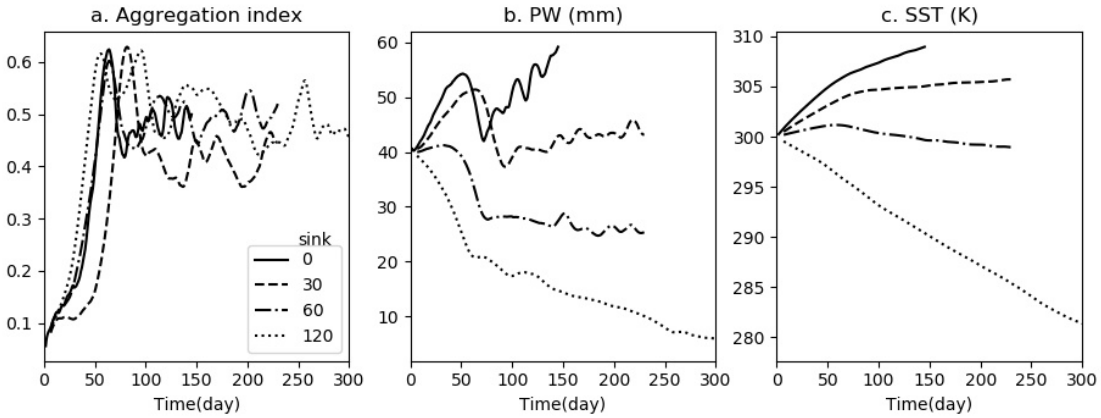

Figure 4.11: Time evolution of aggregation index (black) PW (blue) and domain mean surface temperature (green) for a simulation with constant sink equal to 60 W/m2.

Longwave Radiation, or OLR, cooling, e.g. Wing and Emanuel (2014)) but does not stop it, as the amount of energy reaching the surface is still large and it is thus not in equilibrium energetically. PW shows a sharp reduction with aggregation but with surface warming, it continues increasing. For sink = 30 W m^{-2}, the domain mean SST has a very modest increase after aggregation as the sink of energy is very close to the surface energy imbalance when aggregated (40 W/m^2). The simulation with sink = 60 W/m^2 starts cooling after aggregation but does not disaggregate with cooling (not shown) as the aggregation is favored even at cold SST = 295 K in our simulations (Shamekh et al., 2019).

When the energy sink is large, equal to 120 W m^{-2}, the surface cools strongly and the cooling is enhanced by aggregation. Interestingly, this simulation disaggregates partially around SST = 293 K, but aggregates again when the SST drops below 285 K. The disaggregation - re-aggregation can not be seen easily in the plots as the disaggregation does not happen completely but the dry patch shrinks.

We note that our results do not indicate that self-aggregation could be a

way for tropical temperatures to regulate themselves, as was hypothesized in past studies (e.g. Khairoutdinov and Emanuel (2010)). Indeed, since aggregation is associated with icreased OLR, it was suggested that as SST increases, self-aggregation is favored, yielding more OLR cooling and reducing the SST back towards its initial value. So maybe the tropical atmosphere could "regulate" its temperature through modulation of its convective aggregation. In contrast, the oscillation between aggregation - disaggregation does not happen in our simulations, as the aggregation is favored over a large range of SST.

In summary, independent of the sink, all the simulations aggregate. But the final SST and PW of the simulations depend on the sink of energy. In order to minimize drift in domain mean SST, and also to avoid the sensitivity of results to the strength of the imposed ocean sink, in this study we instead avoid the runaway greenhouse climate by relaxing the domain mean SST towards a target temperature.

4.B Surface pressure computation

The goal of this Appendix is to derive the equation for the surface pressure anomaly in dry regions (equation 4.7). We use standard notations (same as those used in the main text). We suppose hydrostatic balance $dp = -\rho g dz$ which, along with the ideal gas law $p = \rho R_d T_v$, yields

$$\frac{\partial \ln p}{\partial z} = -\frac{g}{R_d T_v}, \tag{4.13}$$

where for simplicity of notations, we drop the z dependence, i.e. it is understood implicitly that $T_v(z)$ is a function of z.

We are interested in surface pressure anomaly in the dry patch compared

to the domain-mean. And we know this pressure anomaly is sourced from just the boundary layer (virtual temperature anomalies are negligible above the boundary layer, see e.g. Figure 4 and 6 of the paper). We therefore integrate the above equation from the surface $z = 0$ to the boundary layer top z_{BL} (with pressure p_{BL}) yielding

$$PSFC = p_{BL} \exp\left[\frac{g}{R_d}\int_0^{z_{BL}} \frac{1}{T_v} dz\right]. \tag{4.14}$$

If we further neglect variations in boundary layer height z_{BL} and pressure p_{BL}, we obtain for the surface pressure anomaly in dry regions:

$$\begin{aligned} PSFC' &= PSFC_d - \overline{PSFC} && (4.15)\\ &\approx p_{BL} \exp\left[\frac{g}{R_d}\int_0^{z_{BL}} \frac{1}{T_{v,d}} dz\right] - p_{BL} \exp\left[\frac{g}{R_d}\int_0^{z_{BL}} \frac{1}{\overline{T_v}} dz\right] && (4.16)\end{aligned}$$

where the overbar denotes domain averaged quantities and subscript d refer to quantities averaged in the dry regions. Since $T_{v,d} = \overline{T_v} + T_v'$ with $T_v' \ll \overline{T_v}$,

$$\begin{aligned} PSFC' &\approx p_{BL} \exp\left[\frac{g}{R_d}\int_0^{z_{BL}} \frac{1}{\overline{T_v}} dz\right]\left(\exp\left[\frac{g}{R_d}\int_0^{z_{BL}} \frac{-T_v'}{\overline{T_v}^2} dz\right] - 1\right) && (4.17)\\ &\approx \overline{PSFC}\left(\frac{g}{R_d}\int_0^{z_{BL}} \frac{-T_v'}{\overline{T_v}^2} dz\right) && (4.18)\end{aligned}$$

Since $T_v \approx T\,(1 + 0.61 q_v)$, we obtain equation 4.7:

$$PSFC' \approx \overline{PSFC}\frac{g}{R_d}\int_0^{z_{BL}} \frac{-1}{\overline{T_v}}\left(\frac{T'}{\overline{T}} + \frac{0.61 q_v'}{1 + 0.61\overline{q_v}}\right) dz \tag{4.19}$$

4.C Sensitivity simulations and low-level radiative cooling

In order to verify the importance of boundary layer radiative cooling, we run 3 sensitivity tests by homogenizing the radiative cooling profile at: 1. all levels (mentioned as homrad in Figure 4.12, 2. in the boundary layer which we crudely define to be up to 1 km above the surface, and 3. in free troposphere (referred to as BL-homorad), above 1 km to the top of the domain (mentioned as FT-homrad).

As figure 4.12 shows for both temperatures, 300 and 305 K, radiative cooling feedbacks are necessary for self-aggregation so that homogenizing the radiation profile prevents the self-aggregation. The results also show that for FT- homrad, in which the radiation is homogenized only in free troposphere, the aggregation proceeds without significant difference from the control simulations (fullrad). But homogenizing the boundary layer radiative feedback (BL-homrad in Figure 4.12) prevents the aggregation. These findings are consistent with Bretherton et al. (2005) who emphasize the role of low-tropospheric / boundary layer radiative cooling, as well as with Muller and Held (2012) who find the shallow clouds radiative feedbacks to be important for the aggregation onset.

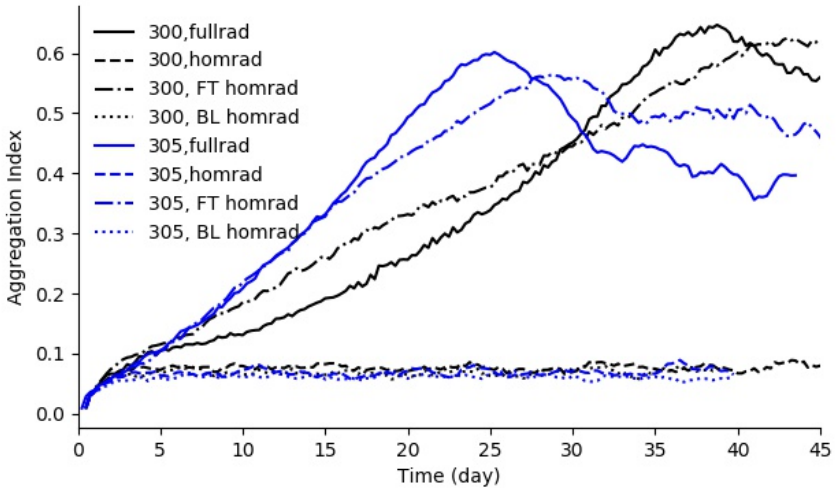

Figure 4.12: Plot shows the aggregation index time series for the sensitivity tests at 300K (black curves) and 305 K(blue curves). Homrad, FT and BL stand for homogenized radiation, free troposphere and boundary layer respectively.

Chapter 5

Impact of the diurnal cycle on the aggregation of convective clouds with interactive surface temperature

Convective aggregation is known to be closely linked to radiative feedbacks, however the aggregation studies are mostly done using a constant incoming solar radiation. Here we investigate how the diurnal cycle (DC) changes the progress of aggregation with an interactive sea-surface temperature (slab ocean). Furthermore, we investigate how the diurnal cycle impacts the circulation and precipitation before and after reaching the aggregated state. Although the daily-averaged profile of radiation evolves similarly between the simulations with and without DC, we find that the presence of a diurnal cycle significantly accelerates the aggregation process. This acceleration is larger for shallower ocean slab depths (more interactive sea-surface temperatures). With DC, persistent dry patches form in a few days, and can be traced back to initial precipitation-driven cold pools and concomitant surface cooling. This new

initiation process for aggregation and its acceleration has important implications for the relevance of self-aggregation to the Earth's atmosphere, which is still debated as the aggregation is often considered to be a slow phenomenon compared to other atmospheric processes.

5.1 Introduction

Studies of tropical deep convections have long noticed the existence of diurnal variation of deep convective activity and precipitation over the tropical ocean (Gray and Jacobson, 1977; Randall et al., 1991; Hendon and Woodberry, 1993; Nesbitt et al., 2000; Duvel, 1988, 1989). These two elements show a strong nocturnal-early morning peak and a weak secondary later afternoon one. The diurnal cycle of convective activity has been found to be more pronounced when the convective clouds are organized (Gray and Jacobson, 1977; Machado et al., 1993; Liu and Moncrieff, 1998; Ruppert and Hohenegger, 2018). The large scale organized convective system such as the one associated with the Inter-tropical Convergence Zone (ITCZ) and ITCZ forced large scale circulation, also shows a clear diurnal pulsing which is mostly explained through the diurnal cycle of deep convection (Deser and Smith, 1998; Bain et al., 2010; Ciesielski et al., 2018). The diurnal cycle has been also identified in the upward mass flux of tropical cyclones (Davis and Ahijevych, 2012; Nicholls, 2015), their precipitation (Bowman and Fowler, 2015), and their cirrus canopy extent (Kossin, 2002). The boundary layer divergent flow which is found to be crucial for the convective organization in idealized simulations (Bretherton et al., 2005; Muller and Held, 2012; Hohenegger and Stevens, 2016) shows a strong enhancement in the morning.

Two main mechanism have been proposed to explain the diurnal cycle

of convective activity over tropical oceans, both invoking the diurnal cycle of incoming solar radiation. Randall et al. (1991) suggested a direct convection-radiation interaction mechanism in which cloud top warming by shortwave absorption stabilizes the column thus weakens the convective activity during daytime. At night, the top cloud long wave radiative cooling destabilizes the cloud layer, enforces the convection thus the vertical mass flux and boundary layer convergence. The second mechanism, proposed by Gray and Jacobson (1977), suggests a clear-cloudy sky differential radiation based mechanisms. The strong night time free tropospheric radiative cooling results in a strong subsidence which then drives a divergent flow out of the clear region and into the clouds and intensifies the convective activity. During the day, reduced radiative cooling due to the shortwave absorption reduces the subsidence and the divergent flow thus the convective activity is weakened. The daytime weakening of boundary layer divergent flow has been confirmed by Deser and Smith (1998) for the Western Pacific region. They hypothesize that the diurnal heating sea surface can weaken the low-level divergent flow during the day and intensifies it at night. Based on either of these mechanisms, the large scale circulation especially the low-level divergent flow shows a diurnal cycle which is more pronounced when the convection is organized.

Although the impact of the organization of convection on the diurnal cycle of convective activity and precipitation has been well studied (Gray and Jacobson, 1977; Chen and Houze, 1997; Liu and Moncrieff, 1998; Ruppert and Hohenegger, 2018), the impact of the diurnal cycle on the formation of convective clusters and aggregation has not received much attention. In numerical simulation of aggregation, very few studies include the diurnal cycle, as it is assumed not to have a significant impact on the equilibrium state (albeit a slight amplification of the precipitation diurnal variation and earlier maximum precipitation (Ruppert and Hohenegger, 2018)). The equilibrium state

of the aggregation, which is determined by the balance between atmospheric radiative cooling and precipitation, seems to be independent of the progress of aggregation. Despite this, it is not clear if the diurnal cycle has an impact on the time scale of triggering and the progress of aggregation.

Hohenegger and Stevens (2016) briefly mentioned that in their 3D RCE simulations with interactive SST, the aggregation is slowed down when the diurnal cycle is included. A recent study by Haerter et al. (2020) shows that the formation of the cloud cluster is significantly accelerated with the diurnal cycle. In their simulation, the surface temperature has a realistic imposed diurnal oscillation and the latent heat flux is reduced to 70 % of its value in order to mimic land properties. They find that the SST oscillation with large amplitude triggers deep convection and strong cold pools which then facilitate the clustering of convection.

In this chapter, we investigate the impact of the diurnal cycle on the aggregation of convective clouds when SST is interactive. Section 5.2 introduces the simulation setup. Section 5.3.1 discusses the diurnal cycle of precipitation and circulation, and the impact of aggregation on their diurnal variability. Section 5.3.2 investigates the formation of dry patches in simulations with DC. In section 5.3.2 we also compare the aggregation progress in the simulation with and without DC in order to clarify the impact of the diurnal cycle. A summary of the main results is provided in section 5.4.

5.2 Experimental setup

In this chapter we use the same simulation setup as in chapter 4 but include the diurnal cycle. Notably, the diurnal mean solar irradiance is the same as chapter 4, but spread over the day (sunrise at 6am, sunset at 6pm) with a

Slab depth (m)	mean SST (K)	solar radiation
1	300, 305	DC, PS
2	300, 305	DC, PS
5	300, 305	DC, PS
10	300, 305	DC, PS
50	300, 305	DC,PS
200	300, 305	DC
Fixed SST	300, 305	PS

Table 5.1: List of the simulations with diurnal cycle (DC) and constant perpetual solar radiation (PS).

maximum at noon following Collins et al. (2004), and the domain mean SST is relaxed towards a target values SST_0 as in Equation 4.2. We also include the results for two more, very shallow, slab depths H=1 and 2 meters to our simulations. The list of simulations is provided in Table 5.1. It should be mentioned that for the shallow slabs 1 and 2 meters, the relaxation time of 2 hours results in respectively 0.2 and 0.1 K warming. One might think that this warming potentially impacts the aggregation speed. To verify this, we run two more simulations with slabs 1 and 2 meters and with relaxation term equals to 1 min. The results is very similar to the one with $\tau = 2$ hours, meaning that the warming of the order of 0.1 K does not have a large impact on the speed of aggregation as the other forcing have not been changed.

Similar to chapter 3, we use column relative humidity (CRH) to define the dry patches so that $\text{Area}_{CRH<0.6}$ is the dry region. To refer to each simulation, we use DC for simulations with the diurnal cycle and PS (perpetual sun) for simulations with constant incoming solar radiation. We add the slab depth and SST_0 so that a simulation is referred to as H-SST-DC(PS). For example, 5-305-DC is a simulation with a slab depth of 5 meters, mean SST of 305 K, and with diurnal cycle.

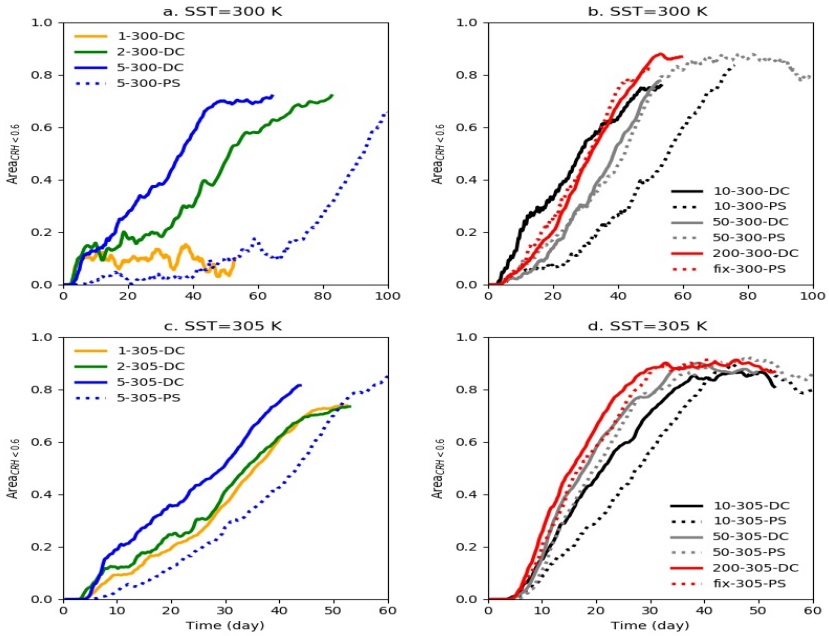

Figure 5.1: Time series of the aggregation index. The lines and dotted lines show the simulations with and without the diurnal cycle respectively. For more readability, the times series are presented in two panels for each SST_0. As the simulations with slab depth of 1 and 2 meters and without DC do not aggregate, we have not included them in the plot.

5.3 Results

Figure 5.1 shows the progress of the aggregation index for simulations with different slab depths at $SST_0 = 300$ and 305 K. Interestingly, for the deepest slabs (200 and 50 meters), the progress of the aggregation index is similar with and without DC. With a deep slab the SST variations (diurnal oscillation as well as SST anomalies) are small. Hence when the SST is approximately constant, including a diurnal cycle has a negligible impact on the aggregation progress without the SST response to the diurnally varying radiation. For the shallower slabs though (H= 10, 5, 2 and 1 m), the aggregation index shows a rapid increase around days 3-7. After this period, the aggregation slows down and then accelerates again. For example, 2-305-DC has a sharp increase at the beginning from day 3 to day 7, followed by a slower period from day 7 to 25, and an accelerated final period to reach its maximum.

With the diurnal cycle, the aggregation occurs even with slab depth = 1 (only at 305 K) and 2 meters. Furthermore, the dependency on the slab depth reduces and the aggregation accelerates for shallow slabs. Compared to PS simulations, it seems that the diurnal cycle removes the latency (defined as in section 4.5.1, i.e. as the initial period when the aggregation index remains approximately constant before starting its monotonic increase) so the aggregation index starts increasing straightaway. For instance, 5-300-PS has a latency of around 60 days that is completely removed in 5-305-DC. The fact that the diurnal cycle impacts the aggregation only for the shallow slabs, indicates a potential role of SST oscillations and anomalies which are significant for shallow slabs.

To investigate the behavior of aggregation with DC, in section 5.3.1, we firstly explore how DC impacts precipitation, shallow flux, and surface latent heat flux and what role the slab depth plays. We explore how the aggregation changes the diurnal variability of these elements. Second, in section 5.3.2, we investigate the accelerated aggregation with DC by exploring the early time increase of aggregation index in shallow slab simulations. We also investigate whether the transient part of aggregation is affected by the diurnal cycle.

5.3.1 The diurnal cycle in aggregating simulation

In this section, we investigate the diurnal variation of variables of interest such as shallow flux, latent heat flux, and precipitation, and how aggregation impacts these variations. In our analysis, we look at two periods: 1- the early stage of the simulation, when the aggregation is not yet started or just started so that the clouds are still randomly distributed over the domain. For this period we select 5 days, day 4 to day 9. We refer to this period as 'non-agg'. 2- When the aggregation is well established. For this period, we select

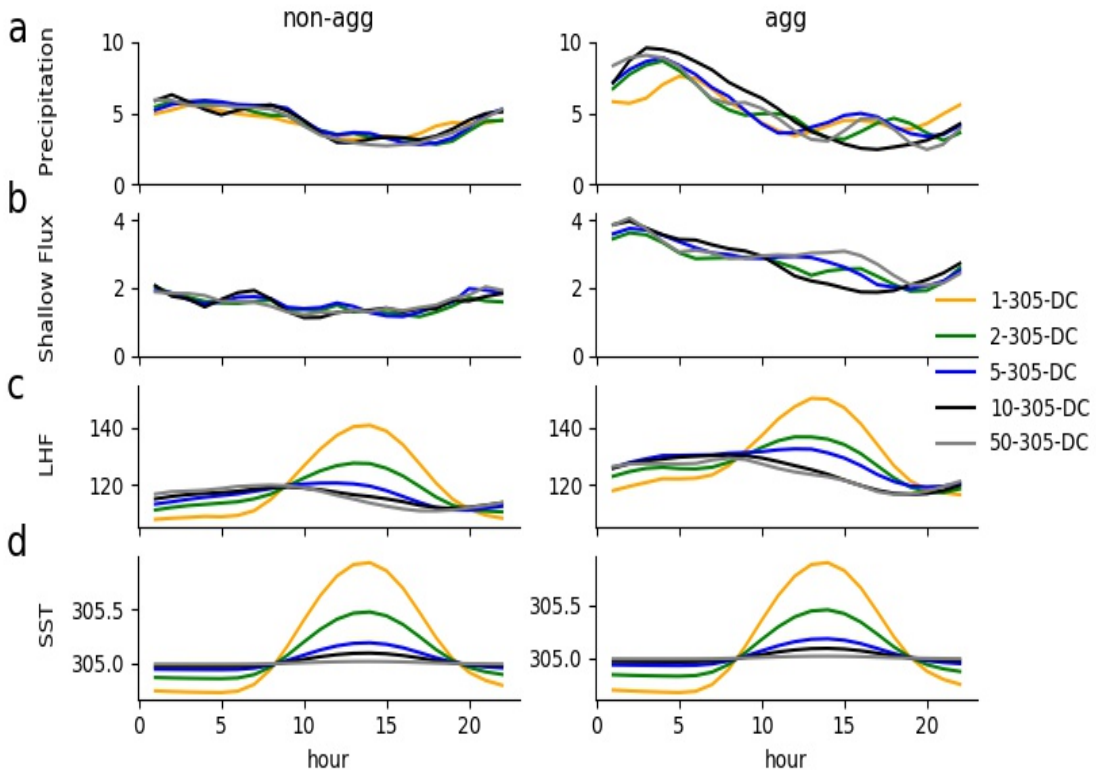

Figure 5.2: Plot shows the composites of a. the domain mean precipitation (mm/day), b. the maximum of shallow flux (kg/m^2/s, and (c) the domain mean surface latent heat flux (W/m^2) for non-aggregated (left column) and aggregated (right column) situations for simulations at 305 K with diurnal cycle. Plot is smoothed by a 3-hour running average.

5 days for which the aggregation index is around its maximum so the clouds are well clustered in a small fraction (about 20-25 %) of the domain. We refer to this period as 'agg'. We must mention that 'agg' state has different timing depending on the slab depth and mean SST (Figure 5.1). As the 3D outputs of all the simulations are not available (due to the cluster limitations), we show the analysis only with SST_0 = 305 K.

Figure 5.2.a shows the diurnal variation of domain mean precipitation. The maximum precipitation occurs around 3 in the morning and its timing is the same for all the slab depths except H = 1 m. This timing does not show a significant dependency on the aggregation state. This is in contrast with Ruppert and Hohenegger (2018) who found that aggregation shifts the

maximum precipitation to earlier morning by 4 hours. Here, the clear impact is that with aggregation, the peak of precipitation is sharper and the precipitation is enhanced by 3-4 mm/day. The enhancement of precipitation with aggregation is probably due to the larger net atmospheric radiative cooling. With aggregation, a large fraction of the domain is dry and cloud free, so that it can effectively cool by radiation, thus subsidence occurs over a larger area and enforces a stronger precipitation, the same mechanism suggested by Gray and Jacobson (1977).

In observations, the precipitation over the ocean usually has a secondary peak which occurs later in the afternoon, around 6 pm (Sui et al., 1997; Yang et al., 2008). This secondary peak is hard to detect in our simulations especially in non-aggregated case, as it is not a significant signal compare to the hourly variation of precipitation. However, a small secondary peak can be detected between 16-18 o'clock (except for 10-305-DC) for aggregated case. An ensemble run is necessary to confirm the existence of this secondary peak, but here we will instead focus on the aggregation time scale and link with the shallow circulation discussed in earlier chapters.

The shallow flux has one peak that happens around 3 in the morning (Figure 5.2.b). The stronger convergence at night has been confirmed in previous studies (Gray and Jacobson, 1977). With the aggregation, the shallow flux strengthens, consistent with chapter 3. The precipitation and shallow flux are strongly correlated and the shallow flux maximum occurs slightly earlier than precipitation maximum.

Figure 5.2.c shows the diurnal variation of surface latent heat flux. These variations and the timing of its minimum and maximum depend on the slab depth and the aggregation state. For non-aggregated cases, LHF plot shows one peak at 7, 8, 12, 14, and 14 for 50-305-DC, 10-305-DC, 5-305-DC, 2-305-

DC, and 1-305-DC respectively. So the shallower the slab the later is the peak of LHF. To explain this pattern, we first mention that near-surface relative humidity does not change significantly with the diurnal cycle so LHF is mostly controlled by the SST variation and the wind magnitude. When the slab is shallow, the SST variation is large so LHF is mostly controlled by SST, especially for non-agg case where the shallow flux is small. This explains why LHF is in phase with SST for 2-305-DC and 1-305-DC. For deeper slabs, the SST anomaly does not have large variation so LHF is mostly controlled by the surface wind which is larger early morning. With aggregation, 2-305-DC and 1-305-DC show a weak secondary peak around 2-4 in the morning. This peak is probably the result of enhanced surface wind which has a maximum overnight/early morning (based on the shallow flux variation). With aggregation, 50-305, 10-305 and 5-305 have a slight shift in their maximum to the earlier morning that further emphasizes the role of shallow flux (or equally surface wind) on surface fluxes. As expected, with aggregation, LHF increases in all 5 simulations studied here due to stronger boundary layer shallow flux and to the reduced relative humidity in the first layer of the atmosphere.

5.3.2 Diurnal cycle vs constant solar radiation

Figure 5.3 shows two DC simulations 2-305-DC and 5-300-DC and one PS simulation 5-305-PS to detect the formation and growth of dry patches. In the two simulations with DC (Figure 5.3.a and b), the dry patches are detectable at day 5 and they grow fast compared to the PS simulation, in which (Figure 5.1 and Figure 5.3.c) the dry patches appear later and grow comparatively slowly. These two differences, faster appearance and faster growth of dry patche,s are the reason for accelerated aggregation in DC cases. This difference is significant when the slab depth is shallow, while for the deep slabs (H >= 50 m) the

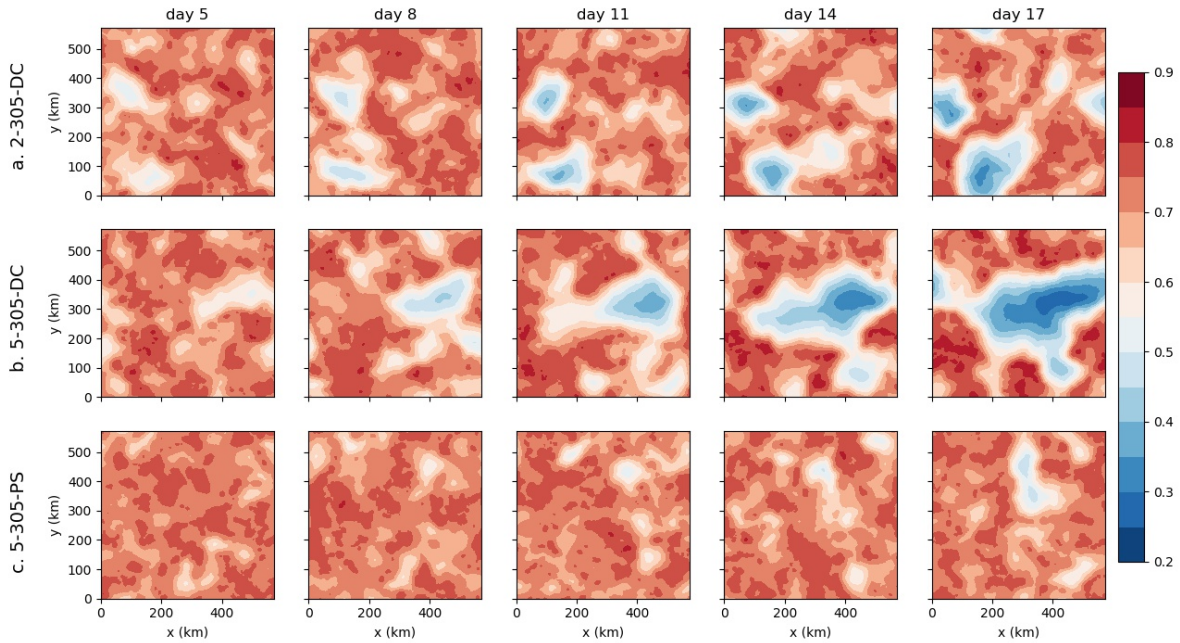

Figure 5.3: The spatial distribution of CRH as a function of time in 2-305-DC (a), 5-305-DC (b), and 5-305-PS (c). Each plot is averaged over one day.

progress of aggregation is fairly similar. In this section, we first investigate the faster initiation and whether it is enough for the faster aggregation. Further on, we compare the transient time of aggregation (after the dry patches first form, but before the full aggregated state is reached) between DC and PS simulations.

a. Dry patch formation

Coppin and Bony (2015) found that the triggering of aggregation is preceded by a rapid expansion of dry/cold patches. In their simulations, these dry/cold regions are associated with a subsiding thus dry mid-troposphere, and the presence of shallow clouds. The time scale of formation of a dry subsiding region is set by the atmospheric overturning circulation (Tompkins and Craig, 1998; Grabowski and Moncrieff, 2004), thus this preconditioning is a slow process. The dry patches that form in the simulation 50-305-PS are likely through this mechanism (Figure 5.4 showing the time evolution of conditions

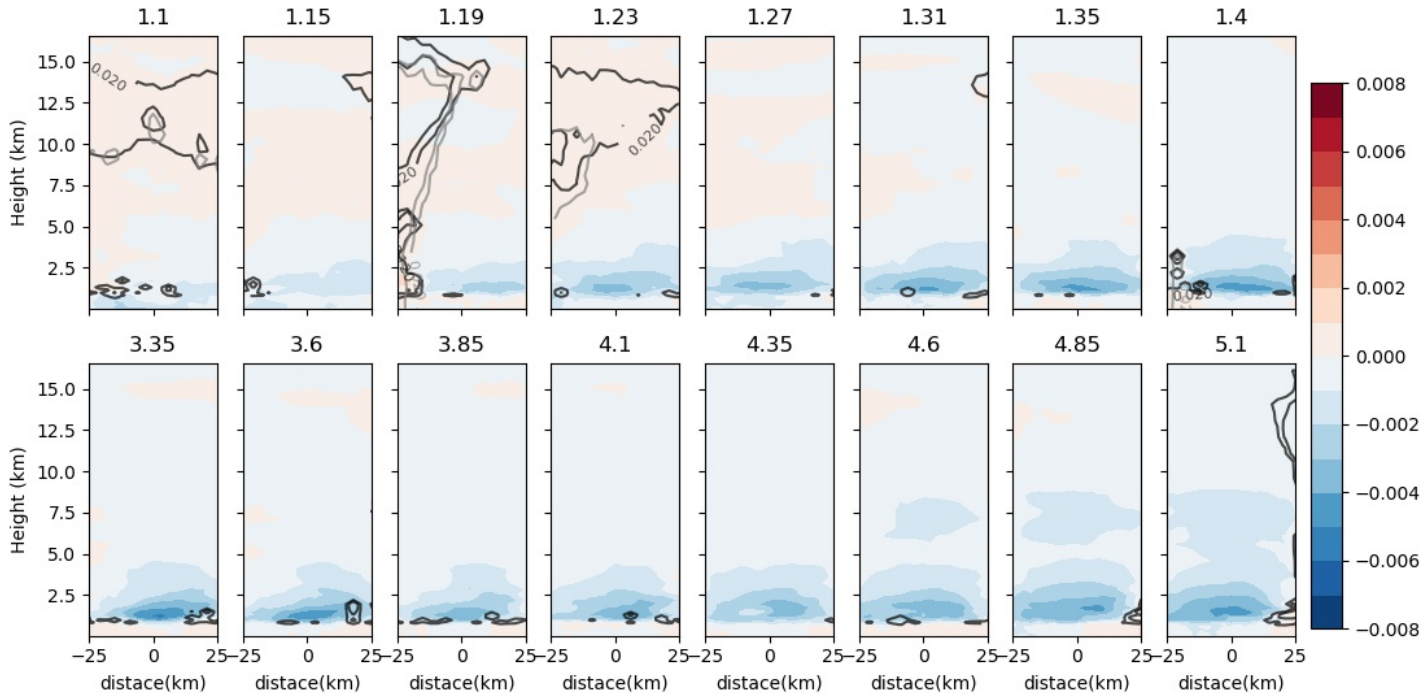

Figure 5.4: The formation of dry patch in 50-305-PS simulation. Color map shows the specific humidity anomaly, black contour shows the cloud condensate, gray contours show the precipitating water.

around a randomly selected dry region at day 5.1 traced back in time to its origin), with dry patches forming outside of deep clouds in clear sky regions, albeit a small shallow cloud coverage.

But in our DC simulations, with shallow slabs ($<= 10m$), the first dry patches form in a couple of days, significantly faster than the processes associated with radiatively driven circulations. For example Figure 5.3.a and b show day 5 of two DC simulations in which the dry patches are already as large as 10 percent of the domain. To understand the mechanism underlying this fast appearance of dry patches, we focus on the regions where the first dry patches appear and visually trace them back in time to their first appearance. In figure 5.5 we select three dry regions A, B, and C. All three regions can be traced back to deep clouds one or two days before. After the convective activity, the surface underneath these clouds is cold due to the cloud shading

and gust-enhanced surface fluxes. The cold SST anomaly persists up to two days, then recovers and becomes warmer due to enhanced shortwave flux at the surface but the dryness does not recover.

During the precipitation, due to the advection of dry air by downdrafts, these regions have negative moisture anomalies which persist and dry further. Figure 5.6 shows the vertical profile of specific and relative humidity anomaly in location C in Figure 5.5. The first column shows one hour after the rain event (located at $x = 0$). The boundary layer and lower free troposphere moisture are both significantly reduced, while the upper troposphere has positive specific and relative humidity. In the following hours,the boundary layer moisture partially recovers but its anomaly remains negative. The free troposphere undergoes a progressive dryness due to subsidence and become completely dry by day 5 at which CRH has already dropped below 0.6 (5.3.

Figure 5.7 shows the averaged profile of point C in Figure 5.5. The plot confirms the negative moisture anomaly in the boundary layer and lower free troposphere after the rain event (which occurs at day 2.25). In following hours the upper and mid troposphere dry progressively. The temperature anomaly is strongly negative at the beginning. With time, the near-surface temperature anomaly recovers while the upper boundary layer temperature anomaly remains slightly negative. The virtual temperature anomaly is negative and equal to -1 *10^{-}3 K. This magnitude is comparable with the one in Figure 4.4, however, with DC, T_v reaches -1*10 $^{-}$3 K in a few days while in Figure 4.4 this value is achieved in 24 days. The radiative cooling, beside its diurnal variability, does not show a significant change during this period.

The vertical velocity is negative and decreasing towards the surface in the boundary layer indicating the existence of a divergent flow. This divergent flow ensures the further removal of moisture from the boundary layer. In the free

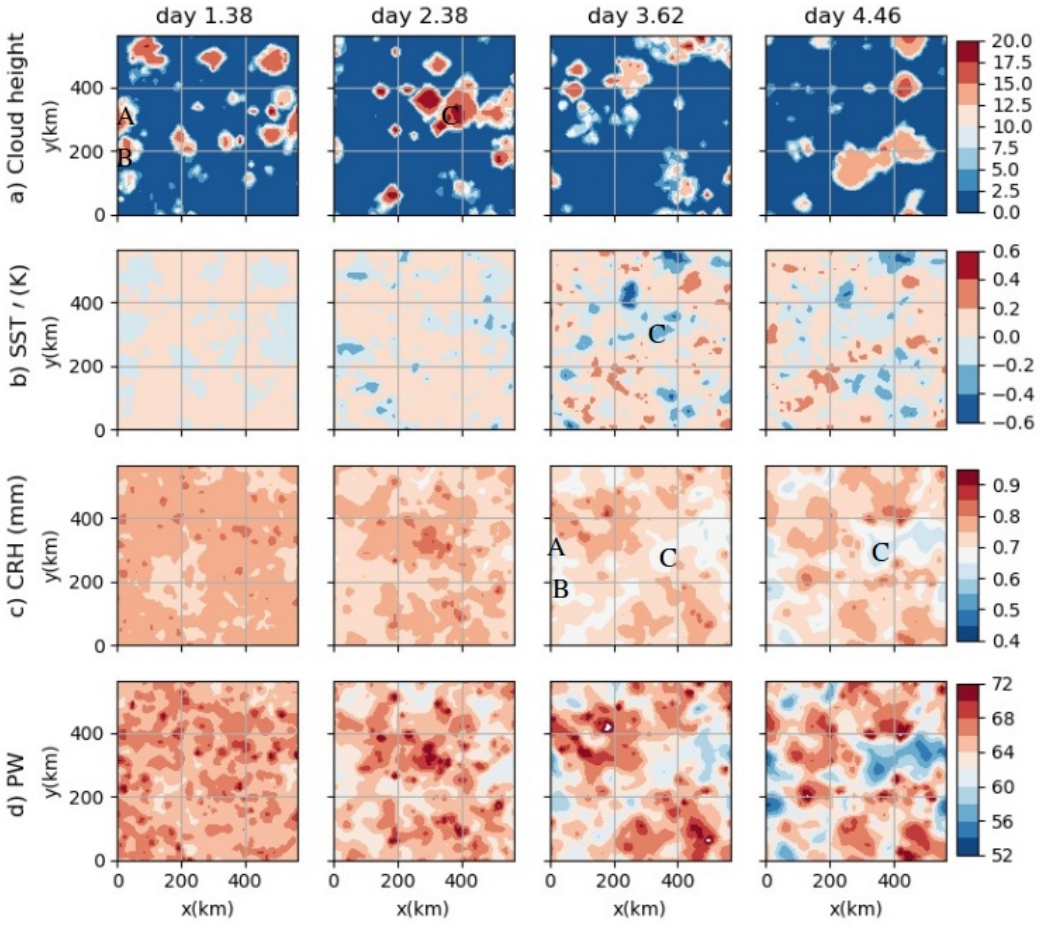

Figure 5.5: The spatial distribution of a. cloud cover, b. SST anomaly, c. CRH, and d. PW as a function of time for the simulation 5-305-DC. Each panel is averaged over one hour and smoothed by 24*24 km^{2}block averaging. The letters A, B and C trace the dry patches.

troposphere, the vertical velocity becomes negative and stronger with time, resulting in the removal of moisture by subsidence (Figure 5.6).

These results thus suggest the following mechanism: when the SST is interactive, a negative SST anomaly forms under the clouds. The colder SST, thus lower LHF, delays the cold pool core moisture recovery. The cold pool divergent flow, driven by negative moisture and temperature anomalies, persists long enough to result in a significant removal of moisture from the boundary layer locally. The negative moisture and temperature anomalies maintain a negative virtual temperature anomaly (thus high pressure by hydrostasy). Consequently, a divergent flow maintains and further dries the region. The free troposphere subsides due to continuity and radiative cooling.

A dry lower free troposphere has been suggested to suppress deep convection through the entrainment of dry air into the updrafts and reduction of their buoyancy (Tompkins, 2001b). We find that for the deep slabs, the dry patches form in the region of low free tropospheric moisture which prohibits convection (Figure 5.4). For the shallow slabs with DC (large SST gradient under the clouds), the negative moisture anomaly in the boundary layer is important as also has been suggested by Yang (2018). This anomaly, which is in this case the consequence of convection, can create a high pressure thus maintains a divergent flow and creates a positive feedback. Nakajima and Matsuno (1988); Jeevanjee and Romps (2013); Yang (2018) showed that cold pools disfavor aggregation by redistributing moisture in the boundary layer. Here we emphasize the local impact of cold pools in cooling the SST, drying the boundary layer and the lower free troposphere. This process instead facilitates the triggering of dry patches.

The persistence of the cold SST anomaly, generated by cloud shading, can play an important role in the formation of the dry patches. Using a fixed SST,

Tompkins (2001a) showed that the temperature perturbation at the center of the cold pool recovers quickly. Here we find that for the shallow slabs, the cold patches that form under the clouds persist for about 2-3 days. This can potentially impact the recovery of temperature in the cold pools further favoring their persistence. Beside this, the cold anomaly reduces the surface latent heat flux thus the moistening of the boundary layer by evaporation.

The question then arises: how do the diurnal cycle and slab depth play a role? When the slab is shallow, the SST gradients that form between the region under and outside the clouds is large. The large SST gradient strengthens the divergent flow of the cold pool. Beside this it can delay the cold pool moisture and temperature recovery.

The other plausible mechanism is the Gray-Jacobson mechanism (differential radiative cooling). Due to stronger night time radiative cooling outside the cloud region, a stronger subsidence thus stronger boundary layer divergent flow form. With a shallow slab, the night time cooling of the surface outside the clouds (including the persisting cloud free cold pools with negative SST anomaly that formed the day before) boosts the boundary layer divergent flow into the convective regions. This process enhances cold pool drying and accelerates triggering of dry patches in those regions. The drying thus the divergent flow persist during the day and prevent the recovery of cold pools.

Dry patches could be triggered by cold pools even without diurnal cycle or with deep slabs but with different time scale. Indeed for these cases as the dry patches form over much longer time, tracing them back in time to their first formation becomes harder. Whether the same mechanism triggers dry patches and how slab depth and diurnal cycle changes the time scale of dry patch formation deserve further investigation.

The fast formation of dry patches with DC removes the latency. From

chapter 4, we know that the latency becomes more important with reducing the slab depth due to the opposition impact of warm SST anomalies in dry regions. By removing the latency, the diurnal cycle reduces the dependency of aggregation on slab depth and results in a faster aggregation. We further investigate whether the diurnal cycle impacts only the latency, thus the triggering of dry patches, or it plays a role also in the transient part. To do so we perform to sensitivity tests with slab depth = 2 and 5. These two simulations start with the diurnal cycle, but after 5 days (enough for triggering) the diurnal cycle is removed and constant solar radiation equal to 413 W/m^2 is implemented similar to PS simulations. We refer to these two simulations as 2-305-DC-PS and 5-305-DC-PS. The aggregation index of these simulations are shown in Figure 5.8. The sensitivity test at slab = 5 m stays between 5-305-DC and 5-305-PS. The test with a 2-meter slab has very similar aggregation progress as 2-305-DC. This indicates that a great part of the accelerated aggregation with DC is due to the faster triggering of dry patches. The fact that 2-305-DC-PS proceeds very similar to 2-305-DC while 5-305-DC-PS shows slower aggregation compared to 5-305-DC can be related to different time scale at which the dry patches are triggered. This time scale can be related to the slab depth. We do not further investigate this dependency.

b. Transient

In chapter 3, we found that the formation of positive surface pressure anomalies (PSFC) in dry regions, drives a divergent flow (shallow flux) in the boundary layer that transport low-level moist air from dry to the moist region and expands the dry patches. Thus to compare the transient period in simulations with DC and PS, we look at the shallow flux.

Figure 5.9.a shows the time series of shallow flux. Indeed, the shallow

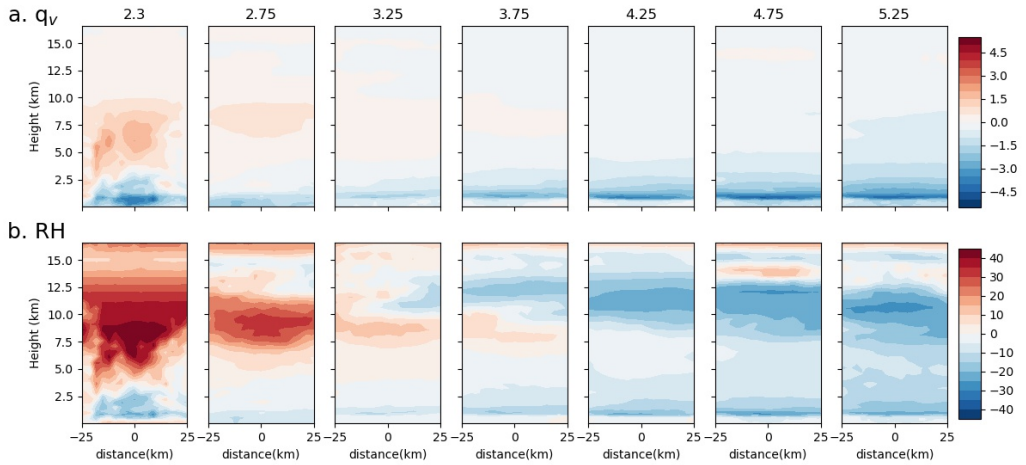

Figure 5.6: Time series of a) specific humidity anomaly and b) relative humidity anomaly for simulation 5-305-DC at point C in Figure 5.5. The anomaly is calculated from the domain mean and each panel is averaged over 2 hours.

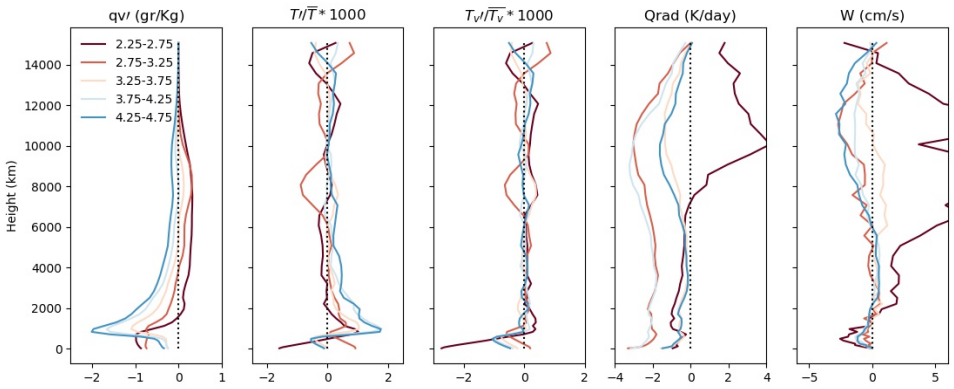

Figure 5.7: The composites of a. specific humidity anomaly, b.normalized temperature anomaly, c. normalized virtual temperature anomaly, d. radiative heating rate, and e. vertical velocity. Composite is 25 km radially and 12 hours temporally averaged over 3 dry patches that formed by convective cold pool. The legend shows time in days.

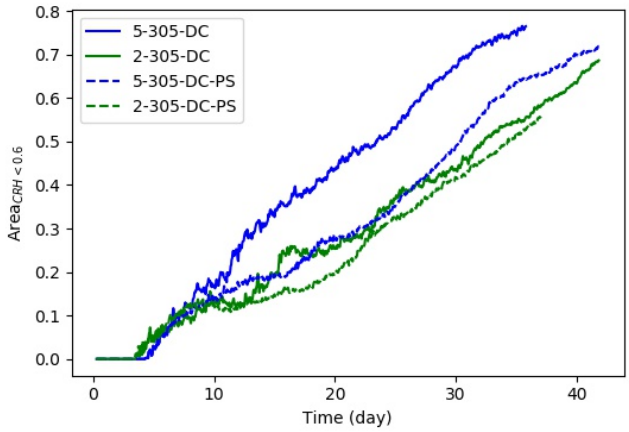

Figure 5.8: Time series of aggregation index for sensitivity tests and the corresponding DC and PS simulations.

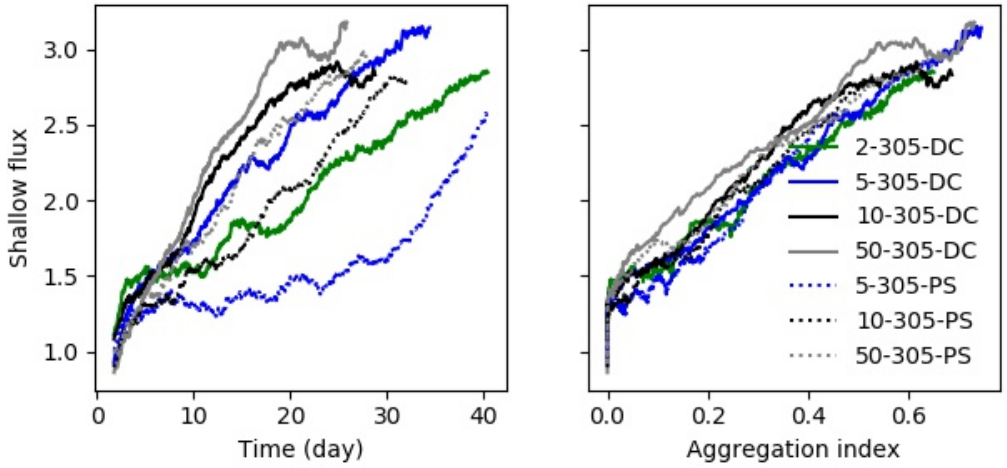

Figure 5.9: Plot shows the evolution of shallow flux ($Kg.m^{-2}.s^{-1}$) with time (left panel) and with aggregation index (right panel).

flux intensifies faster with DC, consistent with the finding of chapter 3. When plotted vs the aggregation index, all plots fall on top of each other, indicating the strong correlation between the shallow flux and the aggregation progress for both cases. The faster enhancement of shallow flux with diurnal cycle is probably mainly due to the removal of the latency. During the latency, the shallow flux has a small value as, based on the finding of chapter 4, the positive SST anomaly opposes the pressure anomaly which drives the shallow flux. When diurnal cycle is included, the early stage warming of SST under the dry patches is precedes by a cooling due to cloud shading. The warming by short-

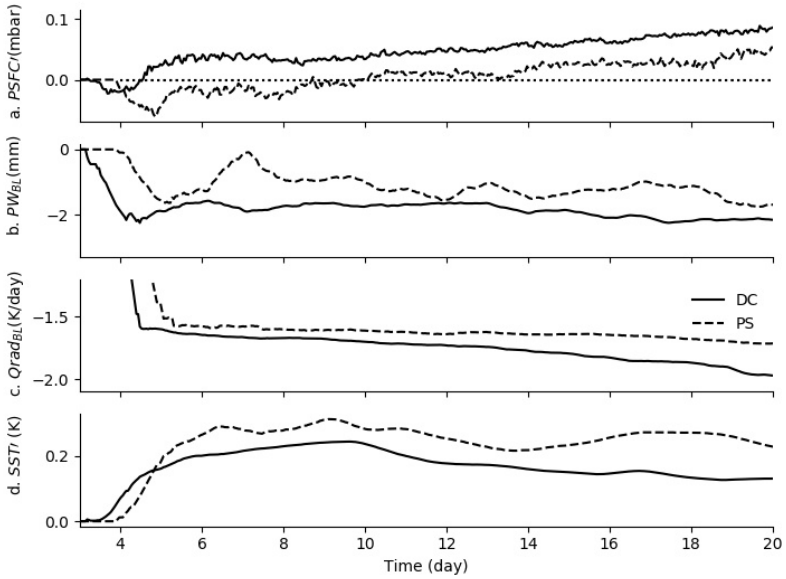

Figure 5.10: Time series of PSFC anomaly , boundary layer precipitable water, boundary layer radiative cooling, and SST anomaly for 5-305-DC (solid line) and 5-305-PS (dashed line), averged over the dry patches and smoothed by 24-hour running average.

wave occurs few days after but its opposition is less effective (5.10.a). The reason is that the early stage dryness is more significant with diurnal cycle (5.10.b) due to different triggering mechanisms. Consequently, it results in a larger pressure anomaly. Furthermore, a larger dryness allows a more efficient surface radiative cooling thus the warm SST anomalies becomes smaller compared to PS case. Consequently, the center of the dry patches becomes cold earlier with DC than PS.

5.4 Conclusion

We run 3D RCE simulations to investigate the importance of the diurnal cycle on the aggregation of convective clouds. The SST is allowed to interact with the atmosphere using a slab ocean which has a fixed mean but locally varying temperature. The finding shows that the aggregation enhances the diurnal variability of shallow flux, precipitation, and LHF. The shallow flux and pre-

cipitation have one maximum which occurs early in the morning (around 3 am) and its timing does not significantly depend on the slab depth.

Our finding shows that, compared to simulations with constant incoming solar radiation, the diurnal cycle reduces the impact of slab depth on the aggregation so that the aggregation proceeds much faster for shallower slabs. For deeper slabs (200 and 50 meters) the speed is insignificantly affected by the diurnal cycle. The main mechanism by which the aggregation proceeds faster with the diurnal cycle is the triggering of dry patches. The triggering is caused by cold pool: the advection of dry mid-tropospheric air by downdrafts into the boundary layer and the following density current remove moisture from the cold pool center. Along with the cold SST anomaly, these yield the persistence of a divergent flow. The strong night time radiative cooling and enhanced subsidence and divergent flow accelerate the removal of moisture from cold-pool regions.

The Gray-Jacobson mechanism can be amplified when the slab is shallow: the strong SST gradient strengthens the divergent flow at night and increases the dry patch growth. When the slab is deep, the SST gradient does not play a role, thus the triggering is similar with and without diurnal cycle. The different triggering time scale with DC and shallow slab, removes the latency, and thus reduces the dependency of aggregation on the slab depth.

After the triggering period, during the transient period, the aggregation slows down for the shallow slabs. This slow down is due to the formation of a positive SST anomaly in dry regions. At this stage, the SST gradient opposes the divergent flow. The transient period of the aggregation is similar between DC and PS cases: in both cases, the shallow flux enhances linearly with aggregation index. Sensitivity tests further confirm that the main impact of the diurnal cycle on the progress of aggregation is through the early triggering

process.

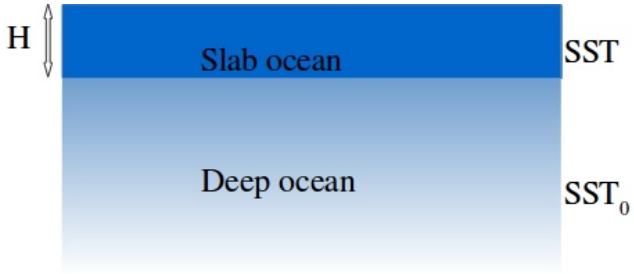

Figure 5.11: Schematic of slab ocean with constant averaged SST

Appendices

5.A Sensitivity to relaxation time

To remove the surplus of energy, the domain means SST is relaxed to a constant SST with a relaxation time (τ) following Equation 4.2. Figure 5.11 shows a simple schematic for the slab set-up. The constant SST (SST_0) is representative of the deep ocean temperature that acts like a thermostat preventing the net cooling or warming of the slab. When the diurnal cycle is included, the mean SST of the slab has a diurnal cycle. Moreover, the amount of energy that is removed by the relaxation term also has a diurnal cycle with the largest removal at midday and negative removal at night.

As the results can be sensitive to τ, we run two more simulations for which τ= 1 hour and 10 min. Figure 5.12 shows the progress of the aggregation index for these two simulations as well as for the simulation with τ =2 hours. The aggregation index does not show a significant dependency on the relaxation time, the same for the main conclusions of the chapter. However, some of the details are different among these simulations, for example, a larger relaxation time results in a larger diurnal variation of the domain mean SST (not shown).

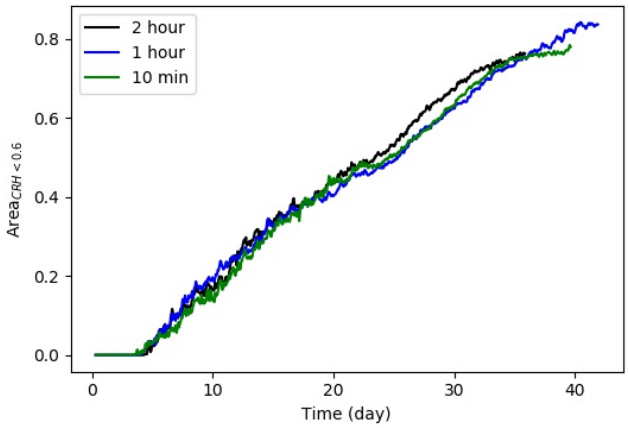

Figure 5.12: The progress of aggregation index for 5-305-DC with three different relaxation time.

Chapter 6

Conclusions and Future Research Directions

6.1 Conclusions

The aggregation of deep convection, which refers to the spontaneous organization of convective clouds into one (or a few) cloud cluster in numerical studies, is known to have a significant impact on domain averaged specific humidity and OLR. If relevant to the Earth's tropics, these two consequences of aggregation could potentially impact the climate sensitivity (Mauritsen and Stevens, 2015; Bony et al., 2015). However, the idealized configuration of simulations in many aggregation studies makes it difficult to quantitatively compare with observed convective organization. Notably, a large number of these studies use a fixed and uniform SST as lower boundary condition, while in nature, SST gradients of different temporal and spatial scales are ubiquitous. One interesting question, which can add to our understanding of aggregation and also makes the numerical studies of aggregation more realistic, is how the aggregating evolves in a domain with SST patterns, and how the feedbacks which

drive the aggregation differ from the simulations with uniform SSTs.

Towards this goal, 3-D cloud resolving simulations of radiative-convective equilibrium with interactive radiation and surface fluxes have been performed in order to investigate the interaction between SST and the aggregation of convective clouds. We investigated three different SST types: fixed and uniform in time and space, fixed in time but heterogeneous in space, and interactive (i.e. evolving in time and space according to the surface energy budget).

Similar to Wing and Emanuel (2014), we find that in a small square domain with fixed and uniform SST (in the range 290 - 305 K), the aggregation occurs above a critical value of SST (295 K) and its speed increases with SST. In all of these simulations, interactive radiation is necessary for aggregation.

In chapter 3, we investigate the impact of a warm ocean anomaly on the aggregation. The warm anomaly is represented as a circular area with radius R and SST anomaly dT which are both spatiotemporally constant. We find that the hot-spot accelerates the aggregation significantly, and the acceleration correlates with R and dT. One interesting result is that even a small hot-spot with a fractional area of 3% can enforce the aggregation at SST below the critical value (295K), thus extending the range of SSTs for which aggregation occurs. However, in this case, the aggregated cluster disaggregates once the hot-spot is removed. The faster aggregation and the extended range of SSTs which favor aggregation, suggest that a hot-spot amplifies the positive feedbacks driving the aggregation: it enhances the surface fluxes, intensifies the low-level convergence of moisture, and increases the buoyancy anomaly locally. Remotely the hot-spot forces the subsidence drying of the environment outside the hot spot and suppresses the convection there. In this sense, a hot-spot can favor the formation of a large scale circulation by localizing the upward mass transport and forcing subsidence drying remotely through mass

continuity. In simulations with a uniform SST, regions of enhanced radiative cooling and reduced moisture appear and grow by suppressing and "pushing" away convection, while in simulations with a hot-spot the locally enhanced instability thus "pulls" the convection over it and deprives the rest of the domain of convection.

To further investigate the necessary versus sufficient feedbacks for aggregation with hot-spot, we performed hot-spot simulations with homogenized radiation. In these cases, the aggregation still proceeds if the hot-spot is large/warm enough (at least larger than 3% with 5 degree temperature anomaly), thus the surface fluxes are sufficient to build up a large scale circulation which transports moisture up-gradient and drives the aggregation.

A spatiotemporally fixed SST rules out the interactions between SST and the convective clouds that potentially affect the aggregation. To include these interaction, chapter 4 is devoted to the impact of an interactive SST on the progress of aggregation. An interactive SST is implemented by a slab ocean with a fixed mean SST using a Newtonian relaxation method. Two mean SSTs (300 and 305 K) and 4 slab depths (5,10,50 and fixed SST for an infinite slab) have been tested. For simplicity, the diurnal cycle is excluded and the incoming shortwave radiation is set to its average over the tropical region. The results show that the aggregation is delayed with interactive SST with larger delay for a shallower slab, consistent with previous studies (Grabowski, 2006; Hohenegger and Stevens, 2016). The first impact of dry patches, which appears after 5-10 days, is SST warming, due to enhanced shortwave flux at the surface as the dry patches are cloud-free. With further dryness at the center of the dry patch, the cooling by surface longwave radiative and latent heat fluxes increase and overcome the warming by shortwave, so that the SST starts decreasing. This cooling at the center leads to the formation of a cold

center surrounded by a ring of warm water which further favors up-gradient transport of moisture.

The pressure anomaly under the dry patches, which becomes positive from the early stage due to a negative moisture anomaly, drives a divergent flow out of the dry patches which further dries and intensifies the dry patches, yielding a positive feedback. The interactive SST opposes the divergent flow at the early stage when it is positive under the dry patches, consistent with previous studies (Grabowski, 2006; Hohenegger and Stevens, 2016; Coppin and Bony, 2017). Later on, when the SST anomaly at the center of the dry patch turns negative, it accelerates the divergent flow. Thus the interactive SST has an opposition-acceleration impact on aggregation through modification of the divergent flow (or shallow flux from dry to moist regions). This result is different from previous studies in which cloud-free regions are always warmer than moist regions thus opposing the divergent flow (Grabowski, 2006; Hohenegger and Stevens, 2016).

Another important mechanism in the dry region is the locally enhanced boundary layer radiative cooling, which cools the boundary layer and favors the formation of a positive surface pressure anomaly in the dry region. The importance of boundary layer radiative cooling has been tested by homogenizing the radiative profile only in the first kilometer of the atmosphere. This simulation does not aggregate while homogenizing the free tropospheric radiative cooling only delays the aggregation by a few days.

The boundary layer divergent flow is key for the aggregation, and it is well correlated with the aggregation index: it increase linearly when plotted versus the aggregation index. The deep circulation is fairly similar between the simulations and does not have a significant variation with aggregation. Our results therefore indicate that once aggregation is triggered, its evolution

is solely dictated by the boundary layer divergence from the dry region in our simulations.

In chapter 5 we investigate the impact of the diurnal cycle on the progress of aggregation when SST is interactive. The results show that the diurnal cycle accelerates the aggregation and also extends the range of slab depths for which aggregation occurs. The acceleration is mostly due to the fast triggering of dry patches, so the latency is removed and dependency on slab depth is reduced. The faster appearance of dry patches is due to cold pools that locally dry the boundary layer especially the sub-cloud layer significantly. The dryness persists as the surface underneath is cold thus the latent heat flux is reduced. The enhanced night time radiative cooling and concomitantly enhanced shallow flux accelerates the drying of dry patches. Consequently, the negative moisture and surface temperature anomaly create a high pressure that drives a divergent flow. By continuity, the whole column subsides and becomes dry. This divergent flow converts the cold pool to a dry subsiding region and triggers the aggregation faster. If confirmed in observations, this new triggering mechanism for aggregation by cold pools could significantly shorten the time scale of this process.

6.2 Future Research Directions

6.2.1 Ocean Eddies

The results of the third chapter suggest that the presence of a hot-spot changes the atmospheric properties such as moisture profile, wind convergence, and cloudiness. A large/warm hot-spot enhances surface fluxes and near-surface instability, so that it can trigger aggregation feedbacks and contribute to the

aggregation of convective clouds. An example of such oceanic hot-spots are the warm ocean mesoscale eddies with radius of $\mathcal{O}$(100 km) (Chelton, 2011) and lifetime of $\mathcal{O}$(10 weeks), comparable to the hot-spots studied here. Although the temperature amplitude of observed ocean eddies is smaller ($\mathcal{O}$(1 degree)) than our hot-spot temperature anomalies, their dynamical and thermodynamical impact on their environment can be important. For instance, numerous studies show that tropical cyclones intensify while passing over a warm ocean eddy as the eddy acts as a heat source providing energy for the cyclone (Wu et al., 2007; Walker et al., 2014; Ma et al., 2015; Sugimoto et al., 2017). Considering this impact, one interesting direction for future work then is to investigate the impact of ocean eddies on cloud organization, and how the aggregation feedbacks play a role. The EUREC^{4}A data provides a great opportunity to investigate these ocean-atmosphere feedbacks (Bony et al., 2017).

Furthermore, a moist region with frequent deep convection is suggested to be favorable for cyclogenesis (Dunkerton et al., 2008). As in low wind shear, a warm ocean anomaly tends to moisten its environment, it is interesting to investigate whether the ocean eddy regions are favorable for cyclogenesis, either in the observation or in RCE simulations with a similar set-up to the hot-spot study.

6.2.2 Boundary Layer Divergent Flow

The boundary layer divergent flow from dry regions has been long noted to be important for convective activity (Gray and Jacobson, 1977; Deser and Smith, 1998; Back and Bretherton, 2009). The results of chapters 3 and 4 confirm this finding, and further show that the boundary layer divergent flow, which transports moisture up-gradient, is linearly correlated with the aggregation progress. These two chapters show the importance of moisture, surface temper-

ature and radiative cooling in driving the divergent flow. Furthermore, chapter 5 shows the nighttime enhancement of boundary layer divergence which can be linked to strong nighttime radiative cooling. The importance of boundary layer radiative cooling on the shallow flux has been suggested by Naumann et al. (2017, 2019). By using a simple conceptual model, they show that an enhanced boundary layer radiative cooling can drive a shallow flux from a dry (larger radiative cooling) to a moist (smaller radiative cooling) region. It would be interesting to investigate the boundary layer divergent flow in observations and the contribution of moisture, radiative cooling, and surface temperature to the divergent flow under different environmental conditions (wind shear, tropospheric moisture, atmospheric stability, etc).

6.2.3 Dry patch triggering

Chapter 5 shows that the dry patches can also be triggered by cold pool dynamics. In this case, the time scale of triggering depends on many parameters such as moisture, SST and boundary layer temperature perturbation due to cold pool properties. The time scale of recovery of each of these perturbations depends on SST (mean and anomaly), slab depth, and the presence of a diurnal cycle. Furthermore, free-tropospheric moisture, radiative cooling and stratification can also play a role by impacting the subsidence velocity in these regions. Quantifying the time scale of each of these processes can improve our understanding of conditions favorable for dry patches to be triggered by cold pools.

6.2.4 Shallow Circulation

As shows in Bretherton et al. (2005) (figure 10) and chapter 4 (Figure 4.7), the stream function shows a low-level inflow from dry to moist (shallow flux) and an outflow that happens all through the column in the moist region. The outflow has one maximum at the top of the boundary layer (shallow circulation) and a secondary maximum in the upper free troposphere. Although the importance of large scale circulation has been emphasized by many numerical studies of self-aggregation (Muller and Held, 2012; Jeevanjee and Romps, 2013; Wing and Emanuel, 2014; Coppin and Bony, 2015; Hohenegger and Stevens, 2016), it is not clear whether it is the total low-level inflow which is important for the aggregation, or whether it is only the fraction of this inflow which returns to dry regions below 2-3km. The former one measures total moisture transport, while the latter is close to the MSE transport up-gradient. Whether MSE transport is important for aggregation or moisture is also controversial among the studies.

One interesting future work would be to study the inflow-outflow profile and how it impacts the aggregation progress. Furthermore, this profile itself depends on the simulation set-up such as domain size and radiation profile (Jeevanjee and Romps, 2013; Bretherton et al., 2005). For instance, Muller and Held (2012); Coppin and Bony (2015) mentioned that removing liquid clouds from radiation destroys the shallow circulation and prevents the aggregation, while in our simulations, sensitivity tests show that removing clouds from radiation delays the aggregation but does not prevent it. Furthermore, chapter 5 suggests that the diurnal cycle imposes a diurnal variability on the inflow-outflow profile that potentially impacts the aggregation speed. A possible continuation is to investigate how the radiation profile impacts the inflow-outflow profile.

6.2.5 Interactive SST with adjusted mean energy removal

In chapter 5, we investigate the impact of a diurnal cycle on the aggregation when the SST is interactive. To keep the mean SST constant, a Newtonian relaxation term has been added to the temperature equation that removes the surplus of energy from the surface, via the SST evolution equation 4.2 repeated here for convenience (with $C_w = \rho_w c_{p,w} H$ slab ocean heat capacity, and $\Sigma EF = Q^N_{SW} + Q^N_{LW} + LHF + SHF$ net energy flux at the surface):

$$C_w \left(\frac{dSST}{dt} + \frac{\overline{SST} - SST_0}{\tau_0} \right) = \Sigma EF.$$

Note that this method yields a diurnal cycle on the relaxation term, at the domain-mean surface temperature $\overline{SST}$ has a diurnal cycle.

But as the sink of energy is supposed to mimic the poleward transport of energy out of the tropics, it probably does not have a significant diurnal variation. One alternative method for energy removal without diurnal cycle, is to remove the averaged surface energy imbalance from the temperature equation:

$$C_w \frac{dSST}{dt} = \Sigma EF - < \overline{\Sigma EF} >, \tag{6.1}$$

where $< \overline{\Sigma EF} >$ is the domain-mean and daily-mean net energy flux at the surface. If used with constant incoming solar radiation, the last term on the RHS can be averaged over a few time steps, while when the diurnal cycle is included, the average has to be taken over a day (or several days) to remove its diurnal variation. This method thus removes the diurnal cycle from the energy sink, and also results in a larger diurnal variability of the domain mean SST. Thus potentially, this other approach could affect the results of chapter 5, and significantly impact the aggregation process.

Bibliography

Abbot, D. S. (2014). Resolved snowball earth clouds. J. Climate, 27(12):4391–4402.

Back, L. E. and Bretherton, C. S. (2009). On the relationship between sst gradients, boundary layer winds, and convergence over the tropical oceans. Journal of Climate, 22(15):4182–4196.

Bain, C. L., Magnusdottir, G., Smyth, P., and Stern, H. (2010). Diurnal cycle of the intertropical convergence zone in the east pacific. Journal of Geophysical Research: Atmospheres, 115(D23).

Bellenger, H., Duvel, J., Lengaigne, M., and Levan, P. (2009). Impact of organized intraseasonal convective perturbations on the tropical circulation. Geophys. Res. Lett., 36:L16703.

Beringer, J. and Tapper, N. (2002). Surface energy exchanges and interactions with thunderstorms during the maritime continent thunderstorm experiment (mctex). J. Geophys. Res., 107(D21):AAC 3–1–AAC 3–13.

Bony, S., Stevens, B., Ament, F., Bigorre, S., Chazette, P., Crewell, S., Delanoë, J., Emanuel, K., Farrell, D., Flamant, C., et al. (2017). Eurec4a: a field campaign to elucidate the couplings between clouds, convection and circulation. Surveys in Geophysics, 38(6):1529–1568.

Bony, S., Stevens, B., and Coauthors (2015). Clouds, circulation and climate sensitivity. Nature Geosci.

Bowman, K. P. and Fowler, M. D. (2015). The diurnal cycle of precipitation in tropical cyclones. Journal of Climate, 28(13):5325–5334.

Bretherton, C. S., Blossey, P. N., and Khairoutdinov, M. (2005). An energy-balance analysis of deep convective self-aggregation above uniform SST. J. Atmos. Sci., 62(12):4273–4292.

Bretherton, C. S. and Smolarkiewicz, P. K. (1989). Gravity waves, compensating subsidence and detrainment around cumulus clouds. J. Atmos. Sci., 46(6):740–759.

Chelton, D. (2011). Global observations of nonlinear mesoscale eddies. Prog. Oceanogr., 91(2):167 – 216.

Chen, S. S. and Houze, R. A. (1997). Diurnal variation and life-cycle of deep convective systems over the tropical pacific warm pool. Quarterly Journal of the Royal Meteorological Society, 123(538):357–388.

Ciesielski, P. E., Johnson, R. H., Schubert, W. H., and Ruppert, J. H. (2018). Diurnal cycle of the itcz in dynamo. Journal of Climate, 31(11):4543–4562.

Collins, W. D., Rasch, P. J., Boville, B. A., Hack, J. J., McCaa, J. R., Williamson, D. L., Briegleb, B. P., Bitz, C. M., Lin, S. J., and Zhang, M. (2006). The formulation and atmospheric simulation of the community atmosphere model version 3 (cam3). J. Climate, 19(11):2144–2161.

Collins, W. D., Rasch, P. J., Boville, B. A., Hack, J. J., McCaa, J. R., Williamson, D. L., Kiehl, J. T., Briegleb, B., Bitz, C., Lin, S.-J., et al. (2004). Description of the ncar community atmosphere model (cam 3.0). NCAR Tech. Note NCAR/TN-464+ STR, 226.

Coppin, D. and Bony, S. (2015). Physical mechanisms controlling the initiation of convective self-aggregation in a general circulation model. J. Adv. Model. Earth Syst., 7(4):2060–2078.

Coppin, D. and Bony, S. (2017). Internal variability in a coupled general circulation model in radiative-convective equilibrium. Geophys. Res. Lett., 44(10):5142–5149.

Craig, G. C. and Mack, J. M. (2013). A coarsening model for self-organization of tropical convection. J. Geophys. Res., 118(16):8761–8769.

Cronin, T. W., Emanuel, K. A., and Molnar, P. (2015). Island precipitation enhancement and the diurnal cycle in radiative-convective equilibrium. Quart. J. Roy. Meteor. Soc., 141(689):1017–1034.

Crook, N. A. (2001). Understanding hector: The dynamics of island thunderstorms. Mon. Wea. Rev., 129:1550–1563.

Daleu, C. L., Plant, R. S., and Woolnough, S. J. (2017). Using the weak-temperature gradient approximation to evaluate parameterizations: An example of the transition from suppressed to active convection. J. Adv. Model. Earth Syst., 9(6):2350–2367.

Davis, C. A. and Ahijevych, D. A. (2012). Mesoscale structural evolution of three tropical weather systems observed during predict. Journal of the Atmospheric Sciences, 69(4):1284–1305.

Deser, C. and Smith, C. A. (1998). Diurnal and semidiurnal variations of the surface wind field over the tropical pacific ocean. Journal of Climate, 11(7):1730–1748.

Dunkerton, T. J., Montgomery, M. T., and Wang, Z. (2008). Trop-

ical cyclogenesis in a tropical wave critical layer: easterly waves. Atmospheric Chemistry and Physics Discussions, 8(3):11149–11292.

Duvel, J. P. (1988). Analysis of diurnal, interdiurnal and interannual variations during northern hemisphere summers using meteosat infrared channels. Journal of climate, 1(5):471–484.

Duvel, J. P. (1989). Convection over tropical africa and the atlantic ocean during northern summer. part i: Interannual and diurnal variations. Monthly weather review, 117(12):2782–2799.

Emanuel, K. A., David Neelin, J., and Bretherton, C. S. (1994). On large-scale circulations in convecting atmospheres. Quarterly Journal of the Royal Meteorological Society, 120(519):1111–1143.

Emanuel, K. A., Wing, A. A., and Vincent, E. M. (2014). Radiative-convective instability. J. Adv. Model. Earth Syst., 6(1):75–90.

Grabowski, W. W. (2006). Impact of explicit atmosphere-ocean coupling on mjo-like coherent structures in idealized aquaplanet simulations. J. Atmos. Sci., 63(9):2289–2306.

Grabowski, W. W. and Moncrieff, M. W. (2001). Large-scale organization of tropical convection in two-dimensional explicit numerical simulations. Quart. J. Roy. Meteor. Soc., 127(572):445–468.

Grabowski, W. W. and Moncrieff, M. W. (2004). Moisture–convection feedback in the tropics. Quart. J. Roy. Meteor. Soc., 130(604):3081–3104.

Gray, W. and Jacobson, R. (1977). Diurnal variation of deep cumulus convection. Mon. Wea. Rev., 105:1171–1187.

Haerter, J. O., Meyer, B., and Nissen, S. B. (2020). Diurnal self-aggregation.

Held, I. M., Hemler, R. S., and Ramaswamy, V. (1993). Radiative-convective equilibrium with explicit two-dimensional moist convection. J. Atmos. Sci., 50(23):3909–3909.

Hendon, H. H. and Woodberry, K. (1993). The diurnal cycle of tropical convection. Journal of Geophysical Research: Atmospheres, 98(D9):16623–16637.

Hennon, C. C., Papin, P. P., Zarzar, C. M., Michael, J. R., Caudill, J. A., Douglas, C. R., Groetsema, W. C., Lacy, J. H., Maye, Z. D., Reid, J. L., Scales, M. A., Talley, M. D., and Helms, C. N. (2013). Tropical cloud cluster climatology, variability, and genesis productivity. Journal of Climate, 26(10):3046–3066.

Hohenegger, C. and Stevens, B. (2016). Coupled radiative convective equilibrium simulations with explicit and parameterized convection. J. Adv. Model. Earth Syst., 8(3):1468–1482.

Holloway, C. E. (2017). Convective aggregation in realistic convective-scale simulations. J. Adv. Model. Earth Syst., 9(2):1450–1472.

Houze, R. A. (1977). Structure and dynamics of a tropical squall–line system. Monthly Weather Review, 105(12):1540–1567.

Houze, Jr., R. A. (2004). Mesoscale convective systems. Rev. Geophys., 42(4):RG4003.

Jeevanjee, N. and Romps, D. M. (2013). Convective self-aggregation, cold pools, and domain size. Geophys. Res. Lett., 40(5):994–998.

Khairoutdinov, M. F. and Emanuel, K. A. (2010). Aggregated convection and the regulation of tropical climate. Preprints, 29th conference on Hurricanes and Tropical Meteorology, Tucson, AZ, Amer. Meteor. Soc., P2.69.

Khairoutdinov, M. F. and Kogan, Y. L. (1999). A large eddy simulation model with explicit microphysics: Validation against aircraft observations of a stratocumulus-topped boundary layer. J. Atmos. Sci., 56(13):2115–2131.

Khairoutdinov, M. F. and Randall, D. A. (2003). Cloud resolving modeling of the ARM summer 1997 IOP: Model formulation, results, uncertainties, and sensitivities. J. Atmos. Sci., 60(4):607–625.

Kossin, J. P. (2002). Daily hurricane variability inferred from goes infrared imagery. Monthly Weather Review, 130(9):2260–2270.

Kuang, Z. (2012). Weakly forced mock walker cells. J. Atmos. Sci., 69:2759–2786.

Lau, N.-C. (1997). Interactions between global sst anomalies and the mid-latitude atmospheric circulation. Bulletin of the American Meteorological Society, 78(1):21–34.

Liu, C. and Moncrieff, M. W. (1998). A numerical study of the diurnal cycle of tropical oceanic convection. Journal of the Atmospheric Sciences, 55(13):2329–2344.

Ma, J., Xu, H., Dong, C., Lin, P., and Liu, Y. (2015). Atmospheric responses to oceanic eddies in the kuroshio extension region. J. Geophys. Res., 120(13):6313–6330.

Machado, L. T., Duvel, J.-P., and Desbois, M. (1993). Diurnal variations and modulation by easterly waves of the size distribution of convective cloud clusters over west africa and the atlantic ocean. Monthly weather review, 121(1):37–49.

Madden, R. A. and Julian, P. R. (1971). Detection of a 40–50 day oscillation in

the zonal wind in the tropical pacific. Journal of the Atmospheric Sciences, 28(5):702–708.

Manabe, S. and Strickler, R. F. (1964). Thermal equilibrium of the atmosphere with a convective adjustment. Journal of the Atmospheric Sciences, 21(4):361–385.

Mapes, B. and Neale, R. (2011). Parameterizing convective organization to escape the entrainment dilemma. J. Adv. Model. Earth Syst., 3(2).

Mapes, B. E. (2001). Water's two height scales: The moist adiabat and the radiative troposphere. Quart. J. Roy. Meteor. Soc., 127(577):2353–2366.

Marshall, J. S. and Palmer, W. M. K. (1948). The distribution of raindrops with size. Journal of Meteorology, 5(4):165–166.

Mauritsen, T. and Stevens, B. (2015). Missing iris effect as a possible cause of muted hydrological change and high climate sensitivity in models. Nature Geoscience, 8(5):346–351.

Muller, C. J. (2013). Impact of convective organization on the response of tropical precipitation extremes to warming. J. Climate, 26:5028–5043.

Muller, C. J. and Bony, S. (2015). What favors convective aggregation and why? Geophys. Res. Lett., 42(13):5626–5634.

Muller, C. J. and Held, I. M. (2012). Detailed investigation of the self-aggregation of convection in cloud-resolving simulations. J. Atmos. Sci., 69:2551–2565.

Muller, C. J. and O'Gorman, P. A. (2011). An energetic perspective on the regional response of precipitation to climate change. Nature Climate Change, 1(5):266–271.

Muller, C. J., O'Gorman, P. A., and Back, L. E. (2011). Intensification of precipitation extremes with warming in a cloud-resolving model. J. Climate, 24(11):2784–2800.

Nakajima, K. and Matsuno, T. (1988). Numerical experiments concerning the origin of cloud clusters in the tropical atmosphere. Journal of the Meteorological Society of Japan. Ser. II, 66(2):309–329.

Naumann, A. K., Stevens, B., and Hohenegger, C. (2019). A moist conceptual model for the boundary layer structure and radiatively driven shallow circulations in the trades. Journal of the Atmospheric Sciences, 76(5):1289–1306.

Naumann, A. K., Stevens, B., Hohenegger, C., and Mellado, J. P. (2017). A conceptual model of a shallow circulation induced by prescribed low-level radiative cooling. Journal of the Atmospheric Sciences, 74(10):3129–3144.

Neelin, J. D. and Held, I. M. (1987). Modeling tropical convergence based on the moist static energy budget. Monthly Weather Review, 115(1):3–12.

Nesbitt, S. W., Zipser, E. J., and Cecil, D. J. (2000). A census of precipitation features in the tropics using trmm: Radar, ice scattering, and lightning observations. J. Climate, 13(23):4087–4106.

Nicholls, M. E. (2015). An investigation of how radiation may cause accelerated rates of tropical cyclogenesis and diurnal cycles of convective activity. Atmospheric Chemistry and Physics, 15(15):9003–9029.

Pauluis, O. and Held, I. M. (2002). Entropy budget of an atmosphere in radiative–convective equilibrium. part i: Maximum work and frictional dissipation. J. Atmos. Sci., 59(2):125–139.

Pierrehumbert, R. T. (2010). Principles of planetary climate. Cambridge University Press.

Qian, J.-H. (2008). Why precipitation is mostly concentrated over islands in the maritime continent. J. Atmos. Sci., 65(4):1428–1441.

Ramsay, H. A. and Sobel, A. H. (2011). Effects of relative and absolute sea surface temperature on tropical cyclone potential intensity using a single-column model. J. Climate, 24(1):183–193.

Randall, D. A., Harshvardhan, and Dazlich, D. A. (1991). Diurnal variability of the hydrologic cycle in a general circulation model. Journal of the Atmospheric Sciences, 48(1):40–62.

Raymond, D. J., Sessions, S. L., Sobel, A. H., and Fuchs, Ž. (2009). The mechanics of gross moist stability. J. Adv. Model. Earth Syst., 1(3).

Robinson, F. J., Sherwood, S. C., Gerstle, D., Liu, C., and Kirshbaum, D. J. (2011). Exploring the land-ocean contrast in convective vigor using islands. J. Atmos. Sci., 68(3):602–618.

Romps, D. M. (2010). A direct measure of entrainment. J. Atmos. Sci., 67(6):1908–1927.

Romps, D. M. (2011). Response of tropical precipitation to global warming. J. Atmos. Sci., 68(1):123–138.

Ruppert, J. and Hohenegger, C. (2018). Diurnal circulation adjustment and organized deep convection. J. Climate.

Semie, A. G. and Tompkins, A. M. (2016). Organization of tropical convection in low vertical wind shears: impact of boundary conditions. In EGU General Assembly Conference Abstracts, volume 18.

Shamekh, S., Muller, C., Duvel, J.-P., and D'Andrea, F. (2019). How do ocean warm anomalies favor the aggregation of deep convective clouds? J. Atmos. Sci.

Shamekh, S., Muller, C., Duvel, J.-P., and D'Andrea, F. (2020). Self-aggregation of convective clouds with interactive sea surface temperature. J. Adv. Model. Earth Syst., submitted.

Simpson, J., Ritchie, E., Holland, G. J., Halverson, J., and Stewart, S. (1997). Mesoscale interactions in tropical cyclone genesis. Monthly Weather Review, 125(10):2643–2661.

Singh, M. S. and O'Gorman, P. A. (2012). Upward shift of the atmospheric general circulation under global warming: theory and simulations. J. Climate.

Sobel, A. H. and Bretherton, C. S. (2000). Modeling tropical precipitation in a single column. J. Climate, 13(24):4378–4392.

Sobel, A. H., Burleyson, C. D., and Yuter, S. E. (2011). Rain on small tropical islands. J. Geophys. Res., 116(D8).

Sobel, A. H., Nilsson, J., and Polvani, L. M. (2001). The weak temperature gradient approximation and balanced tropical moisture waves. J. Atmos. Sci., 58:23.

Stephens, G. L., Van Den Heever, S., and Pakula, L. (2008). Radiative–convective feedbacks in idealized states of radiative–convective equilibrium. J. Atmos. Sci., 65:3899–3916.

Sugimoto, S., Aono, K., and Fukui, S. (2017). Local atmospheric response to warm mesoscale ocean eddies in the kuroshio-oyashio confluence region. Scientific Reports, 7(11871).

Sui, C.-H., Lau, K.-M., Takayabu, Y. N., and Short, D. A. (1997). Diurnal variations in tropical oceanic cumulus convection during toga coare. Journal of the Atmospheric Sciences, 54(5):639–655.

Tan, J., Jakob, C., Rossow, W. B., and Tselioudis, G. (2015). Increases in tropical rainfall driven by changes in frequency of organized deep convection. Nature, 519(7544):451.

Tobin, I., Bony, S., and Roca, R. (2012). Observational evidence for relationships between the degree of aggregation of deep convection, water vapor, surface fluxes, and radiation. J. Climate, 25:6885–6904.

Tompkins, A. M. (2001a). Organization of Tropical Convection in Low Vertical Wind Shears: The Role of Cold Pools. J. Atmos. Sci., 58:1650–1672.

Tompkins, A. M. (2001b). Organization of tropical convection in low vertical wind shears: The role of water vapor. J. Atmos. Sci., 58(6):529–545.

Tompkins, A. M. and Craig, G. C. (1998). Radiative-convective equilibrium in a three-dimensional cloud-ensemble model. Quart. J. Roy. Meteor. Soc., 124:2073–2097.

Tompkins, A. M. and Semie, A. G. (2017). Organization of tropical convection in low vertical wind shears: Role of updraft entrainment. Journal of Advances in Modeling Earth Systems, 9(2):1046–1068.

Walker, N. D., Leben, R. R., Pilley, C. T., Shannon, M., Herndon, D. C., Pun, I.-F., Lin, I.-I., and Gentemann, C. L. (2014). Slow translation speed causes rapid collapse of northeast pacific hurricane kenneth over cold core eddy. Geophysical Research Letters, 41(21):7595–7601.

Wang, S. and Sobel, A. H. (2011). Response of convection to relative sea surface temperature: Cloud-resolving simulations in two and three dimensions. J. Geophys. Res., 116(D11).

Wang, S. and Sobel, A. H. (2017). Factors controlling rain on small tropical

islands: Diurnal cycle, large-scale wind speed, and topography. J. Atmos. Sci., 74(11):3515–3532.

Wing, A. (2019). Self-aggregation of deep convection and its implications for climate. Current Climate Change Reports, 5(1):1–11.

Wing, A., Emanuel, K., Holloway, C., and Muller, C. (2017). Convective self-aggregation in numerical simulations: A review. Surv. Geophys., 38(6):1173–1197.

Wing, A. A. and Cronin, T. W. (2016). Self-aggregation of convection in long channel geometry. Quart. J. Roy. Meteor. Soc., 142(694):1–15.

Wing, A. A. and Emanuel, K. A. (2014). Physical mechanisms controlling self-aggregation of convection in idealized numerical modeling simulations. J. Adv. Model. Earth Syst., 6(1):59–74.

Wu, C.-C., Lee, C.-Y., and Lin, I.-I. (2007). The effect of the ocean eddy on tropical cyclone intensity. Journal of the Atmospheric Sciences, 64(10):3562–3578.

Yang, D. (2018). Boundary layer diabatic processes, the virtual effect, and convective self-aggregation. Journal of Advances in Modeling Earth Systems, 10(9):2163–2176.

Yang, S., Kuo, K.-S., and Smith, E. A. (2008). Persistent nature of secondary diurnal modes of precipitation over oceanic and continental regimes. Journal of Climate, 21(16):4115–4131.

Zuidema, P., Torri, G., and Muller, C. (2017). Precipitation-induced atmospheric cold pools over oceans and their interactions with the larger-scale environment. Surv. Geophys., 38(6):1283–1305.

Résumé

Cette thèse examine l'impact des hétérogénéités de température de surface de la mer (SST) sur l'agrégation des nuages convectifs, à l'aide de simulations 3D de l'équilibre radiatif-convectif. Les hétérogénéités de température étudiées sont soit imposées, soit interactives. Dans le premier cas, un point chaud de rayon R et d'anomalie de température ΔT est introduit à la surface. Le point chaud accélère l'agrégation et étend les valeurs de SST pour lesquelles la convection agrège. L'augmentation de l'instabilité sur le point chaud renforce la convection et la circulation grande échelle, forçant la subsidence et l'assèchement à l'extérieur du point chaud. Une anomalie suffisamment large ou chaude provoque l'agrégation même sans rétroactions radiatives. Dans le cas d'hétérogénéités interactives, l'océan est modélisé par une couche de température moyenne constante mais variant dans l'espace. La SST interactive ralentit l'agrégation, d'autant plus que la couche océanique est peu profonde. L'anomalie de SST dans les régions sèches est d'abord positive, s'opposant à la circulation divergente dans la couche limite, connue pour favoriser l'auto-agrégation. À un seuil de sécheresse plus élevé, l'anomalie devient négative et favorise cette circulation. La circulation peu profonde est corrélée à la vitesse d'agrégation. Elle est due à une haute pression, elle-même liée aux anomalies de SST et au refroidissement radiatif de la couche limite. L'inclusion d'un cycle diurne dans les simulations avec SST interactive accélère l'apparition de zones sèches et l'agrégation pour les couches océaniques peu profondes, réduisant ainsi la dépendance de l'agrégation à la profondeur de la couche océanique.

Mots Clés

Nuages convectifs, Agrégation, Température de surface de la mer

Abstract

This study investigates the impact of Sea Surface Temperature (SST) heterogeneities on the aggregation of convective clouds, using 3D cloud-resolving simulations of radiative-convective equilibrium. The SST heterogeneities are either imposed or interactive. In imposed cases, a spatiotemporally fixed warm SST anomaly (Hot-spot) with radius R and temperature anomaly ΔT is introduced at the center of the domain. The hot-spot significantly accelerates aggregation and extends the range of SSTs for which aggregation occurs. A convective instability over the hot-spot leads to stronger convection and generates a large-scale circulation, forcing subsidence drying outside the hot-spot. A large/warm hot-spot drives the aggregation even without radiative feedbacks. In cases where SST heterogeneities are interactive, the ocean is modeled as one layer slab ocean, with a constant mean but spatially varying temperature. The interactive SST decelerates the aggregation, especially with shallower slab. SST anomaly in dry regions is positive at first, thus opposing the diverging shallow circulation known to favor self-aggregation. With further drying, it becomes negative and favors the shallow circulation. The shallow circulation is found to be well correlated with the aggregation speed. It can be linked to a positive surface pressure anomaly, itself the consequence of SST anomalies and boundary layer radiative cooling. Including a diurnal cycle in simulations with interactive SST results in faster triggering of dry patches and accelerates the aggregation for shallow slabs, thus reducing the dependency of aggregation on slab depth.

Keywords

Deep convective clouds, Aggregation of convection, Sea surface temperature